ALMA MATER STUDIORUM - UNIVERSITÀ DI BOLOGNA

DOTTORATO DI RICERCA IN

Meccanica e scienze avanzate dell'ingegneria

Ciclo 29°

Settore Concorsuale di afferenza 09/A2

Settore Scientifico disciplinare ING-IND-13

MODELING, COMPONENT SELECTION AND OPTIMIZATION OF SERVO-CONTROLLED AUTOMATIC MACHINERY

Presentata da: **Francesco Meoni**

Coordinatore Dottorato

Prof. Nicolò Cavina

Relatore

Prof. Marco Carricato

Esame Finale anno 2017

Modeling, Component Selection and Optimization of Servo-controlled Automatic Machinery

Alma Mater Studiorum - Università degli Studi di Bologna

Francesco Meoni

March 2017

Abstract

A servo-controlled automatic machine can perform tasks that involve coordinated or synchronized actuation of a significant number of *servo-axes*, namely one degree-of-freedom (DoF) electromechanical actuators. Each servo-axis comprises a servo-motor, a mechanical transmission and an end-effector. It is responsible for generating the desired motion profile and providing the power required to achieve the overall task. The design of a such a machine must involve a detailed study from a mechatronic viewpoint, due to its electric and mechanical nature. This raises new challenges, which are not tackled when mechanical and electrical components are considered separately. Our effort in meeting such challenges are justified by the fact that the traditional approach will only lead to an optimum design at a sub-system level. An integrated approach allows for achieving, instead, a global optimal design. Therefore, analyzing the whole system instead of a specific part is of fundamental importance for embracing the different nature of the machine, in order to achieve an optimal design.

The first objective of this thesis is the development of an overarching electromechanical model for a servo-axis, thus providing a global view on the system from the electric grid to the end effector. Such model enables us to evaluate the influence of all components, such as the servo-motor, the mechanical transmission and the motion law of the system. Every source of losses is taken into account, be it mechanical or electrical. The mechanical transmission is modeled by means of a sequence of lumped-parameter blocks: each block is a single-input-single-output subsystem, whose behavior is encoded in a transfer function that prescribes interaction among kinematic and dynamic parameters. In parallel to the mechanical model, an electric model of the servo motor and the inverter is defined, which takes into account winding losses, iron losses and controller switching losses. The permanent magnet synchronous motor efficiency is defined as a function of load and speed. No experimental characterizations are needed to implement the electric model, since the parameters are inferred from the data available in commercial catalogs.

Once the model is defined, we may obtain a comprehensive set of information from simulations involving both inverse and forward dynamics. For instance, once the task is given and the inverse dynamic problem is solved, the stress born by the components, the torque to be provided by the motor, and the maximum rotational speed can be inferred. The determination of such quantities serves as indispensable prerequisites for the design phase. More specifically, the impact of several design choices is evaluated, such as the influence of the motion profile on global efficiency, or the selection of a certain component over another, etc. With the global model at disposal, a second objective of this work is pursued: the optimization analysis for automatic machine design. The components selection and the motion profile design procedure are optimized in order to minimize a set of objective functions, such as the root-mean-square of the motor torque, peak values of electric power, and overall absorbed energy. The integration of electrical and mechanical aspects guarantees the derivation of a global optimal design.

Among the several design choices to be analyzed, this thesis focuses on the selection of the motor-reducer unit, which has a great impact on the dynamic performance of a machine. The limitations of both components must be simultaneously taken into account. The optimal transmission ratios that minimize several objective functions are found: in particular,

since energy efficiency is a growing concern in today's mechatronic design paradigm, the optimal transmission ratio that minimizes the energy absorbed by the motor is highlighted. The mechanical transmission is first assumed to be ideal and a feasibility analysis on a discrete set of candidate motors is made. For each candidate, the optimization is carried out and then the non-ideal reducer characteristics are taken into account. This process is practical and automatizable, but is iterative and must be repeated for each motor. In order to overcome these drawbacks we present a novel method where the discrete set of available motor is extended to a continuous domain by fitting manufacturer data. The optimization is then carried out without iterations, and it is applicable to the general case of a real transmission with limited operation range. The problem becomes a two-dimensional nonlinear optimization subject to nonlinear constraints, and the solution gives the optimal choice for the motor-reducer system.

The presented electromechanical model, along with the implementation of optimization algorithms, forms a complete and powerful simulation tool for servo-controlled automatic machines. On the one hand, the tool offers an all-around support to the machine designer, guiding him/her through the process of selection and sizing of components. The tool is versatile, allowing the determination of a wide range of electric and mechanical parameters related to machine operation. The user can take advantage of this versatility in order to define an optimal machine set-up, thus choosing which objective function to prioritize. On the other hand, the behaviour of the system in different operating conditions can be simulated and, thus, evaluated.

Contents

Chapter 1

Introduction

1.1 Motivations, State of Art and Goals

1.1.1 Prologue

A machine can be formulated is *a system that uses energy to perform a given task*. In the general sense, machines may be traced to the beginning of human civilization: tools like pulleys or other form of lifting equipment were present in ancient times. During the Industrial Revolution, in the eighteenth and nineteenth centuries, several developments on manufacturing, transportation and agriculture were made and had a fundamental impact on human activities and social improvement. One of the main reasons for this sudden development is the availability of new forms of energy, like steam power. In fact, the general improvement made in several technology fields allowed an easy and more efficient access to raw materials. Among its numerous consequences, the energy available to operate machines switched from purely mechanical (provided by animal or directly humans) to different forms such as thermodynamic, and eventually electrical.

During the last few centuries, increasingly complex mechanisms have been developed in order to achieve manipulation or processing tasks repeatedly, such as in tailoring, milling, printing and packaging. On the other hand, the development and refinement of internal-combustion and electric motors provided reliable and consistent sources of energy, thus allowing the convenient production of mechanical energy converted from electric, thermal or chemical sources. In particular, the application of electric motors to complex mechanisms apt to execute repetitive tasks gave rise to the modern concept of *automatic machinery*.

In the first half of the twentieth century, the introduction of production lines, i.e. the decomposition of the production process in smaller and repeatable tasks, favored the development of automatic machines. The integration of electric actuation and mechanical design made a great impact on the manufacturing industry. In the second half of the century, the introduction of computers further sped up the development process. The word *mechatronics* was coined in the early seventies to refer to the new discipline at the intersection of several engineering fields, such as mechanical engineering, electronic engineering, computer science and control theory. Nowadays, in order to maximize efficiency and productivity, the design of an automatic machine must encompass the simultaneous consideration all these fields.

In recent years, electric motors and their control systems have seen an exponential

growth in development. The role of electric actuation is not only confined to being an energy source, but it required to accomplish complex tasks such as motion profile generation, which were historically realized by the mechanical transmission. In this scenario, a mechatronic perspective has a paramount importance for the optimal design of an automatic machine.

1.1.2 Context and motivations

In mechatronic applications, such as robotic or automatic machinery, the task to be executed often consists in the achievement of a certain motion profile under specific load conditions varying over time. The device responsible for executing the task is called the *end-effector*: a typical task varies from a motion execution (e.g. moving a product along an assembly line or positioning a tool) to operations on a product (e.g. machining, welding). An electrically controlled *motor*, called *servo-motor*, provides the needed power, while a mechanical transmission both transfers the energy to the end-effector and occasionally generates a suitable motion profile. The composition of these components forms a one degree-of-freedom (DoF) electro-mechanical actuator, which is referred as a *servo axis*.

In servo-controlled automatic machines, several tasks are performed simultaneously, and a significant number of servo-axes are mounted on a single machine. With the fast development of servo-motors for generating accurate motion profiles, the traditional role of the mechanical transmission as motion generator is becoming less important, even if it cannot be completely omitted in the absence of direct coupling between the motor and the end-effector. In this scenario, where the electric and mechanical part are inseparably integrated, many new challenges must be faced during the design of the automatic machine.

The main objective of this thesis is to study the design process behind the selection of components in servo controlled automatic machinery. In general, this project aims at integrating mechanical and electrical aspects during the design phase. In order to do that, a comprehensive view of the automatic machine is much needed: analyzing the behavior of the whole system, and not only of its specific parts, is of fundamental importance for embracing the different natures of the system in order to achieve an optimal design. A modular approach, which treats mechanical and electrical components separately, will lead to a feasible solution, or, even better, to a *local* optimum for that specific sub-system. However, an integrated approach may allow one to obtain a *global* optimal design otherwise missed. It is worth mentioning that, for certain *objective functions* that take into account environmental and economic reasons, like energy efficiency, even an incremental improvement can be significant. Motivated by the aforementioned discussion, a global model of the automatic machine servo axis is needed, which takes both mechanical and electric losses into account. Once the transmission is defined and the motion and load profile are known, the model must determine the torque and the electric power to be provided to the motor shaft, the requested rotational speed, the total power drawn by the system from the electric grid, and finally the operating range of the actuator.

Once the model is available, the impact of several design choices (such as the components' selection and the input motion profile) may be evaluated and, thus, the automatic machine design may be optimized in order to minimize a set of objective functions, e.g. the required motor torque, the peak values of electric power, the overall energy absorbed from the grid, etc.

In particular, the problem of servo-motor and gearbox reducer selection is considered. Given a task specification, the goal is to choose among all available possibilities the best

solution while ensuring that the task can be achieved. The process may appear trivial, since the force load and movement are fully defined. However, the introduction of a gearbox reducer on the one hand introduces an additional freedom for the optimization process, while on the other it impacts the dynamic behavior of the system, as well as changing task requirements. Conversely, the determination of anoptimal transmission ratio (e.g. one that minimizes energy consumption) cannot be carried out without taking into account the influence of motor inertia, which is unknown until the motor has been chosen. The selection procedure is thus iterative.

1.1.3 State of the Art and Goals

Given the spread of electromechanical actuators in automatic machinery and the importance of the problem, the selection of servo-motor and gearbox reducer is studied by several authors in the literature. In [1] the concept of *inertia matching* is introduced: this paper shows that the best performance on accelerating a purely inertial load (i.e. achieving the minimum time to execute a particular trajectory) is obtained when the inertia of the load reflected to motor shaft is equal to the inertia of the motor itself. This condition gives a first optimal value for the transmission ratio. Chen et al. [2] extend this result to multi-DOF systems. These outcomes, however, only serve as indications for a preliminary choice, since the selection of the motor is not involved. Van de Straete [3, 4] is the first to propose a robust procedure for motor selection: a normalization of the problem is introduced, and dimensionless parameters are used for torque and rotor speed. The simulations made for a convenient reference motor (e.g. with unitary inertia) can be extended to other motors, and a suitable transmission-ratio range is determined (i.e. the minimum and maximum values that allow the motor to drive the load). The procedure is still try-and-error, but it can be partially automatized, since motors that aren't admissible are discarded regardless of the transmission ratio. Van de Straete later [4] proposes a method to optimize a *variable* transmission ratio, but this method seems to lack a practical use. In all these works, the assumption of an ideal gearbox is made, i.e. the gearbox is assumed to have zero inertia and unit efficiency: this implies that the reducer influences the system's dynamic performance only with the variation of speed, which ends up being a reasonable approximation.

Roos et al. [5] introduce the reducer mechanical efficiency and inertia in the process: these quantities are set constant during the selection stage, and then verified. Cusimano minimizes the root-mean-square (RMS) value of the motor torque by means of diagrams for a purely inertial load [6]. Then the treatise is generalized to include a generic dynamic load [7, 8], non-rectangular dynamic range [9] and reducer efficiency on direct and inverse power flow [10]. In Legnani [11] a different approach is presented to obtain similar results: a performance index, called the *accelerating factor* or *power rate*, is defined for every commercially available motor. The index is compared with the so-called *load factor* (representing the loading conditions) to verify its feasibility. This concept is further developed in [12] and [13], where a practical graphical representation is presented.

As for the choice of objective functions, the aforementioned works are focused on a purely mechanical point of view. In particular, the RMS value of the motor torque is the most representative index for the selection of a servo-motor, since the thermal criterion of the motor admissibility requires the RMS torque being smaller than the rated torque. Minimizing the RMS torque ensures the selection of the smallest possible motor, since the size (and thus the cost) is proportional to the rated torque. Besides, a selective diagram-based procedure based on maximizing the peak torque (with some limiting constraints) is

proposed in [14, 15], but it generates less general results due to the variance of the type of constraint.

Electric quantities have also been investigated in the motor selection procedure: in [5], for instance, the power loss due to Joule effect is introduced, and the energy efficiency is used as a criterion to select a motor among several candidates after a first round of mechanical selection. In [16], since the accelerating factor's selection procedure does not allow a direct comparison between motors, a relation between such factors and electrical motor inner parameters is investigated, but the results do not seems to be consistent. In [17], an analytical expression for optimal transmission ratio is presented to increase the energetic efficiency of the motor, but only Joule resistive losses are considered. Besides, the impact of frequency bandwidth is also studied from a control point of view. In [18, 19] an electromechanical model for a one degree-of-freedom mechatronic application is presented: it features a geared DC motor, and the electric efficiency map is shown. In [19] a comparison between energy computation methods is made, which also opens a discussion on the appropriate definition of motor efficiency.

Park [20] introduces the so-called *Park's transformation* between fixed and rotating reference systems for modeling a permanent magnet synchronous motor. Based on Park's work, the *direct-quadrature axes* reference system (*dq model*) is commonly utilized to model synchronous rotating machines, such as in [21] or more recently in [22]. The study of core losses, resistive losses and saturation is carried on further by means of the equivalent-circuit method [23, 24, 25].

The ultimate goal of our work is to develop a reliable tool which supports the optimal selection of a mechatronic actuator. In order to select the *best* solution with respect to a set of suitable objective functions, we take into account both electric and mechanical quantities. The first step is to define a comprehensive and easily characterizable electromechanical model: only rated data available in catalogs are used, and no experimental characterization of the servo-motor is needed. This allows us to characterize a permanent magnet synchronous motor, regardless of its type and manufacturer. Once this is done, the selectable motor database ideally coincides with the whole list of commercially available motors. Then, the implementation of the electrical model in the optimization process allows us to obtain the optimal transmission ratio to achieve the best motor efficiency in the most general case, including core losses along resistive losses.

Up to this point, the selection procedure it requires the evaluation of a *discrete* set of candidate motors. For each of them, the optimization is carried on and the optimal gearbox reducer is found. An admissibility verification must be made to take into account the non-ideal reducer characteristics. In order to avoid these iterative steps, we present a method to extend the discrete commercially available motor catalog to a *continuous* catalog obtained by fitting manufacturers data. Then, the optimization is carried out in its most general case for every component (efficiencies, inertias, electric losses). Finally, a nonlinear optimization problem with inequality constraints is solved in order to find the best admissible motor-reducer pair.

1.1.4 Outline

Section 2.1 presents the general architecture of a servo-controlled automatic machine. A parallel-axes architecture is considered: each servo-axis is connected to a DC bus that provides the electric energy, exchanging it with the grid. A generic servo axis is a one degree-of-

freedom electromechanical actuator, which comprises a synchronous brushless servo motor, a mechanical transmission and an end-effector. An electric drive (i.e. an inverter) is responsible of the servo-motor control. Due to the parallel architecture, there is no interaction between servo axes, i.e. the behavior of a specific servo-axis is not influenced by the others.

Chapter 2 presents the mechanical model of a 1-DOF servo- axis. A *lumped-parameter model* is introduced. The transmission chain, mechanically connecting the motor with the end effector, is represented as a sequential block diagram. Each block is modeled as a single-input-single-output (SISO) subsystem: at the input node, it receives motion and torque from the previous block and transfers them to the next one. The relation between input and output quantities is determined by a multi input-multi-output (MIMO) *transfer function* defined for each block. The transfer functions take into account both kinematic and dynamic properties. A procedure to define a block model representing a generic mechanism, with the support of a CAD model, is introduced. The generic mechanism creation tool, together with a set of predefined models of linkages of common usage (four-bar, crank-lever, etc.), defines a ready-to-use mechanisms library. The ideal equation of motion is found by means of Lagrange equations. Then, mechanical losses are taken into account by means of an efficiency function, which considers both direct motion, when the power flows from the motor to the end-effector, and inverse motion, when the power flows towards the motor. By equating motion and torque at the nodes, the global equation of motion is determined. Both *inverse* and *forward* dynamics are solved. The main focus is on inverse kinematics, since once the transmission is known (geometry, inertias, etc.) and the end-effector motion and load are given, the motor operating conditions (rotating speed, torque) are determined.

Chapter 3 presents the electric model of the servo axis, comprising a *permanent magnets synchronous motor* (PMSM) and *voltage source inverter* (VSI). The electric model proposed here is reliable and simply implementable, since no experimental measures are required and all parameters can be determined by the nominal data available on motor and inverter catalogs. The model is developed in two steps: the first step aims at defining a novel general torque-current relation, while in the second step the electric energy losses are evaluated in order to determine the global efficiency. As for the torque-current relation, a quadratic curve is proposed, and the least square fitting method is used in order to find a curve that fits the reference torque-current points provided by the catalog. A comparison with an experimental model is made to ensure that the new curve represents the motor in a better way than the standard linear curve proposed by the manufacturer. As for energy evaluation, three main losses sources are introduced: *winding losses* due to Joule effect, *iron losses* (divided into *Eddy current losses* and *hysteresis losses*) and *switching losses*. While windings losses are proportional to the square current, iron losses are assumed to be a function of the motor rotational speed. Switching losses are prevalently present in the inverter drive, and they are proportional to switching frequency and current. A novel procedure to infer losses coefficients is presented, and, as for the torque-current relation, the input data are entirely gathered from commercial catalogs. A case study comparison with an experimental model is made, and the efficiency motor map is defined over the motor operating range as a function of torque and rotational speed. Eventually, the model allows us to evaluate the total electric power absorbed by the servo axis when operation task is given.

Chapter 4 investigates the problem of optimal selection of motor and gearbox reducer. A discrete approach is utilized, and the procedure is divided into two phases: the feasibility phase and the optimization phase. While evaluating feasibility, each motor is studied assuming an ideal transmission (zero inertia and unit efficiency). Since the main parameters of each motor (such as the rotor inertia) are known, the range of admissible transmission

ratios is found by imposing motor constraints on the operative range (thermal problem, maximum instantaneous torque and speed), and the motors that cannot drive the load regardless of the transmission ratio are discarded. The optimization phase aims at minimizing a set of objective functions, such as the RMS torque and the total energy consumption. In particular, the analytic expression of the transmission ratio optimal value that minimizes the energy absorbed by the motor is found in its most general form, implementing both the loss model (iron and winding losses) and the quadratic torque-current relation. As for the instantaneous peak torque, a procedure is presented to determine the pattern of local stationary points, regardless of load profile, and to find the optimal transmission ratio that guarantees the lowest torque peak.

In Chapter 5, the discrete motor catalog is extended to a continuous domain. In order to do that, a *size index* is defined over the motor catalog, ranging from zero (smallest motor in terms of rated torque) to one (largest motor). Every real value of the size index represents a possible selection, while the actual motor population is a discrete subset of the continuous domain. Every motor parameter, both electrical and mechanical (such as motor inertia, stator resistance, etc.) is extended as a continuous function of the size index by means of spline interpolation or polynomial fitting.The approach is used for loss coefficients. The feasibility and optimization are studied simultaneously without iterations, in the general case of a real transmission (inertia an efficiency are taken into account at the outest). The optimization problem becomes a 2-dimensional nonlinear programming problem, which is solved by means of the imposition of *Karush-Khun-Tucker conditions*, i.e. the conditions under which a point is the solution of a minimization problem under non-linear constraints. The optimal pair, namely size index and transmission ratio that minimize the energy drawn by the motor is found, and several consideration are made on the comparison with the discrete approach case. In the last part of the chapter, the process is extended to include inverter losses.

Chapter 6 presents the results of this work, and gives some guidelines for further improvement. A stand-alone application was created using the MATLAB *Graphical User Interface* (GUI) [26]. The key features are described in Appendix A. The software allows the user to compose the mechanical transmission by selecting predefined blocks representing basic mechanisms (four-bar, crank-lever, crank and slotted lever mechanism, Geneva wheel, gears and belt drives) or by generating the custom block of a generic mechanism. The software solves forward and inverse dynamics, and evaluates kinematic and dynamic quantities at each nodes. Electric losses and global efficiecny are evaluated. Finally, the optimization procedures presented in Chapters 4 and 5 are applied, and the optimal motor-reducer combination is recommended.

Chapter 2

Mechanical Model

In this chapter, we present a lumped-parameter mechanical model for a single *servo-axis* of a servo-controlled automatic machine. The servo-axis chain of mechanically connected components from the motor to end-effector. Section 2.1 introduces the standard architecture of a modern servo-controlled automatic machine. Sections 2.3 and 2.4 present the mechanical model of the lumped-parameter single block and of the entire transmission. Section 2.5 offers some guidelines to model a real mechanism. Finally, Section 2.6 reports the equations that defining the model of some standard mechanism.

2.1 Servo-controlled automatic machine architecture

2.1.1 Machine architecture

In servo-controlled automatic machines by several end-effectors are present in a single machine. The majority of tasks usually consists in positioning problems: the product is positioned in sequential stations, and in each one of them an operation is performed (machining, bending, welding, etc.). This process is repeated for each machine cycle. Each end-effector must follow a fixed trajectory with a specific motion profile. The trajectory, be it planar or spatial, can be parametrized as a periodic 1-DoF motion. The way by which this motion is achieved varied significantly through the years, following the development of electronic control.

The traditional architecture of automatic machines includes a single main motor driving a series of 1-DoF mechanical transmission systems, which move the end-effectors of the machine (see Fig. 2.1). The role of the motor is to provide the power requested to move the entire machine. Each branch exchanges power with the main motor in both directions, and the total power absorbed by the machine is the algebraic sum of these power flow. Typically, an asynchronous 3-phase electric motor is used, which is characterized by small variations of its rotational speed. The mechanical transmission has two main purposes: first, it is in charge of generating the motion profile for each end-effector; second, it transfers the power from the motor to the end-effector. The rigid coupling grants a rigorous constant phase between end-effectors.

This architecture has the advantage of simplicity, but it is *rigid*, as it does not allow for modification of motion laws of the end-effectors, unless the transmission is re-designed.

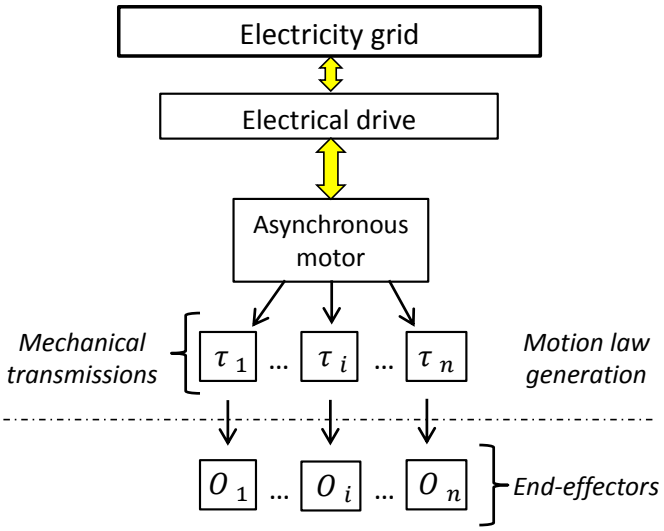

(a)

Figure 2.1: Standard automatic machine architecture.

Moreover, in order to obtain complex motion profile, the transmission is often composed by a great number of members. This introduces undesired clearances and member elasticities, which eventually lead to a lower accuracy.

More recently, this architecture was superseded by a more flexible one (see Fig. 2.2), due to the development of servo-controlled motor, able to generate accurate motion laws. In this new-generation architecture, each end-effector is actuated by a dedicated drive-motor group. In this way, it is possible to change the motion law for each end-effector independently by acting on the drive, with no need to reconfigure the mechanical transmission. Thus, this architecture allows product format changes to be accommodated more easily and is therefore more flexible.

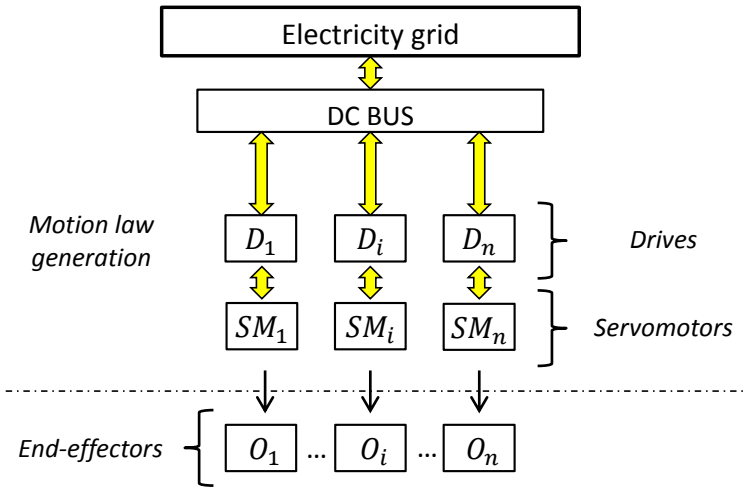

Figure 2.2: New generation servo-controlled automatic machine architecture.

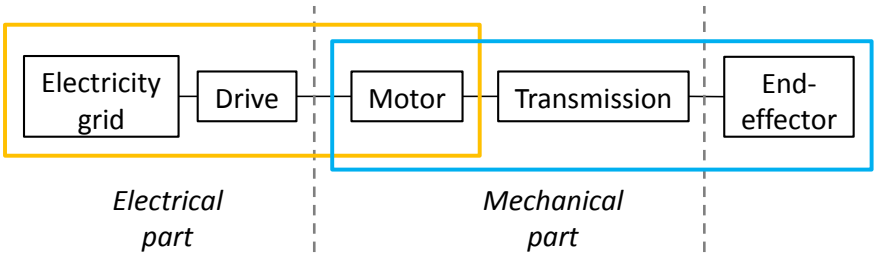

Figure 2.3: Model of one axis.

2.1.2 The mechanical transmission

In electronic control automatic machines, the drive generates the motion profile the motor must achieve. This implies that, for instance, the use of linkages is not mandatory anymore in order to obtain alternate motion, such as index mechanisms. Furthermore, the presence of several (thus smaller) servomotors allows more freedom in motor placement and mounting. This reduces the need of transferring power from a central engine to every machine branch. If the servomotor can be mounted in proximity of end-effector operating zone, the mechanical transmission may be reduced or even omitted.

All this being said, the mechanical transmission is still a key component in automatic machines. In fact, the electric motor can only provide rotational (in some cases, translational): if a different trajectory path is needed, closed-chain mechanisms can be used to generate a planar (or even spatial) 1-DoF motion on desired path. It is not uncommon to see a linear movement actuated by a rotational motor and mechanical transmission, rather than by a linear electric motor. Furthermore, because of space constraints, the motor cannot be placed everywhere at will, as high-dynamic automatic machines have a strict product line architecture in order to allow efficient product movement. The processes constraints must be taken into account as well, as in certain operations the product atmosphere must be kept clean (e.g. food production, pharmaceutic), electromagnetic field are not allowed near the end-effector, or the environment is not suitable for an electric machine (e.g. under water, explosive areas). Even in the generation of the motion profile, the mechanical transmission can contribute to the task, as the mechanical advantage [27] can be used the help the motor to sustain the load. For the aforementioned reasons, the nature of the transmission varies with machine architectures, typologies, processes and design choices.

2.1.3 Modeling assumptions

Ultimately, any multi-axis automatic machine, no matter how complex its structure is, may be somewhat reduced to a system of one-degrees-of-freedom (1-DoF) servo-axes acting in parallel and non-interactively. Each axis works independently: the axes' movements are phased, but since every motion has 1-DoF, their dynamic behaviors are not mutually influenced. It may happen that an external load is shared between two or more end-effectors. In that case, however, the load can be split between the affected axes by considering the geometry of the problem. To fully model the electrical and mechanical operation of the whole machine, it is therefore sufficient to obtain a complete, generic model of one of the servo-axes, as shown in Fig. 2.3, where both the electrical and mechanical part are represented. This Chapter focuses on the mechanical part, whereas the electric part is treated in Chapter

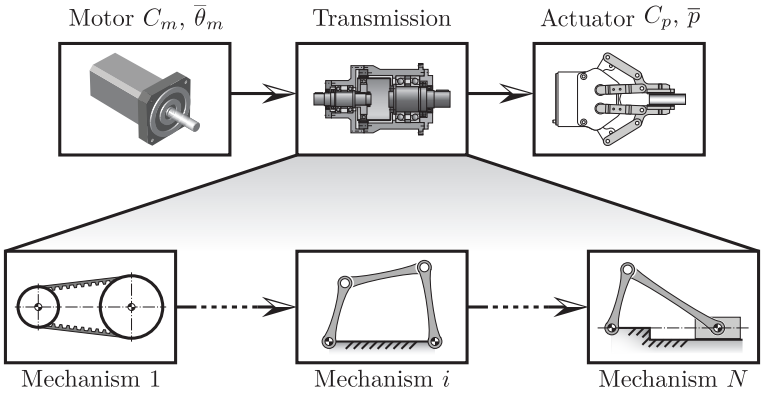

Figure 2.4: Servo-axis model: the transmission is composed of serial 1-DOF mechanisms

3. The mechanical part comprises three interacting components: the ***motor*** (providing mechanical power), the ***end-effector*** (achieving the desired task) and the ***transmission*** in between.

2.2 Components

The ***end-effector*** is responsible for performing motion and/or force operations on the load that are required by the production task. The *displacement* parameter of a generic end-effector will be denoted by p, which may represent the output angle of a revolving end-effector, the position of a translational end-effector, or even a suitably chosen parameter for the coupler curve of a 1-DoF linkage. Consequently, when parametrizing p over time, the derivatives $\dot{p} \triangleq dp/dt$ and $\ddot{p} \triangleq d^2p/dt^2$ may correspond, respectively, to speed and acceleration of an angular, linear or curvilinear variables. For our purpose, it suffices to consider $\overline{p}(t) \triangleq (p, \dot{p}, \ddot{p})^T \in \mathbb{R}^3$ for representing the *kinematic state* of the end-effector.

Usually, during the automatic machine design phase, $\overline{p}(t)$ may either be subject to kinematic constraints or be fully determined according to the production process requirement. Besides, the end-effector may be required to not only achieve displacement tasks, but also counteract external disturbances introduced by other end-effectors. Such situation may arise, for example, when the end-effector has to position a load while another operation is being performed on it, or when the end-effector is to perform a manufacturing process that induces disturbance forces on the servo. The external load C_p may depend either solely on time or also on end-effector state. For instance, friction effect is usually modeled as being proportional to $\dot{p}$ [28, Ch. 37], while a the aerodynamic force on a rotating fan is approximately proportional to square velocity [29]. Therefore, we shall consider C_p as a function of time and state, i.e. $C_p = C_p(\overline{p}, t)$.

As it is mentioned in Sec. 2.1, the ***transmission*** architecture may vary widely due to machine-specific design of the servo-axis. To take this variety into account, we model the transmission system by means of a cascade of N 1-DoF mechanisms (see Fig. 2.4). As shown in Fig. 2.4, the motor, the transmission, and the end-effector are represented by blocks connected by arrows to highlight the structural decomposition of the transmission.

Finally, the ***motor*** converts the electric power received from the drive into mechanical power. We shall denote by $\dot{\theta}_m$ the motor rotational speed, and by C_m the torque generated at the motor shaft. We shall also, for consistency, use $\overline{\theta}_m(t) \triangleq (\theta_m, \dot{\theta}_m, \ddot{\theta}_m)^T \in \mathbb{R}^3$ to

denote the motor kinematic state. The mechanical power of the motor is thus given by $P_m = C_m \cdot \dot{\theta}_m$. The total power required for the servo-axis is given by the sum of two major contributions: the external power $P_p = C_p \cdot \dot{p}$ and the inertial power generated by bodily inertial forces. The inertial power dominates the external power in high speed applications such as packaging, whereas it is dominated by the external power in high external force applications, such as metal forming. Besides, the mechanical transmission efficiency has to be taken into account.

2.3 Lumped-parameter model

2.3.1 Evaluation of Equivalent Inertia

Even the simplest 1-DoF mechanism such as a linkage may comprise multiple bodies, with each one contributing to a fraction of the total kinetic energy of the mechanism. The general expression for the kinetic energy of a body moving in a plane is given by:

$$T_b = \frac{1}{2} J_G \omega_G^2 + \frac{1}{2} m \, \overline{v}_G^2 = \frac{1}{2} J_G \omega^2 + \frac{1}{2} m \left(v_{Gx}^2 + v_{Gy}^2 \right) \tag{2.1}$$

where G denotes the center of mass of the body, J_G the mass moment of inertia with respect to the axis passing through G and perpendicular to the motion plane, ω_G the angular velocity of the body, and $\overline{v}_G$ the vector representing the velocity of the center of mass. After defining a planar reference system, $\overline{v}_G$ may be represented by its two scalar components along the **x** and **y** axes, i.e. v_{Gx} and v_{Gy}.

In reference to Eq. (2.1), the kinetic energy of a body in planar motion may be conveniently decomposed into up to three components: one for rotation and two for translation. The total kinetic energy of the system (in this case a 1-DoF mechanism) is then the sum of the components of all bodies in the system. Let T_j be the kinetic energy contributed by the jth component. T_j is proportional to the square of a scalar velocity v_j (rotational or translational) and to the inertia parameter J_j (the mass moment of inertia or the mass). Let q denote the generalized coordinate of the 1-DoF mechanism. The generic velocity v_j is related to $\dot{q}$ by the *transmission ratio* τ_j:

$$\tau_j = \frac{v_j}{\dot{q}} \tag{2.2}$$

where $\tau_j = \tau_j(q)$ depends only on the configuration q of the mechanism. By summing up all components T_j's while replacing v_j with $\tau_j \dot{q}$, we have the following expression for the total kinetic energy T of the mechanism:

$$T = \frac{1}{2} \sum_j J_j \left(\tau_j \dot{q} \right)^2 = \frac{1}{2} \underbrace{\left(\sum_j J_j \tau_j^2 \right)}_{J} \dot{q}^2 = \frac{1}{2} J \, \dot{q}^2 \tag{2.3}$$

J is referred to as the *reduced* or *reflected moment of inertia*. We emphasize that $J = J(q) = \sum_j J_j \tau_j(q)^2$ is generally a function of the mechanism configuration q.

2.3.2 Analysis of a generic transmission block

We model the transmission chain of each servo-axis as a serial chain of blocks without considering parallel interactions between servo-axes. We may conveniently associate each

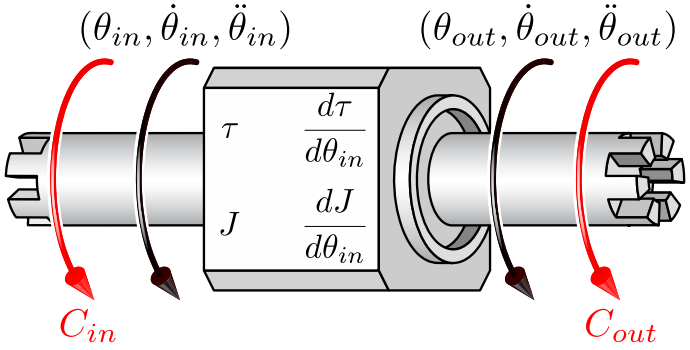

Figure 2.5: Kinematic and force variables associated to the input and output ports of a transmission block.

mechanism in a transmission chain, as shown in Fig. 2.4, with a single-input-single-output (SISO) block, so that we may represent the entire transmission chain as a sequential block diagram: each block takes the motion and force output of its predecessor as its input, and in turn generates an output for the succeeding block. This defines, for each block, a *transfer function* parameterized by the configuration q of the block. The type of input and output of the blocks are determined by the type of their corresponding mechanisms.

The block model is graphically presented in Fig. 2.5. The motion and force variables sampled at the input (motor side) and output (end-effector side) ports of the block are denoted by subscripts *in* and *out* respectively. Thus $\overline{\theta}_{in}$ and $\overline{\theta}_{out}$ denote, respectively, the input and output state vectors comprising displacement, velocity and acceleration, and C_{in} and C_{out} are the external forces/torques acting at the input and output port, respectively. Such a notation must not be confused with input-output relation in the physical sense. In practice, the mechanical power in a servo-axis may flow from the motor to the end-effector, or back from the end-effector to the motor. For example, it often occurs in inertial load applications that the power flow is reversed one or more times during a single cycle. When studying the behavior of a 1-DoF mechanism as a generic block, we shall always take θ_{in} to be the generalized coordinate that characterizes its motion. Further details will be given in Sec. 2.5.

The determination of input/output ports in a mechanism depends on its intended function. For instance, consider a crank-rocker four-bar linkage where the crank rotation (*in*) is transferred to that of the rocker link (*out*). Both ports are characterized by a rotation and θ_{in} and θ_{out} are measured in radians, and C_{in}, C_{out} are measured in [Nm] (torque). Depending on the application, the crank rotation (*in*) may also be used to move a point attached to the coupler link (*out*). In this case, while θ_{in} is still measured in radians, displacement θ_{out} is measured in meters and C_{out} in [N] (pure force).

2.3.3 Kinematic properties

Let τ be the transmission ratio of the block, defined as the ratio between output speed $\dot{\theta}_{out}$ and the input speed $\dot{\theta}_{in}$.

$$\tau = \frac{\dot{\theta}_{out}}{\dot{\theta}_{in}} = \frac{d\theta_{out}}{d\theta_{in}} \tag{2.4}$$

τ is in general a function of the generalized coordinate θ_{in}. The dimensions of τ depends on the mechanism type. For rotation-to-rotation or translation-to-translation mechanisms,

τ is dimensionless. For rotation-to-translation or translation-to-rotation mechanisms, τ is measured in meters [m] or [1/m] respectively. In order to determine the relation between input and output accelerations, we take the time derivative of Eq. (2.4):

$$\ddot{\theta}_{out} = \frac{d}{dt}\left(\tau\dot{\theta}_{in}\right) = \tau\ddot{\theta}_{in} + \frac{d\tau}{d\theta_{in}}\frac{d\theta_{in}}{dt}\dot{\theta}_{in} = \tau\ddot{\theta}_{in} + \frac{d\tau}{d\theta_{in}}\dot{\theta}_{in}^2 = \tau\ddot{\theta}_{in} + \tau'\dot{\theta}_{in}^2 \tag{2.5}$$

where τ' denotes the derivative of τ with respect to θ_{in}. By integrating Eq. (2.4) with respect to θ_{in} over the time interval $[t_0, t_1]$, the expression of θ_{out} as a function of θ_{in} is given by:

$$\begin{aligned}\theta_{out}(t_1) &= \theta_{out}(t_0) + \int_{\theta_{in}(t_0)}^{\theta_{in}(t_1)} \tau(\theta_{in})\, d\theta_{in} \\ &= \theta_{out}(t_0) + \int_{t_0}^{t_1} \tau(\theta_{in}(t)) \cdot \dot{\theta}_{in}\, dt\end{aligned} \tag{2.6}$$

where $\theta_{out}(t_0)$ is the preassigned initial condition.

2.3.4 Equation of motion

The equation of motion of a single block is derived by using Lagrange equation. If the contribution of conservative forces is emphasized, the potential energy V of the block can be evaluated as a function of θ_{in} only, and V' is its derivative with respect to θ_{in}. Since the block has 1-DoF, we have one Lagrange equation depending on generalized coordinate q:

$$\frac{d}{dt}\left(\frac{\partial T}{\partial \dot{q}}\right) - \frac{\partial T}{\partial q} + \frac{\partial V}{\partial q} = Q \tag{2.7}$$

where T is given by Eq. (2.3). The generalized force Q associated with q is found by equating the virtual work done by Q over the virtual displacement δq of q with the virtual work done by external forces C_j's over their corresponding virtual displacements $\delta\theta_j$'s:

$$\delta W = Q\delta q = \sum_{j=1}^{n} C_j \delta\theta_j \qquad \Rightarrow \qquad Q = \sum_{j=1}^{n} C_j \frac{\partial\theta_j}{\partial q} \tag{2.8}$$

In the examined case, where $q = \theta_{in}$, the generalized force is:

$$Q = \sum_{j=1}^{n} C_j \frac{\partial\theta_j}{\partial q} = C_{in} + C_{out}\frac{\partial\theta_{out}}{\partial\theta_{in}} = C_{in} + \tau C_{out} \tag{2.9}$$

The first two terms of Eq. (2.7) may be differentiated as follows:

$$\begin{cases} \dfrac{d}{dt}\left(\dfrac{\partial T}{\partial \dot{\theta}_{in}}\right) = \dfrac{d}{dt}\left(J\dot{\theta}_{in}\right) = J\ddot{\theta}_{in} + \dfrac{\partial J}{\partial\theta_{in}}\dfrac{d\theta_{in}}{dt}\dot{\theta}_{in} = J\ddot{\theta}_{in} + J'\dot{\theta}_{in}^2 \\ \dfrac{\partial T}{\partial\theta_{in}} = \dfrac{1}{2}J'\dot{\theta}_{in}^2 \end{cases} \tag{2.10}$$

where J' denotes the derivative of J with respect to θ_{in}. Substitute Eq. (2.10) into Eq. (2.7) and we have:

$$J\ddot{\theta}_{in} + \frac{1}{2}J'\dot{\theta}_{in}^2 + V' = C_{in} + \tau C_{out} \tag{2.11}$$

Equation (2.11) is used to determine the relation between C_{in} and C_{out}.

2.3.5 Efficiency

So far, we have not considered energy loss in the equation of motion. Since our servo-axis model is defined by means of lumped parameters, we shall correspondingly define a *lumped efficiency* η to account for energy losses from the system. However, several considerations must be taken into account for this seemingly trivial task.

First of all, the efficiency of a system can usually be uniquely defined as the ratio of the energy generated at the output versus the energy entering the system. However, such a definition may lead to ambiguities when considering a complex mechanism. Besides, there are multiple sources of energy loss in a transmission system. For example, the relative motion between two bodies connected by a mechanical joint will inevitably induce friction loss. For a linkage with multiple joints, the functional dependence of the efficiency η on the linkage kinematic state might be difficult to determine analytically. The fact that η is in general a non-linear function of the linkage state makes experimental measurement equally difficult.

We propose a method to derive a simple efficiency model from the basic definition of efficiency, as follows. We denote by W_{in}, W_{out} and W_{loss} the energy, respectively, introduced into the system, the output work and the energy loss over an infinitesimal time interval Δt. By introducing the contribution of the variation of potential and kinetic energies, we have following energy balance equation:

$$W_{in} + W_{out} + W_{loss} = \Delta T + \Delta V \tag{2.12}$$

where a positive variation indicates the amount of energy entering the system, and a negative one indicates the amount leaving the system. Thus a resistant load implies $W_{out} < 0$. Even if some kind of energy is introduced in the system (e.g. $W_{in} > 0$) it does not necessarily mean that the energy is available at the output (i.e. $W_{out} < 0$), since it may happen that the energy entering the system is used to increase kinetic energy (e.g., accelerating the end-effector) or potential energy (e.g. elevating the end-effector). We also define the *required energy*:

$$W_{req} = \Delta T + \Delta V - W_{out} \tag{2.13}$$

When $W_{req} > 0$, the energy flows from the motor to the load (i.e., from *in* to *out*), leading to a *direct motion* of the servo-axis. When $W_{req} < 0$, the system is generating energy and the power flows from load to motor, resulting in *inverse motion*.

Efficiency model: case one

The instantaneous efficiency may be evaluated by dividing both sides of Eq. (2.12) by Δt and taking the limit $\Delta t \to 0$:

$$\frac{dW_{in}}{dt} + \frac{dW_{out}}{dt} + \frac{dW_{loss}}{dt} = \frac{dT}{dt} + \frac{dV}{dt} \tag{2.14}$$

In direct motion, dW_{in}/dt is positive and dW_{loss}/dt is a negative quantity. The correspondent required power is:

$$\frac{dW_{req}}{dt} = \frac{dT}{dt} + \frac{dV}{dt} - \frac{dW_{out}}{dt} \tag{2.15}$$

We define the *direct efficiency* η_{dir} to be the ratio of dW_{req} versus dW_{in}:

$$\eta_{dir} = \frac{dW_{req}}{dW_{in}} = \frac{\dfrac{dW_{req}}{dt}}{\dfrac{dW_{in}}{dt}} \qquad \Rightarrow \qquad \frac{dW_{in}}{dt} = \frac{1}{\eta_{dir}} \frac{dW_{req}}{dt} \tag{2.16}$$

Applying this definition to the transmission block model, and evaluating and substituting the following quantities

$$\begin{aligned} \frac{dW_{in}}{dt} &= C_{in}\dot{\theta}_{in} & \frac{dV}{dt} &= V'\dot{\theta}_{in} \\ \frac{dW_{out}}{dt} &= C_{out}\tau\dot{\theta}_{in} & \frac{dT}{dt} &= \left(J\ddot{\theta}_{in} - \frac{1}{2}J'\dot{\theta}_{in}^2\right)\dot{\theta}_{in} \end{aligned} \tag{2.17}$$

into Eq. (2.16), finally gives the relation between input and output actions for direct motion:

$$C_{in} = \frac{1}{\eta_{dir}}\left[J\ddot{\theta}_{in} + \frac{1}{2}J'\dot{\theta}_{in}^2 + V' - C_{out}\tau\right] \tag{2.18}$$

In inverse motion (i.e., power is flowing from the load to the motor), the system is giving back energy. Therefore, both dW_{req}/dt and dW_{in}/dt are negative quantities, while $dW_{loss}\,dt$ remains positive for reducing the energy recovered by the motor. In this case the following absolute value expression is more informative:

$$\left|\frac{dW_{in}}{dt}\right| - \left|\frac{dW_{loss}}{dt}\right| = \left|\frac{dW_{req}}{dt}\right| \tag{2.19}$$

and the efficiency is the ratio of power recovered from the electrical machine as a generator versus the power given back by the system.

$$\eta_{inv} = \frac{\dfrac{dW_{in}}{dt}}{\dfrac{dW_{req}}{dt}} \qquad \Rightarrow \qquad \frac{dW_{in}}{dt} = \eta_{inv}\frac{dW_{req}}{dt} \tag{2.20}$$

Equation (2.20) leads to:

$$C_{in} = \eta_{inv}\left[J\ddot{\theta}_{in} + \frac{1}{2}J'\dot{\theta}_{in}^2 + V' - C_{out}\tau\right] \tag{2.21}$$

Finally, Eqs. (2.21) and (2.18) may be written as:

$$C_{in} = \frac{1}{\hat{\eta}}\left[J\ddot{\theta}_{in} + \frac{1}{2}J'\dot{\theta}_{in}^2 + V' - C_{out}\tau\right] \tag{2.22}$$

where $\hat{\eta}$ is defined as:

$$\hat{\eta} = \begin{cases} \eta_{dir} & W_{req} > 0 \\ \dfrac{1}{\eta_{inv}} & W_{req} < 0 \end{cases} \tag{2.23}$$

The above efficiency model is notably nonlinear, and may overestimate energy losses: all the energy contributes are reduced by the lumped efficiency.

Efficiency model: case two

An alternative efficiency model can be derived making further considerations on the periodicity of motion profile. The evaluation of instantaneous efficiency can be troublesome due to the fact that in general the behavior of friction loss varies with the operating condition of the machine, and also since instantaneous measurements are difficult to take. Besides, it is preferable to evaluate energy exchanges over a period of time, in particular when motion conditions are regularly repetitive. If there is a time interval after which the mechanism returns to the same kinematic state, the time interval will be naturally referred to as a *period* and the mechanism is said to be in a *periodic duty*. Under the premise of automatic machines, such periodic condition is ubiquitous. At every stage of production, operations on products are repeated several times per second. In order to achieve final product homogeneity, motion and force repeatability is a mandatory requirement. The *cycle time* t_c is usually specified by the application for each servo-axis in an automatic machine, and may differ from axis to axis. In particular, end-effectors working on the same operation share the same period time t_c.

If the work efficiency is evaluated for every period, the finite variations of kinetic and potential energy are zero, that is, the right hand side of Eq. (2.12) is equal to zero. Under these circumstances, the output power is equal in magnitude to the required power $W_{req} = -W_{out}$, since no energy is stored at the end of the cycle. In both direct and inverse motion, W_{in} and W_{out}, should be equal and opposite, with the difference being W_{loss}. Consequently, the direct and inverse efficiencies are defined as:

$$\eta_{dir} = \frac{|W_{out}|}{|W_{in}|}, \qquad \eta_{inv} = \frac{|W_{in}|}{|W_{out}|} \tag{2.24}$$

and for every period:

$$C_{in} = -\frac{\tau}{\hat{\eta}} C_{out} \tag{2.25}$$

By summing the torque contributions due to energy variation, we define an alternative efficiency model ($\hat{\eta}$ is the same as in Eq. (2.23)):

$$C_{in} = J\ddot{\theta}_{in} + \frac{1}{2}J'\dot{\theta}_{in}^2 + V' - \frac{\tau}{\hat{\eta}} C_{out} \tag{2.26}$$

In comparison to Eq. (2.22), the efficiency loss in Eq. (2.26) are underestimated, since the efficiency does not affect inertia terms of the same block, that is, the inertias are assumed to move at velocity $\dot{\theta}_{in}$. In Sec. 2.5, we shall make several considerations on modeling efficiency for particular mechanisms.

2.4 Servo-axis global model

In the previous section, we have presented the lumped parameter block model as the component of an individual transmission chain. Equations (2.4), (2.5), (2.6) and(2.11) together prescribe the relation between respectively input and output kinematic quantities and input and output torques (forces). In this section, we shall present the complete motor-to-load block scheme composed from concatenation of all transmission blocks in the servo-axis.

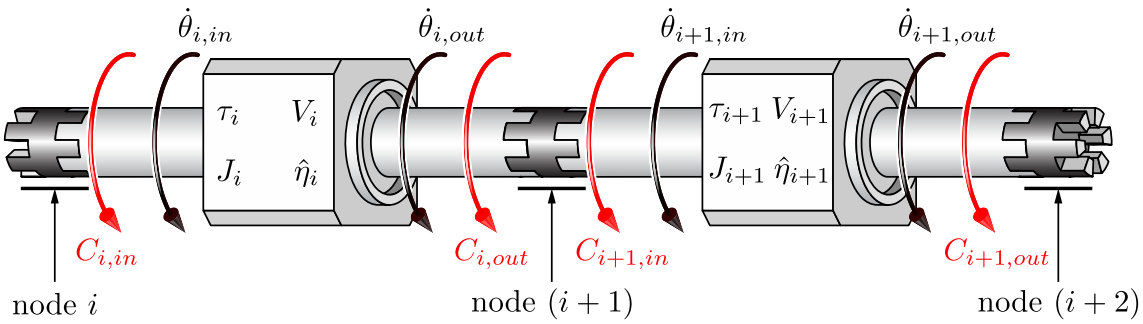

Figure 2.6: Assembling two neighboring blocks.

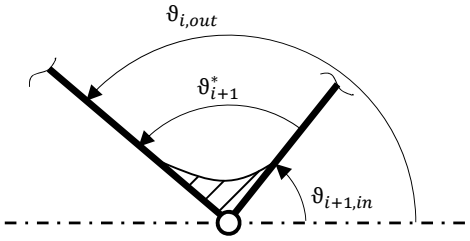

Figure 2.7: Mechanical phase angle between block i and $i+1$

2.4.1 Node compatibility equations

Let N be the number of blocks in the transmission under consideration. Considering two neighboring blocks, the i-th and the $(i+1)$-th, as shown in Fig. 2.6. For each block, the reduced inertia J_i, the transmission ratio τ_i and the potential energy V_i are defined as functions of the block generalized coordinate θ_{in}. For variables having two subscripts, the first subscript indicates the block which the variable is associated to, and the second indicates the port of the variable. Imposing compatibility equations at the $(i+1)$-th node connecting block i and $i+1$ gives:

$$\begin{cases} C_{i,out} = -C_{i+1,in} & \text{(2.27a)} \\ \dot{\theta}_{i,out} = \dot{\theta}_{i+1,in} & \text{(2.27b)} \\ \ddot{\theta}_{i,out} = \ddot{\theta}_{i+1,in} & \text{(2.27c)} \\ \theta_{i,out} = \theta_{i+1,in} + \theta^*_{i+1} & \text{(2.27d)} \end{cases}$$

In Eq. (2.27d), θ^*_{i+1} is the *mechanical phase* of block $i+1$, defined as the difference $\theta^*_{i+1} = \theta_{i,out} - \theta_{i+1,in}$. It is a constant and depends on how the block mechanism are mechanically connected to each other. For instance, at a node committing rotation transmission, the final member of block i and the first member of block $(i+1)$ are attached to the same shaft, that is, they have the same rotational speed. The rotation angles of two members can be measured with respect to the same reference direction (the horizontal direction in Fig. 2.7) only if the angle phase between the two members is taken into account. At a translation node, θ^*_{i+1} prescribes the distance between the two reference systems with respect to which the block translations are expressed with respect to.

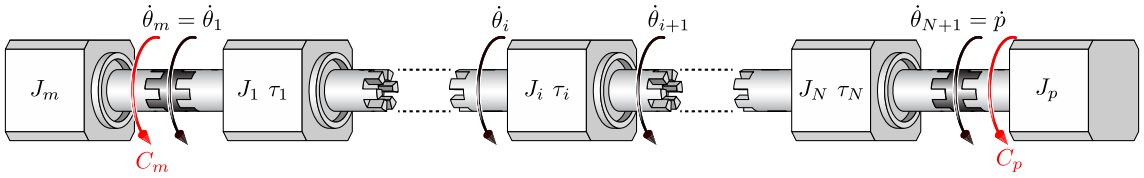

Figure 2.8: Full serial transmission model for a servo-axis with N blocks.

2.4.2 Global transmission chain

When assembling a serial chain of N blocks, we may simply repeat the process discussed in Sec. 2.4.1 with an increasing index i. For the sake of clarity, the input variables of block i are chosen to represent the node behavior (see Eq. (2.27)), and the subscript in will be dropped. The complete model and notations for a N-block servo-axis is presented in Fig. 2.8. At the beginning of the chain or node 1, the motor is modeled as a pure inertia and its velocity serves as the input of the first block, which leads to $\dot{\theta}_m = \dot{\theta}_1$. Similarly, at the output node of block N, or node $N+1$, the inertia of the load/end-effector J_p moves at velocity $\dot{p}$. For consistency, the output velocity of block N is denoted by $\dot{\theta}_{N+1}$ and is equal to $\dot{p}$.

2.4.3 Kinematic Analysis

We first recall Eqs. (2.4), (2.5) and (2.6) from Sec. 2.3. Once the transmission ratio $\tau_i(\theta_i)$ and its derivative $\tau_i'(\theta_i)$ with respect to θ_i are determined for each block, the relation between the states $\overline{\theta}_i$ and $\overline{\theta}_{i+1}$ is given by:

$$\begin{cases} \theta_{i+1} = f_i(\theta_i) \\ \dot{\theta}_{i+1} = \tau_i \, \dot{\theta}_i \\ \ddot{\theta}_{i+1} = \tau_i \ddot{\theta}_i + \tau_i' \dot{\theta}_i^2 \end{cases} \tag{2.28}$$

where f_i is the (block) forward kinematics map derived from position analysis, with $df_i/d\theta_i = \tau(\theta_i)$. When solving inverse kinematics, the end-effector vector state $\overline{p}$ is assumed to be a known quantity, and Eq. (2.28) is applied recursively N to 1. The solution of each step gives $\overline{\theta}_i$, until eventually the motor state vector $\overline{\theta}_m$ is found. When solving the forward kinematics, $\overline{\theta}_m$ is assumed to be known, and we perform a forward recursion with Eq. (2.28) until $\overline{p}$ is found.

2.4.4 Global Equation Of Motion

Equation (2.11) prescribes the ideal relation between torques (or forces). Equations (2.22) and (2.26) also take into consideration efficiency, and either the former or the latter can be implemented. Using Eq. (2.26), the equation that relates input force at node i to input force at node $i+1$ is obtained via Eq. (2.27):

$$C_i = J_i \ddot{\theta}_i + \frac{1}{2} J_i' \dot{\theta}_i^2 + V_i' + \frac{\tau_i}{\hat{\eta}_i} C_{i+1} \tag{2.29}$$

It may be useful to replace the sequence of N transmission blocks by a single equivalent block connecting the motor to the load. Correspondingly, Eq. (2.29) and Eq. (2.28) must

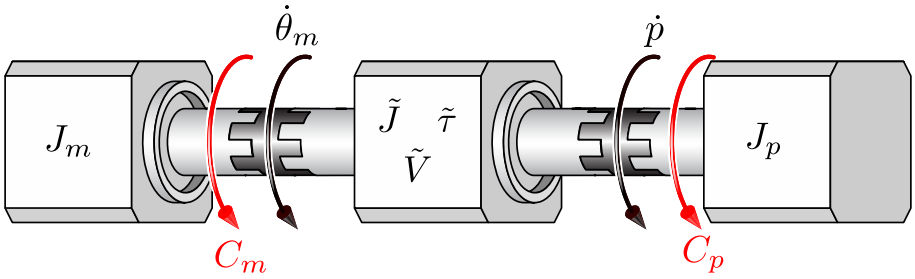

Figure 2.9: Equivalent block representation: N blocks are summarized in a single equivalent block.

be rearranged into an equation of the same form, but with input and output variables $\overline{\theta}_m$ and $\overline{p}$, C_m and C_p. The velocity at node i with respect to $\dot{\theta}_1$ is given by:

$$\dot{\theta}_i = \dot{\theta}_1 \prod_{k=1}^{i-1} \tau_k \tag{2.30}$$

By evaluating Eq. (2.30) at $i = N$, the equivalent transmission ratio is easily found:

$$\tilde{\tau} = \prod_{i=1}^{N} \tau_i \tag{2.31}$$

Before taking the derivative of $\tilde{\tau}$ with respect to θ_1, we shall consider the derivative of a generic transmission ratio τ_i with respect to θ_1 using Eq. (2.30):

$$\frac{d\tau_i}{d\theta_1} = \frac{d\tau_i}{d\theta_i}\frac{d\theta_i}{d\theta_1} = \tau_i' \prod_{k=1}^{i-1} \tau_k \tag{2.32}$$

Then, according to Leibniz product rule:

$$\begin{aligned} \tilde{\tau}' = \frac{d\tilde{\tau}}{d\theta_1} &= \sum_{i=1}^{N} \left[\left(\frac{d\tau_i}{d\theta_1} \right) \left(\prod_{l=1, l\neq i}^{N} \tau_l \right) \right] \\ &= \sum_{i=1}^{N} \left[\tau' \left(\prod_{l=1}^{i-1} \tau_l \right) \left(\prod_{l=1, l\neq i}^{N} \tau_l \right) \right] \\ &= \sum_{i=1}^{N} \left[\tau' \left(\prod_{l=1}^{i-1} \tau_l^2 \right) \left(\prod_{l=i+1}^{N} \tau_l \right) \right] \end{aligned} \tag{2.33}$$

It is important to notice in Eq. (2.29) that when $i = N$, C_{i+1} (or $C_{in,i+1}$ in its extended form) is undefined. Then, for consistency, we define $C_{i+1,in} = -C_{i,out} = -C_p$. The load force/torque C_p is influenced by every lumped efficiency and transmission ratio:

$$\tilde{C}_p = \prod_{i=1}^{N} \frac{\tau_i}{\hat{\eta}_i} C_p \tag{2.34}$$

while the i-th component of the potential energy is influenced by the transmission blocks placed before it:

$$\tilde{V}' = \frac{d\tilde{V}}{d\theta_1} = \sum_{i=1}^{N} \left[V_i' \left(\prod_{l=1}^{i-1} \frac{\tau_l}{\hat{\eta}_l} \right) \right] \tag{2.35}$$

Table 2.1: Expressions of global reduced inertia and its derivative for i=1,2,3

i	$\tilde{\mathbf{J}}$	$\tilde{\mathbf{J}}'$
1	J_1	J_1'
2	$J_1 + J_2\frac{\tau_1^2}{\hat{\eta}_1}$	$J_1' + J_2'\frac{\tau_1^3}{\hat{\eta}_1} + 2J_2\frac{\tau_1\tau_1'}{\hat{\eta}_1}$
3	$J_1 + J_2\frac{\tau_1^2}{\hat{\eta}_1} + J_3\frac{\tau_1^2\tau_2^2}{\hat{\eta}_1\hat{\eta}_2}$	$J_1' + J_2'\frac{\tau_1^2}{\hat{\eta}_1} + J_3'\frac{\tau_1^3\tau_2^3}{\hat{\eta}_1\hat{\eta}_2} + 2J_2\frac{\tau_1\tau_1'}{\hat{\eta}_1} + 2J_3\left(\frac{\tau_1\tau_1'\tau_2}{\hat{\eta}_1\hat{\eta}_2} + \frac{\tau_2\tau_2'\tau_1^3}{\hat{\eta}_1\hat{\eta}_2}\right)$

By recalling Eq. (2.3) and the lumped efficiency in Eq. (2.29), we may calculate the equivalent reduced inertia as follows:

$$\tilde{J} = \sum_{i=1}^{N}\left[J_i\left(\prod_{l=1}^{i-1}\frac{\tau_i^2}{\hat{\eta}}_i\right)\right] \tag{2.36}$$

We proceed by taking the derivative of Eq. (2.36) with respect to θ_1. Extra attention must be paid to the fact that both J_i and τ_i depend on θ_1:

$$\begin{aligned}
\tilde{J}' = \frac{d\tilde{J}}{d\theta_1} &= \sum_{i=1}^{N}\left[\frac{d}{d\theta_1}\left(J_i\prod_{l=1}^{i-1}\frac{\tau_l^2}{\hat{\eta}_l}\right)\right] \\
&= \sum_{i=1}^{N}\left[\left(\frac{dJ_i}{d\theta_1}\right)\left(\prod_{l=1}^{i-1}\frac{\tau_l^2}{\hat{\eta}_l}\right) + J_i\frac{d}{d\theta_1}\left(\prod_{l=1}^{i-1}\frac{\tau_l^2}{\hat{\eta}_l}\right)\right] \\
&= \sum_{i=1}^{N}\left\{\left(\frac{dJ_i}{d\theta_i}\right)\left(\prod_{l=1}^{i-1}\tau_l\right)\left(J_i\prod_{l=1}^{i-1}\frac{\tau_l^2}{\hat{\eta}_l}\right) + J_i\sum_{r=1}^{i-1}\left[\frac{d}{d\theta_1}\left(\frac{\tau_r^2}{\hat{\eta}_r}\right)\left(\prod_{l=1,l\neq r}^{i-1}\frac{\tau_l^2}{\hat{\eta}_l}\right)\right]\right\} \\
&= \sum_{i=1}^{N}\left\{\left(\frac{dJ_i}{d\theta_i}\right)\left(J_i\prod_{l=1}^{i-1}\frac{\tau_l^3}{\hat{\eta}_l}\right) + J_i\sum_{r=1}^{i-1}\left[2\frac{\tau_r}{\hat{\eta}_r}\frac{d\tau_r}{d\theta_i}\left(\prod_{l=1}^{r}\tau_l\right)\left(\prod_{l=1,l\neq r}^{i-1}\frac{\tau_l^2}{\hat{\eta}_l}\right)\right]\right\}
\end{aligned} \tag{2.37}$$

Once all block parameters are reduced at the motor side to functions of θ_1, θ_1 is replaced by θ_m and C_1 by C_m, while motor inertia is added to $\tilde{J}$. Alternatively, the motor can be modeled as a generic block component with unit efficiency and transmission ratio, and the inertia J_m is computed via Eq. (2.36). Here, it is preferable to highlight the contribution of motor inertia. Finally the complete equation of motion is given by:

$$C_m + \tilde{C}_p = \left(J_m + \tilde{J}\right)\ddot{\theta}_m + \frac{1}{2}\tilde{J}'\dot{\theta}_m^2 + \tilde{V}' \tag{2.38}$$

which gives a direct relation between C_m and C_p while taking into account the inertia of all N blocks. We give in Tab. 2.1 some examples of functions $\tilde{J}, \tilde{J}'$ for the simplest case of $i = 1, 2, 3$.

Viscous Damping effect

The mechanical model defined by Eq. (2.38), which gives the motor torque C_m to be provided to achieve a given task, may be extended by considering the effect of viscous damping on

the rotor. In facts, the mechanical friction on bearings, or fluid interaction (e.g air friction) generate a resistive torque proportional to the rotational speed. If these effects can be evaluated at the end-effector or along the transmission chain, the damping contribution may be included inside $\tilde{C}_p$, or inside the blocks efficiencies $\hat{\eta}_i$. Alternatively, in order to take into account the contribution of the viscous damping on the motor, a resistive torque is introduced [17]:

$$C_d = b_m \dot{\theta}_m \tag{2.39}$$

where b_m is the damping coefficient measured in [N·m·s]. The equation of motion becomes:

$$C_m + \tilde{C}_p = \left(J_m + \tilde{J}\right) \ddot{\theta}_m + \frac{1}{2}\tilde{J}'\dot{\theta}_m^2 + \tilde{V}' + b_m \dot{\theta}_m \tag{2.40}$$

The coefficient b_m, however, is not of easy calculation, since it requires experimental measures [30]. In facts, the evaluation of b_m as a constant coefficient is challenging, given the highly non-linear nature of the friction phenomenon.

2.4.5 Dynamic Analysis

Inverse Dynamics

Given the task intended for the automatic machine in consideration, the external actions and the end-effector kinematic state may be promptly computed for the duration of the operation on the product (e.g. a process of transformation or a simple movement). Even during repositioning, the necessity to introduce several phases of movements leads to multiple kinematic constraints on end-effector motion. Therefore it is a natural choice to represent the task motion and force by the end-effector state $\overline{p}(t)$ and end-effector force $C_p(t)$. For this reason, the inverse dynamics problem of determining the motor torque C_m from task specification is common in motor selection for automatic machine design.

Inverse dynamics is an algebraic problem. Similarly to inverse kinematic analysis, the inverse dynamics is performed by performing a backward recursion (from C_p to C_m) using Eq. (2.29), and eventually adding to the motor torque the term in Eq. (2.39). Furthermore, every action exchanged between neighboring blocks is found as well. Alternatively, Eq. (2.40) can be used, although the evaluation of equivalent quantities is not trivial and may be computationally expensive.

Forward Dynamics

If the torque generated by the motor is given to find the end-effector state $\overline{p}$, the second-order ordinary differential equation (ODE) Eq. (2.40) must be integrated. The equivalent parameters $\tilde{J}$, $\tilde{J}'$ and $\tilde{V}'$ depend on motor displacement θ_m, while $\tilde{C}_p$ in general depends on both $\overline{\theta}_m$ and time. The solution $\overline{\theta}_m(t)$ is found by means of numerical quadrature algorithms, such as the Runge-Kutta algorithm [31] implemented in the MATLAB ODE solvers.

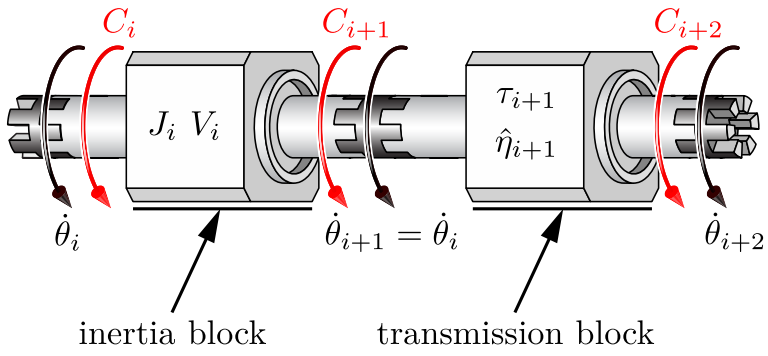

Figure 2.10: Two typologies of blocks: inertia block takes into account variation of energy, transmission block takes into account variation of speed and efficiency

2.5 Modeling techniques

Once the lumped-parameters model has been defined, the issue of modeling an actual mechanism arises. In particular, several questions must be answered: how many blocks are needed to model a mechanism? Which parameter should each block contain? In this section, these issues are addressed, and several techniques of modeling are presented.

2.5.1 Inertia and transmission blocks

Mechanical loss in a linkage mechanism is caused by friction between bodies that move one with respect to the other. Thus, in every kinematic pair (e.g. revolute, prismatic, screw joint), energy dissipation occurs. In Sec. 2.3.5, two different models were presented for efficiency. In the first model, the efficiency $\hat{\eta}$ influences the energy exchange ratio of the whole block (including the variations of both kinetic and potential energy), that is, the sources of loss are concentrated at the input block. Conversely, in the second model, the loss is concentrated just before the output and only influences the output torque. The introduction of a unique efficiency parameter for the entire block leads to inevitable approximations if the block represents a complex mechanism, where there are multiple sources of loss. Furthermore, it may occur that such multiple sources of loss affect the mechanical components in parallel, rather than sequentially. A partial solution to this problem can be found by defining two sub-classes of blocks: the *inertia block* and the *transmission block*. The former considers energy variations, while the latter takes into account velocity variation and concentrates on mechanical friction losses. The two blocks are considered to be sequentially connected, and since two subsequent blocks of the same type can be composed into a single one, an alternate order of the two is also considered.

Let i denote the inertia block and $i+1$ the transmission block. The inertia block is characterized by unit efficiency and transmission ratio. The reduced inertia J_i is easily computed by directly summing all inertias moving at velocity $\dot{\theta}_i$.

If a change of velocity occurs in the mechanism, a transmission block is introduced. A transmission block the contains no inertia J_{i+1} and no contribution of potential energy V_{i+1}. The transmission ratio τ_{i+1} depends on θ_{i+1}. Each transmission block is neighbored by two inertia blocks: this allows one to correctly account for the inertia moving at a given velocity. In fact, the losses are concentrated where a change of speed happens, while the inertia of the transmission is split between two inertia blocks neighboring the transmission block.

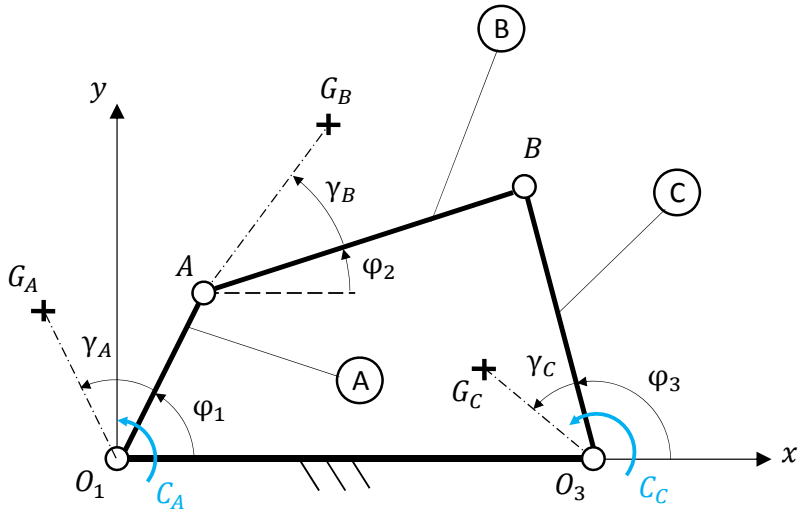

Figure 2.11: 4-bar linkage mechanism

Example: a motoreducer Consider a motor connected to a gearbox speed reducer to move a flywheel load. Assume that the speed reducer is a single-stage parallel-axes gearbox with a constant transmission ratio. This system may be described by a three-block model: a first inertia block takes into account the motor inertia, the reducer fast shaft inertia and the first gearwheel. A transmission block takes into account reducer efficiency and speed reduction. A third inertia block takes into account the reducer slow shaft inertia and the second gearwheel along with the flywheel load inertia.

2.5.2 Example: modeling a 4-bar linkage

In this section, a detailed modeling example is given. A Grashof-type 4-bar mechanism is used to transmit motion between a crank and a rocker. The only forces acting on the system are: a torque on crank A, a torque on the rocker C, and gravity (the 4-bar linkage is assumed to move on a vertical plane).

Kinematic and Dynamic analysis

As shown in Fig. 2.11, a reference system is defined with origin in O_1 and the **x** axis passing through revolute joint O_3. The poses of the members A, B, C are defined by angles $\varphi_1, \varphi_2, \varphi_3$. Their lengths are respectively l_A, l_B, l_C. The position of centers of mass G_A, G_B, G_C are prescribed by angles $\gamma_A, \gamma_B, \gamma_C$ and distances r_A, r_B, r_C, with respect to reference systems attached to mobile members. The transmission ratios of $\dot{\varphi}_3$ and $\dot{\varphi}_2$ versus $\dot{\varphi}_1$ are given by [32]:

$$\begin{aligned} \varphi_3' &= \frac{\dot{\varphi}_3}{\dot{\varphi}_1} = \frac{l_A \sin(\varphi_1 - \varphi_2)}{l_B \sin(\varphi_3 - \varphi_2)} \\ \varphi_2' &= \frac{\dot{\varphi}_2}{\dot{\varphi}_1} = \frac{l_A \sin(\varphi_1 - \varphi_3)}{l_C \sin(\varphi_3 - \varphi_2)} \end{aligned} \tag{2.41}$$

where φ_3' and φ_2' are functions of φ_1. The analytical dependence of φ_2 and φ_3 on φ_1 can be obtained by solving the loop-closure equations [32]. The solution of the position-analysis

problem is not unique, but once the initial assembly configuration is defined, the one-to-one correspondences $\varphi_2 = f_2(\varphi_1)$ and $\varphi_3 = f_3(\varphi_1)$ can be established.

Deriving coordinates of point G_B with respect of time gives the center of mass velocity $\dot{G}_B$, where the **x** and **y** components are $\dot{G}_{B,x}$ and $\dot{G}_{B,y}$. This in turn defines two projected transmission ratios:

$$\begin{aligned} G'_{B,x} &= \frac{\dot{G}_{B,x}}{\dot{\varphi}_1} = -l_A \sin(\varphi_1) - r_B \varphi'_2 \sin(\varphi_2 + \gamma_B) \\ G'_{B,y} &= \frac{\dot{G}_{B,y}}{\dot{\varphi}_1} = -l_A \cos(\varphi_1) + r_B \varphi'_2 \cos(\varphi_2 + \gamma_B) \end{aligned} \tag{2.42}$$

Repeating the above process for G_A and G_C leads to analogous expression for $G'_{A,x}$, $G'_{A,y}$, $G'_{C,x}$, $G'_{C,y}$.

If the members' masses are m_A, m_B and m_C, and member's mass moments of inertia are J_{A,O_1}, J_{B,G_B} and J_{C,O_3} (the second subscript indicates the axis with respect to which the moment of inertia is calculated), the total kinetic energy of the mechanism is:

$$T = \frac{1}{2}\dot{\varphi}_1 \left[J_{A,O_1} + m_B \left(G'_{B,x}\right)^2 + m_B \left(G'_{B,y}\right)^2 + J_{B,G_B} \varphi'^2_2 + J_{C,O_3} \varphi'^2_3 \right] \tag{2.43}$$

while the potential energy is:

$$V = m_A G_{A,y} + m_B G_{B,y} + m_C G_{C,y} \tag{2.44}$$

1) Single block model

Since a rotational motion about O_1 is transmitted to one about O_3, the determination of input and output ports is straight forward: $\theta_{in} = \varphi_1$ and $\theta_{out} = \varphi_3$. The overall transmission ratio τ is thus given by the first relation in Eq. (2.41), so $\tau = \varphi'_3$. We also need the second derivative of φ_3 with respect to θ_{in}, which we denote by $\tau' = \varphi''_3$. The reduced inertia is evaluated by means of Eq. (2.43),

$$J = J_{A,O_1} + m_B \left(G'_{B,x}\right)^2 + m_B \left(G'_{B,y}\right)^2 + J_{B,G_B} \varphi'^2_2 + J_{C,O_3} \varphi'^2_3 \tag{2.45}$$

Introducing the second derivatives of $\varphi_3, \varphi_2, G_{B,x}, G_{B,y}$, with respect to φ_1, denoted as $\varphi''_3, \varphi''_2, G''_{B,x}, G''_{B,y}$, it is (see Eq. (2.44)):

$$\begin{aligned} J' &= 2m_B G'_{B,x} G''_{B,x} + 2m_B G'_{B,y} G''_{B,y} + 2J_{B,G_B} \varphi'_2 \varphi''_2 + 2J_{C,O_3} \varphi'_3 \varphi''_3 \\ V' &= m_A G'_{A,y} + m_B G'_{B,y} + m_C G'_{C,y} \end{aligned} \tag{2.46}$$

We then introduce the efficiencies η_{inv}, η_{dir} to model the mechanical losses of the mechanism. $\hat{\eta}$ is defined as in Eqs. (2.23) and (2.26). The final equation of motion is given by:

$$C_A = J\ddot{\varphi}_1 + \frac{1}{2}J'\dot{\varphi}_1^2 + V' - \frac{\tau}{\hat{\eta}} C_C \tag{2.47}$$

2) Sub-blocks decomposition

While the single-block model represented by Eq. (2.47) provides a good representation of the behavior of the mechanism, it is dependent on a suitable efficiency model to be determined.

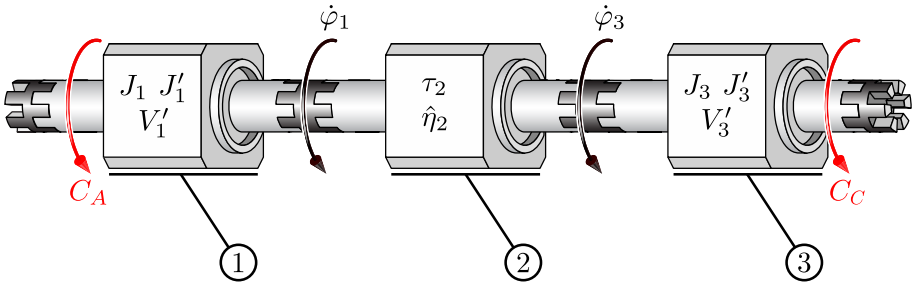

Figure 2.12: Three-block model of a 4-bar mechanism

Table 2.2: Parameters for three-block model of 4-bar mechanism.

i	*1*	*2*	*3*
τ_i	1	φ_3'	1
$\frac{d\tau_i}{d\varphi_i}$	0	φ_3''	0
$\hat{\eta}_i$	1	$\hat{\eta}$	1
J_i	$J_{A,O_1} + m_B\left(G_{B,x}'\right)^2 + m_B\left(G_{B,y}'\right)^2 + J_{B,G_B}{\varphi_2'}^2$	0	J_{C,O_3}
$\frac{dJ_i}{d\varphi_i}$	$2m_B G_{B,x}' G_{B,x}'' + 2m_B G_{B,y}' G_{B,y}'' + 2J_{B,G_B}\varphi_2'\varphi_2''$	0	0
$\frac{dV_i}{d\varphi_i}$	$m_A G_{A,y}' + m_B G_{B,y}'$	0	$m_C \frac{G_{C,y}'}{\varphi_3'}$

The losses are concentrated either at the beginning or at the end of the block, and the energy variation contributions cannot be split. In order to minimize the efficiency model, the mechanism can be decomposedin two inertia blocks and a single transmission block, as is shown in Fig. 2.12.

The first inertia block, i.e. block 1, contains the parameters describing the kinetic and potential energy variations for member A and member B. The inertia related to member B must be reduced to fit into block 1, since the only two velocities available in the model are $\dot{\varphi}_1$ and $\dot{\varphi}_3$. Block 2 is responsible for velocity variation and energy loss. Block 3 only contains the kinetic and potential energy variation parameters of member C. The values for the block parameters are reported in Tab. 2.2. It is useful to rewrite Eq. (2.47) by noticing that $J = J_1 + J_3{\varphi_3'}^2$, $V' = \frac{dV_1}{d\varphi_1} + \varphi_3'\frac{dV_3}{d\varphi_3}$, $\tau = \tau_2 = \varphi_3'$ and $J' = \frac{dJ_1}{d\varphi_1} + 2J_3\varphi_3'\varphi_3''$. Please also notice that the relation $\frac{dV_3}{d\varphi_1} = \frac{dV_3}{d\varphi_3}\frac{d\varphi_3}{d\varphi_1} = \varphi_3'\frac{dV_3}{d\varphi_3}$ has been used. Rearranging we obtain:

$$C_A = J_1\ddot{\varphi}_1 + \frac{1}{2}\frac{dJ_1}{d\varphi_1}\dot{\varphi}_1^2 + \frac{dV_1}{d\varphi_1} + \varphi_3'\left(J_3\varphi_3'\ddot{\varphi}_1 + J_3\varphi_3''\dot{\varphi}_1^2 + \frac{dV_3}{d\varphi_3} - \frac{C_C}{\hat{\eta}}\right) \tag{2.48}$$

which still refers to single-block model, but expressed in three-block-model quantities. Now, in order to infer the expression of C_A for the three-block model, Eq. (2.26) is applied.

It leads to the system:

$$\begin{cases} C_1 = C_A = J_1\ddot{\varphi}_1 + \dfrac{1}{2}\dfrac{dJ_1}{d\varphi_1}'\dot{\varphi}_1^2 + \dfrac{dV_1}{d\varphi_1} + C_2 \\ C_2 = \dfrac{\tau_2}{\hat{\eta}_2} C_3 \\ C_3 = J_3\ddot{\varphi}_3 + \dfrac{dV_3}{d\varphi_3} + C_4 = J_3\left(\tau_2\ddot{\varphi}_1 + \dfrac{d\tau_2}{d\varphi_2}\dot{\varphi}_1^2\right) + \dfrac{dV_3}{d\varphi_3} - C_C \end{cases} \tag{2.49}$$

where $\ddot{\varphi}_3$ is computed by using Eq. (2.28). Rearranging Eqs.(2.49) and introducing quantities in Tab. 2.2 lead to:

$$C_A = J_1\ddot{\varphi}_1 + \frac{1}{2}\frac{dJ_1}{d\varphi_1}'\dot{\varphi}_1^2 + \frac{dV_1}{d\varphi_1} + \frac{\varphi_3'}{\hat{\eta}}\left(J_3\varphi_3'\ddot{\varphi}_1 + J_3\varphi_3''\dot{\varphi}_1^2 + \frac{dV_3}{d\varphi_3} - C_C\right) \tag{2.50}$$

A difference can be identified by comparing Eq. (2.50) with Eq. (2.48). The efficiency $\hat{\eta}$ influences the terms involving inertia of member C, but not of A and B. The three-block model is more accurate than the single block model. The contribution of member B is accounted by reflecting it on A; different choices are available, such as reflecting the contribution of B on C, or splitting the inertia of B partly on A and partly on C. C. It was worth mentioning that the evaluation of the efficiency $\hat{\eta}$ may not always be straightforward, because an extremely accurate model or an experimental evaluation may be difficult to achieve.

2.6 Mechanism Library

In Sec. 2.5.2 the modeling of a four-bar mechanism linkage was presented. In particular, the single block model was determined with a trade-off between accuracy and simplicity. In this section, we present some additional examples of elementary mechanisms modeled as single blocks. Once a standard library of mechanism is defined, more complex transmission chains can be resolved by means of sequentially assembling such elementary pre-characterized mechanisms.

2.6.1 Generic mechanism

In this section, a procedure to generate a single-block model of a generic mechanism with the support of a multi-body simulation software is presented.

A block is fully determined if and only if parameters J, J', τ, τ', V', $\hat{\eta}$ are given for each value of the input angle θ_i. If these parameters are given, the block serves as a 'black box', and no other information about the mechanism is required. In order to obtain such functions analytically, the geometry of the mechanism and the distribution of masses must be known in advance. In complex linkage mechanisms, the derivation may not be trivial, and the architecture may not be suitable for division into serially-connected elementary mechanisms; in the domain of automatic machinery, this scenario is common.

Here, we introduce a specific procedure to determine the parameters of a an assigned transmission by the assistance of a multi-body simulation software, such as Camlinks,

ADAMS, RecurDyn or the dynamic simulation module integrated in most mainstream CAD softwares. The procedure features the execution of a few simulations with conveniently specified conditions.

The first step is to identify input and output ports, i.e. θ_{in} and θ_{out}. The mechanism must be analyzed for every admissible value of θ_{in}. Let $\Delta\theta_{in}$ be the difference between the maximum and the minimum value of θ_{in}. In case of a rotational crank, for example, $\Delta\theta_{in} = 2\pi$. We then assume a constant input velocity $\dot{\theta}_{in} = \omega_1$, i.e. $\ddot{\theta}_{in} = 0$, ignore the efficiency and set external torques equal to zero. Equation (2.11) then gives:

$$C_{in}\Big|_{\dot{\theta}_{in}=\omega_1} = \frac{1}{2}J'\omega_1^2 + V' \tag{2.51}$$

which is valid for $t \in [0, t_{s1}]$, $t_{s1} = \Delta\theta_{in}/\omega_1$. Repeating the same simulation for a different constant speed $\dot{\theta}_{in} = \omega_2$ gives:

$$C_{in}\Big|_{\dot{\theta}_{in}=\omega_2} = \frac{1}{2}J'\omega_2^2 + V' \tag{2.52}$$

which is valid for $t \in [0, t_{s1}]$, $t_{s2} = \Delta\theta_{in}/\omega_2$. The simulation duration is chosen so that both simulations achieve the same displacement range $\Delta\theta_{in}$. J' and V' remain the same in both Eq. (2.51) and Eq. (2.52), with θ_{in} being the only independent parameter. Subtracting Eqs. (2.51) and (2.52) and rearranging gives:

$$J'(\theta_{in}) = 2\frac{\left(C_{in}\Big|_{\dot{\theta}_{in}=\omega_1} - C_{in}\Big|_{\dot{\theta}_{in}=\omega_2}\right)}{\omega_1^2 - \omega_2^2} \tag{2.53}$$

Since all parameters at the right-hand side of Eq. (2.53) are known (the input speeds are given, whereas the input torques are computed by the multi-body simulations), $J'(\theta_{in})$ is thus determined. To find the reduced inertia J, we may integrate J' with respect to θ_{in}, but the evaluation of $J(\theta_{in})$ in (at least) one point is needed. For this purpose, we run a third simulation, where the mechanism starts from a full stop and moves with a constant acceleration $\ddot{\theta}_{in} = \dot{\omega}_3$. Since the initial velocity at $t = 0$ (where $\theta_{in} = \theta_{in,0}$) is zero, we have:

$$C_{in}\Big|_{\ddot{\theta}_{in}=\dot{\omega}_3} = J(\theta_{in,0})\dot{\omega}_3 + V'(\theta_{in,0}) \tag{2.54}$$

which gives the value of J at $\theta_{in} = \theta_{in,0}$. Note that Eq. (2.54) is a single-point evaluation. By using Eqs. (2.53) and (2.54), we finally determine the reflected inertia as:

$$J(\theta_{in}) = J(\theta_{in,0}) + \int_0^{\theta_i} J'\, d\theta_{in} \tag{2.55}$$

The transmission ratio is found from the first or the second simulation, by simply computing the ratio $\dot{\theta}_{out}/\dot{\theta}_{in}$. Once this ratio is known, its derivative is determined by using Eq. (2.5), so that:

$$\ddot{\theta}_{out} = \tau'\dot{\theta}_{in}^2 + \tau\cancel{\ddot{\theta}_{in}} \Rightarrow \tau' = \frac{\ddot{\theta}_{out}}{\dot{\theta}_{in}^2} \tag{2.56}$$

The potential energy may also be easily evaluated by either Eq. (2.51) or Eq. (2.52).This concludes the determination of all essential dynamic parameters.

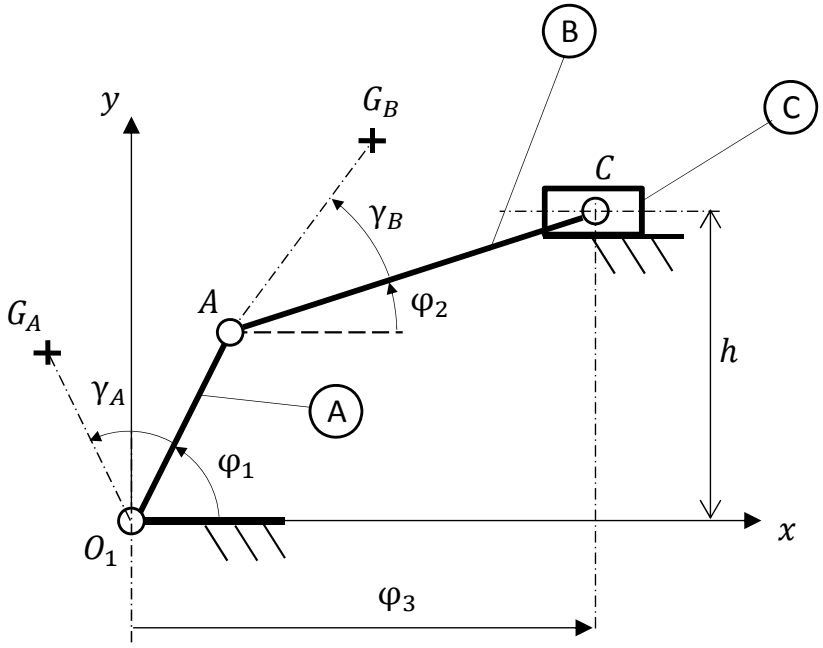

Figure 2.13: Crank slider mechanism: notations.

2.6.2 Crank-slider mechanism

In Fig. 2.13, a crank-slider mechanism is shown. It is composed by a crank A, a rod B and a slider C. A reference system is defined with origin in O_1. The prismatic joint axes is parallel to the $\mathbf{x}$ axis, at distance h. The poses of the members A, B are defined by angles φ_1, φ_2, and the pose of slider C is given by the distance φ_3, measured from O_1 along $\mathbf{x}$. The lengths of A, B are denoted by l_A, l_B. The three members have masses m_A, m_B, m_C. The position of centers of mass G_A, G_B are prescribed by angles γ_A, γ_B and distances r_A, r_B, with respect to reference systems attached to mobile members. The member's mass moments of inertia are J_{A,O_1}, J_{B,G_B} (the second subscript indicates the axis with respect to which the moment of inertia is calculated). The transmission ratios of $\dot{\varphi}_3$ and $\dot{\varphi}_2$ versus $\dot{\varphi}_1$ are given by [32]:

$$\begin{aligned} \varphi_3' &= \frac{\dot{\varphi}_3}{\dot{\varphi}_1} = -\frac{l_A \sin(\varphi_1 - \varphi_2)}{\cos(\varphi_2)} \\ \varphi_2' &= \frac{\dot{\varphi}_2}{\dot{\varphi}_1} = -\frac{l_A \cos(\varphi_1)}{l_B \cos(\varphi_2)} \end{aligned} \tag{2.57}$$

Equation (2.42) still holds for the crank lever mechanisms, and it gives the expressions of the projected transmission ratios $G'_{B,x}$ $G'_{B,y}$. The total kinetic energy of the mechanism is:

$$T = \frac{1}{2}\dot{\varphi}_1 \left[J_{A,O_1} + m_B \left(G'_{B,x}\right)^2 + m_B \left(G'_{B,y}\right)^2 + J_{B,G_B}\, {\varphi'_2}^2 + m_C\, {\varphi'_3}^2 \right] \tag{2.58}$$

while the potential energy is (mechanism moving on a vertical plane):

$$V = m_A G_{A,y} + m_B G_{B,y} + m_C h \tag{2.59}$$

Let assume $\theta_{in} = \varphi_1$ as the input and $\theta_{out} = \varphi_3$ as the output. Therefore, denoting with x'' the second derivative of quantity x with respect to φ_1, the expressions for single-block

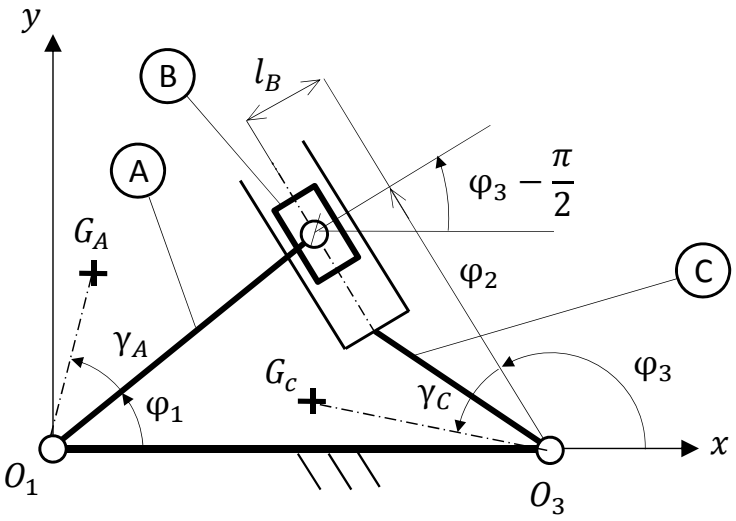

Figure 2.14: Crank and slotted lever mechanism: notations.

characteristic parameters are:

$$\begin{cases} \tau = \varphi_3' \\ \tau' = \varphi_3'' \\ J = J_{A,O_1} + m_B \left(G'_{B,x}\right)^2 + m_B \left(G'_{B,y}\right)^2 + J_{B,G_B} {\varphi_2'}^2 + m_C {\varphi_3'}^2 \\ J' = 2m_B G'_{B,x} G''_{B,x} + 2m_B G'_{B,y} G''_{B,y} + 2J_{B,G_B} \varphi_2' \varphi_2'' + 2m_C \varphi_3' \varphi_3'' \\ V' = m_A G'_{A,y} + m_B G'_{B,y} \end{cases} \tag{2.60}$$

2.6.3 Crank and slotted lever mechanism

In Fig. 2.14 a crank and slotted lever mechanism is show. A slider B is coupled with a revolute joint to a crank A, which rotates around the center O_1 of the reference system $x - y$. The slider is mounted inside a slotted lever C, which is able to rotate around O_3. The poses of the members A, C are defined by angles φ_1, φ_3; the position of the slider is identified by the projections l_B and φ_2 on the lever C. Length l_B is constant once the mechanism geometry is defined. The lengths of A, C are denoted by l_A, l_C. The three members have masses m_A, m_B, m_C. The position of centers of mass G_A, G_C are prescribed by angles γ_A, γ_C and distances r_A, r_C, with respect to reference systems attached to mobile members. The members' mass moments of inertia are J_{A,O_1}, J_{C,O_3} (the second subscript indicates the axis with respect to which the moment of inertia is calculated), while the slider is considered as a punctual mass. The transmission ratios of $\dot{\varphi}_3$ and $\dot{\varphi}_2$ versus $\dot{\varphi}_1$ are given by [32]:

$$\begin{aligned} \varphi_3' &= \frac{\dot{\varphi}_3}{\dot{\varphi}_1} = \frac{l_A \cos(\varphi_1 - \varphi_3)}{\varphi_2} \\ \varphi_2' &= \frac{\dot{\varphi}_2}{\dot{\varphi}_1} = l_B \varphi_3' - l_A \sin(\varphi_1 - \varphi_3) \end{aligned} \tag{2.61}$$

The total kinetic energy of the mechanism is:

$$T = \frac{1}{2}\dot{\varphi}_1 \left[J_{A,O_1} + m_B\, l_A^2 + J_{C,O_3}\, {\varphi_3'}^2 \right] \tag{2.62}$$

while the potential energy is (mechanism moving on a vertical plane):

$$V = m_A G_{A,y} + m_B l_A\, \sin(\varphi_1) + m_C G_{C,y} \tag{2.63}$$

Let assume $\theta_{in} = \varphi_1$ as the input and $\theta_{out} = \varphi_3$ as the output. The expressions for the single-block characteristic parameters are:

$$\begin{cases} \tau = \varphi_3' \\ \tau' = \varphi_3'' \\ J = J_{A,O_1} + m_B\, l_A^2 + J_{C,O_3}\, {\varphi_3'}^2 \\ J' = 2 J_{C,O_3} \varphi_3' \varphi_3'' \\ V' = m_A G_{A,y}' + m_B l_A \cos(\varphi_1) + m_C\, G_{C,y}' \end{cases} \tag{2.64}$$

Chapter 3

Electrical Model

In this chapter, the model of the electric part of the servo-controlled axis is presented. The goal of the chapter is to derive a model solely based on rated data of motor and drives, and also to estimate electric efficiency. Section 3.1 introduces the electric components of the servo-axis and the phenomena that are responsible for power losses. Section 3.2 presents the working principle of a permanent magnet synchronous motor. In Section 3.3 and 3.3 the motor model is described: the former Section presents the torque-current correlation, whereas the latter introduces the loss model. Section 3.4 shows the map efficiency within the motor operation range.

3.1 Introduction

3.1.1 Components

The electric model takes two components into consideration: the motor and the drive. Synchronous machines have been applied in servo-driven operations for a long time. In a synchronous machine, a power supply feeds excitation to the stator to create a rotating magnetic field. The rotor generates a magnetic field that lock on the stator field so that they rotate at the same speed. The main advantage of synchronous machines over induction motors is the absence of rotor slip losses; they also have smaller weights and inertia, and thus higher power density in comparison to DC motors.

Permanent Magnet Synchronous Motors (PMSM)

The most commonly employed type of synchronous motor in automatic machines is the *Permanent Magnet Synchronous Motor (PMSM)*, where the rotor magnetic field is generated by permanent magnets. These motors do not require a secondary energy supply to create the rotor magnetic field, unlike, for instance, excited-rotor motors. As a result, these motors are robust, reliable and simple to build. The drawback is that the intensity of the rotor field is fixed, as it is determined by the rotor magnets , and it cannot be varied as a controllable parameter. The development of high quality permanent magnets allowed manufacturers to produce PMSMs in a wide range of sizes, ranging from 100W up to 500kW. Beyond these limits, excited-rotor motors are still used, as they can generate up to a few MWs [33].

Several names are assigned to PMSMs in the literature, sometimes based on different classification criteria and sometimes based on historical reason. In early 1970s, PMSMs were referred as *Brushless DC* or *BLDC (Brushless Direct Current)*motors, because they are essentially the inside-out version of a standard DC motor (which features permanent magnets on the stator and armature windings on the rotor), and they were considered as a direct replacement of DC motors, equipped with brushes. PMSMs share with DC motor, also (up to a certain accuracy) the linear relation between current and torque, and voltage and speed. The label DC, as opposed to AC, prescribes the pattern of source back-electromotive force (or back-EMF) shape: BLDC motors are powered by quasi-square current waveforms and they feature a trapezoidal back-EMF shape, while *Brushless AC motors* or *PMAC* motors are excited by three-phase currents and have a sinusoidal back-EMF shape [34]. With respect to permanent-magnets position on the rotor, PMSMs can be classified as *interior permanent magnet (IPM)* if the magnets are buried inside the rotor, or *surface permanent magnet (SPM)* if the magnets are attached to the surface. This choice not only influences the mechanical characteristics of the rotor (e.g. inertia and robustness), but also magnetic properties such as flux distribution between rotor and stator [21]. Another rotor characteristic is saliency. A non-salient (cylindrical) rotor has axial symmetry and its magnetic properties do not depend on radial direction. On the other hand, a salient pole rotor with variable inductance can be used to produce reluctance torque, as will be analyzed in Section 3.2.

For the rest of this and later chapters, when referring to a PMSM, the AC excited motor is implied, as they are widely used in industry automation for their ability to provide constant torque at variable speeds.

Voltage Source Inverter (VSI)

A variable-frequency converter is needed as an interface between the utility power system and the synchronous motor. The converter must adjust the frequency according to the desired output speed, and be able to provide the rated current at any frequency [35]. In PMSMs, the rotor speed is exactly determined by the supply frequency. The inverter drive is commonly referred to as *Voltage Source Inverter (VSI)*, and it can be based on MOSFET (metal-oxide-semiconductor field-effect transistor) or IGBT (Insulated Gate Bipolar Transistor).

3.1.2 Types of Energy Losses

There are two categories of power loss in a electrical machine. The first one is due Joule effect, which causes heating to be dissipated in a conductor with non-zero Ohmic resistance during electric current flow. The second one is related to the hysteretic nature of magnetic materials.

If the source of losses is a current flowing in a conductor, it is commonly referred as *copper loss*. considering the fact that the Joule effect is present whether conductors are made by copper or not (e.g. by aluminum), the more general name of *windings losses* is preferred here. If the source of loss is a metallic material subject to time-varying magnetic fluxes, it is referred to *iron loss* (or *core loss*). Iron losses are divided into two subtypes: *Eddy current losses* are caused by Joule effect dissipations associated with induced currents, whereas *hysteresis losses* are caused by magnetic hysteresis of the material.

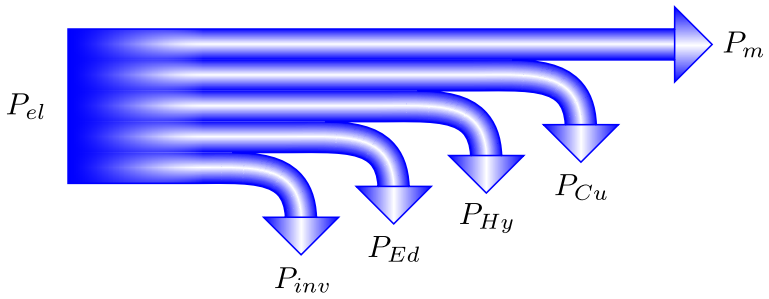

Figure 3.1: Servo-axis power flow

In Fig. 3.1 a visual representation of power losses along the servo-axis is given. $P_{el,tot}$ is the total electric power supplied to the servo-axis (and provided by the DC bus in a parallel-architecture automatic machine). In order to provide mechanical power P_m to the shaft, the power associated with copper losses P_{Cu}, Eddy current and hysteresis losses P_{Ed} and P_{Hy} (total iron losses are denoted by P_{Fe}), inverter losses P_{inv} must be taken into account.

$$P_{el,tot} = P_m + P_{Cu} + P_{Ed} + P_{Hy} + P_{inv} \tag{3.1}$$

If the term P_{inv} is disregarded, the term P_{loss} is used to indicate the overall motor losses concerning only the motor, i.e. $P_{loss} = P_{Cu} + P_{Ed} + P_{Hy}$. A brief introduction to the physical principles responsible for the aforementioned losses is given hereafter.

Windings losses. These losses are directly related to Joule heating, which occurs when an electric current flows through a resistance. The passage of charges causes the conductor to heat, and the heating is proportional to electric power $P = V\,I$. If the load is pure resistive, Ohm's law $V = R\,I$ is applicable: the common form of Joule heating dissipation is proportional to resistance and square current:

$$P_{Cu} \propto RI^2 \tag{3.2}$$

For this reason, Joule heating is also referred to Ohmic heating or resistive heating.

Hysteresis losses. Hysteresis loss is caused by the hysteresis of ferromagnetic materials used in the construction of electric machines. In non-transient situation, the ratio of the flux density B versus the magnetic field intensity H is defined as *permeability* μ, and is a property of the material the magnetic field acts on. Due to hysteresis effect, the relation between B and H is both non-linear and multivalued. In Fig.3.2 a hysteresis loop for a ferromagnetic material is shown: during a time-dependant excitation, the material will complete a loop varying between edge values B_{max} and $-B_{max}$. During this process, every time a cycle is completed, energy is given to the material, proportional to the area inside the loop. This energy is used to move dipoles inside the material [36] and is eventually dissipated via heat. Due to the energy-per-cycle nature of the dissipation, hysteresis losses are directly proportional to excitation frequency ω. To evaluate the dependence of the area inside the $B-H$ cycle under maximum flux density, empirical equations have been developed. In the Steinmetz equation [37], for example, hysteresis losses P_Hy are:

$$P_{Hy} = k_H\,\omega\,B_{max}^{1.6} \tag{3.3}$$

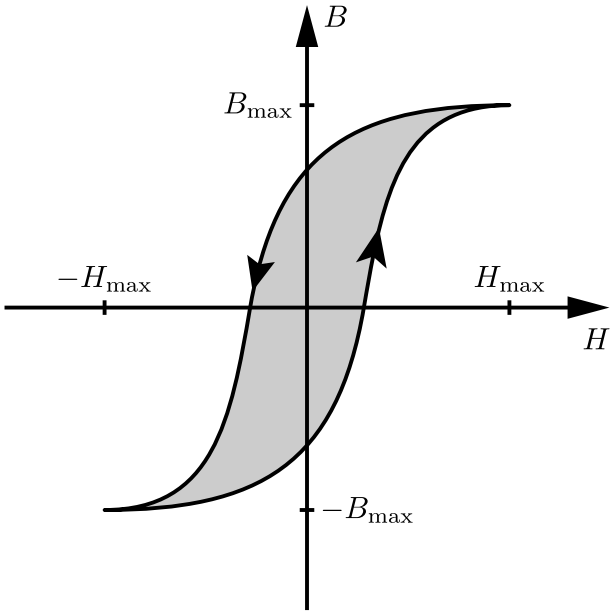

Figure 3.2: Hysteresis loop for a ferromagnetic material [36]

where k_H is a coefficient depending on motor characteristics.

Eddy Currents losses. When a magnetic field varies with time, an electric field is produced as stated by *Faraday's law* [36]:

$$\oint_C E\, ds = -\frac{d}{dt}\int_S B\, da \tag{3.4}$$

The path integral of electric field intensity E on a closed contour C is equal to the time derivative of the magnetic flux linking that contour. In magnetic materials, these induced electric fields generate induced currents, which are in opposition with magnetic field variations. These unwanted currents are a source of ohmic dissipation. Usually the core magnetic material is laminated in layers, with the direction of lamination being the same as the flux direction. Each layer is insulated from adjacent ones, in order to interrupt current paths and stop or reduce the generation of eddy currents. In general, eddy current losses P_{Ed} increases as the square of excitation frequency, and they are proportional to the square of the flux density peak value as well [38] [39].

$$P_{Ed} = k_{Ed}\, \omega^2\, B_{max}^2 \tag{3.5}$$

where k_{Ed} is a coefficient dependent on motor characteristics.

Switching losses. These losses arise when a gate switches its state from ON to OFF or vice versa. During the switching from a state of conduction, when current flows and voltage drops is ideally zero, to a state of non-conduction, when current is zero and voltage drops, there is a transient period where both voltage and current are non-zero. This non-instantaneous switching dynamics causes a power loss proportional to the switching frequency f_s. Controller drives are mainly responsible for this type of loss.

3.2 PMSM Principles of Operation

In this section the main principles of operation of a PMSM are presented.

3.2.1 Excitation and Induced MMF

Synchronous motors are supplied by a three-phase alternate voltage source. It is assumed that the system is balanced and symmetrical, and is excited at frequency ω [Hz]. The phases are denoted by a, b, c, and their voltages are [40]:

$$v_{a,b,c} = \sqrt{2}V \cos\left(\omega t - (i-1)\frac{2\pi}{3}\right) \quad i = 1, 2, 3; \tag{3.6}$$

where V is the effective voltage value of the symmetric system. It can be shown that each phase generates an alternate periodic *MMF (magnetomotive force)* acting along a magnetic axis associated with that phase. The distribution of the magnetic field is a square wave inside the air gap, but when several coils are combined, the results is a periodic function which can be written in Fourier series, and the fundamental frequency of the periodic function is ω. The combination of three phases with same frequency, but at distance of 120° , creates a rotating MMF with a constant module, rotating at a speed of ω. With the assumption of sinusoidal windings spatial distribution, the MMF created by the phase stator current can be assumed to be a sinusoidal function of the position. This allows for setting all the harmonics of the Fourier transform to zero, except for the one with the fundamental frequency [41]. For a machine with uniform air gap, the above analysis for MMF is also valid for the magnetic field strength and the flux density in the air gap. On top of that, the generated back-EMF is sinusoidal as well.

In a synchronous machine, there is no slip and the rotor is locked to the rotating magnetic field generated by the stator. For a two-pole machine, the mechanical rotor speed ω_m equals the frequency ω of the exciting source. Thus, the mechanical angle θ_m that defines the position of the rotor with respect to a stator-fixed reference frame is the same as the electrical angle θ. For a multi-pole machine with p poles, we have the following relation:

$$\frac{d\theta_m}{dt} = \omega_m = \frac{p}{2}\omega \tag{3.7}$$

For the sake of clarity, we shall hereafter consider only a two-pole machine and drop the subscript p, unless otherwise stated.

3.2.2 Reference Systems and Park Transformation

A three-axis reference system *a-b-c* is defined and fixed to the stator. Axis a is defined along the direction of the magnetic axis relative to phase a, and it represents the horizontal axis of the reference system. Consequently, b-axis and c-axis are respectively 120° and 240° ahead of the a-axis if a counterclockwise rotation speed is assumed, as shown in Fig. 3.3. Thus, all periodic quantities can be seen as rotating phasors, and they all have the same frequency and rotational speed. For this reason, in the study of synchronous machines, it is convenient to define a rotating reference system fixed to the rotor, called *d-q*. This system is composed of axis d, called *direct axis*, and axis q, called *quadrature axis*; θ indicates the angle between a fixed axis (i.e. a) and a rotating axis (i.e. d). The d axis is defined along the direction of

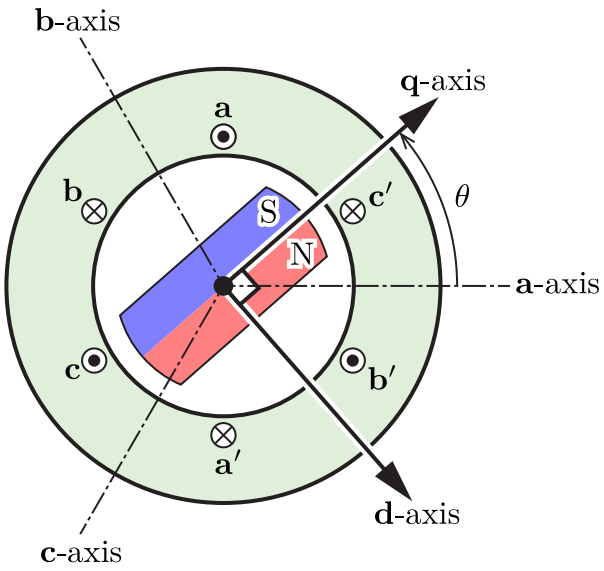

Figure 3.3: *d-q* frame and fixed stator *a-b-c* frame

the permanent magnet flux direction, and it is 90° ahead of q. For a multi-poles machine, where the directions of magnets dipoles are multiple, q can lie in between those direction, thus forming with d an angle smaller than 90°.

The transformation which allows to express fixed system quantities with respect to the rotating system is called Park's transformation [20]. Given a set of three quantities in the coordinate system *a-b-c* Park transformation allows their corresponding equivalents v_d, v_q in the *d-q* system to be found. The Park transformation is defined as:

$$\begin{bmatrix} v_d \\ v_q \\ v_0 \end{bmatrix} = \frac{2}{3} \begin{bmatrix} \cos(\theta) & \cos(\theta - \frac{2\pi}{3}) & \cos(\theta + \frac{2\pi}{3}) \\ \sin(\theta) & \sin(\theta - \frac{2\pi}{3}) & \sin(\theta + \frac{2\pi}{3}) \\ \frac{1}{2} & \frac{1}{2} & \frac{1}{2} \end{bmatrix} \begin{bmatrix} v_a \\ v_b \\ v_c \end{bmatrix} \tag{3.8}$$

The first member of Eq. (3.8) is also referred to as the *space vector* and it is indicated with a subscript s; term v_0 is called the homopolar component. In a balanced system this term is always equal to zero and therefore sometimes it is not included in the space vector definition. The following short notation uses the associated matrix T_P:

$$\boldsymbol{V}_S = T_p \boldsymbol{V}_{a,b,c} \tag{3.9}$$

Since the transformation is invertible, T_P^{-1} always exists.

3.2.3 Equivalent Circuit and Torque Expression

The *d-q* reference system is often used to study the behavior of synchronous machines, and in particular of PMSMs. For example, the *d-q* equivalent circuit is used in [23, 42, 22, 43], and [21, 41]. The *d-q* circuit reported here is determined under the following assumptions [43]:

A1. currents are balanced

A2. the induced EMF is sinusoidal

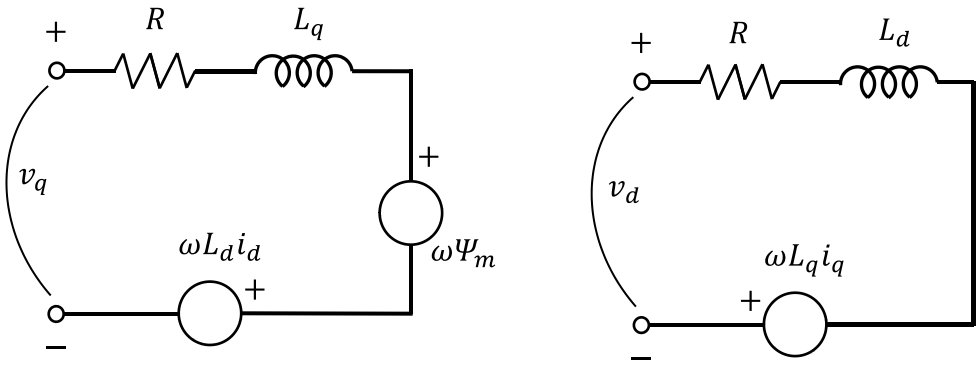

Figure 3.4: d and q equivalent circuits

A3. saturation is neglected

A4. eddy currents and hysteresis losses are disregarded while solving the circuit to find the motor torque

A5. the motor has no squirrel cage rotor or damper windings

A1 and A2 were already discussed in Sec. 3.2.1. As far as A3 is concerned, saturation occurs as currents increase. Although it is neglected in our case, it can be taken into account by parameter changes in the model (see Section 3.3.2 for further information). As for A4, losses are neglected in the equivalent circuit, only to allow a simplified torque expression to be obtained (see Sec. 3.4). As for A5, squirrel cage rotors or damper windings are used to self start the machine as an induction motor. Standard windings are adopted to simplify the equivalent circuit and obtain a torque expression which can preferably represent both average values and instantaneous values (there are no dynamic response related to damper effects).

The voltage equations can be written in d- and q-axes as

$$\begin{aligned} v_d &= R_s i_d + \frac{d}{dt}\Psi_d - \omega\Psi_q \\ v_q &= R_s i_q + \frac{d}{dt}\Psi_q + \omega\Psi_d \end{aligned} \tag{3.10}$$

where R_s is the statoric Ohmic resistance, i_d, i_q, v_d, v_q are d-q stator currents and voltages; Ψ_d and Ψ_q are the stator magnetic flux linkages, and are given by:

$$\begin{aligned} \Psi_d &= L_d i_d + \Psi_m \\ \Psi_q &= L_q i_q \end{aligned} \tag{3.11}$$

where Ψ_m is the magnetic flux linkage created by the permanent magnets on the stator and is directed along d; L_d, L_q are stator self inductances along d- and q- axis . The d and q circuits are represented in Fig. 3.4. The instantaneous input power can be obtained with Park transformation from the three-phase expression:

$$P_{input} = v_a i_a + v_b i_b + v_c i_c = \frac{3}{2}\left(v_d i_d + v_q i_q\right) \tag{3.12}$$

Replacing v_d and v_q in Eq. (3.12) with the values calculated in Eqs 3.10, we obtain the output power and, dividing it by mechanical speed ω, we obtain the general torque expression as:

$$M = \frac{3}{2}\frac{p}{2}\left(\Psi_m i_q + (L_d - L_q) i_d i_q\right) \tag{3.13}$$

The first term in Eq. (3.13) is the most important one and it is related to the permanent magnet flux linkage and stator current perpendicular to the flux linkage. The second term is called *reluctance torque*. It is worth observing that, for a salient-rotor machine, where axis d and axis q inductances are equal ($L_d \approx L_q$), the second term vanishes (see for examples [22, 43]).

Standard $i_d = 0$ control A practical and common control system is to keep i_d equal to zero. This amounts to minimizing the overall current for a given torque value. The space vector of stator current $\boldsymbol{I}_s$, with magnitude $\sqrt{i_d^2 + i_q^2}$, is directed along the q axis in this case. By imposing $i_d = 0$, the drive seeks to maintain $\boldsymbol{I}_s$ to be perpendicular to the direct axis in order to maximize the torque at every operating point. Being a rotating system, the PMSM needs a sensor such as an encoder to detect the rotor position at every instant. With an optimal control of $i_d = 0$, the power factor $\cos\phi$, with ϕ being phase between current and voltage space vectors, can reach a value of around 0.98 [44] Notice that, when $i_d = 0$, the motor torque M is simply proportional to i_q (see Eq. (3.13)).

Reluctance torque control The second term in Eq. (3.13) can be used to produce a positive torque. Rotor saliency (i.e. difference between inductance L_d and L_q) can be used. Typically L_q exceeds L_d so that i_d should be kept negative in order to generate torque. Keeping i_d negative also creates a demagnetizing effect while taking into account saturation of iron [45]. A particular case where the condition $L_d > L_q$ occurs is IPM motors with interior magnets, where the supply system requires a different excitation [23].

3.3 Motor Model

In this section, the operative model of the motor is introduced: the goal is to infer a relation between mechanical parameters (rotational speed, torque) of the motor and its electric operating condition (exciting frequency and current). Then, the model can be used to evaluate losses and efficiency.

The first relation that defines the behavior of a motor is the function g that relates the motor torque to the absorbed current:

$$M = g(I) \qquad \Leftrightarrow \qquad I = g^{-1}(M) \tag{3.14}$$

where T is the motor torque and I is the effective value of stator current. Function g is assumed to be a continuous and is necessarily bijective function. It is defined on the domain $I \in [-I_{max}, I_{\max}]$, where $I_{\max}$ is the maximum admissible current of the motor. The co-domain is $M \in [-M_{max}, M_{\max}]$, with M_{max} being the absolute value of the maximum torque that the motor can provide.

Another fundamental relation links exciting frequency ω and rotor speed ω_m. As seen in Eq. (3.7), this relation is an equality, $\omega = \omega_m$, since the exciting frequency defines the speed of the rotating magnetic field and, thus, also the speed of the rotor.

3.3.1 Linear model

Given Eq. (3.13), for a PMSM that doesn't implement a reluctance mechanism to produce torque, the torque-current dependency can be expressed as a linear relation $M = k'_t\, i_q$. If i_d is assumed to be kept around zero ($i_d \simeq 0$), and by introducing the effective current $I = i_q/\sqrt{2}$, the function g defined in Eq. (3.14) is:

$$M = g_l(I) = k_t\, I \tag{3.15}$$

where k_t is a constant depending on motor construction characteristics and subscript l emphasizes that g is a linear function of I. Together with Eq. (3.7), Eq. (3.15) gives a simple model of a PMSM, which can be used to determine electrical quantities from its operating conditions. This model is widely used by motor manufacturers [46]. By using Eq. (3.15), it is trivial to infer current from motor torque: $I = g_l^{-1}(M) = M/k_t$.

3.3.2 Quadratic model

Premise

The first step to improve the torque-current model is to disregard one or more simplifying assumptions made, in particular A3 and A4. In general, the resulting equivalent circuit is different from those shown in Fig. 3.4.

In order to take saturation into account, several authors developed detailed models to consider inter-saturation [47, 48, 49]. However, the evaluation of this effect is beyond the scope of this work. A more simplified approach is to consider some lumped parameters of the circuit as variables. For example, the magnet flux linkage can be modeled with an equivalent current i_m and a magnetizing inductance L_{md} generating $\Psi_m = L_{md}\, i_m$ [21]; considering L_{md} not constant allows saturation to be modeled. At the same time, it can be assumed that the torque expression Eq. (3.13) remains valid.

Evaluation of iron losses and their dependence on operation parameters will be discussed in Sec. 3.4, while the modification of the equivalent circuit is analyzed here. There are several examples where iron losses are taken into account with the addition of a resistor R_m coupled to the stator flux and in parallel with both inductances L_d and L_q [25, 50, 42]. In this case, assumption A2 still holds, because the additional resistor does not perfectly represent higher harmonics of induced EMF and MMF. In order to overcome this limit, several methods have been used to consider higher harmonics, such as finite element analysis [24].

In [42], both windings and iron losses are evaluated, together with mechanical losses. Disregarding the latter, the resulting torque-current relation, including iron and windings losses, is still linear. Although the coefficient in this case is different from the case with no losses, Eq. (3.15) still holds. Even if this is not entirely true, the linear model may still serve as a good approximation of the behavior of the motor.

The purpose of this section is to define a novel function g which takes into account all losses with a reasonable level of details, by using only rated data available from manufacturers. In fact, the evaluation of motor internal parameters, such as self and mutual inductances, can be done experimentally, but it is not suitable for automatic machine design, where an entire motor catalog has to be characterized in order to make an optimal selection.

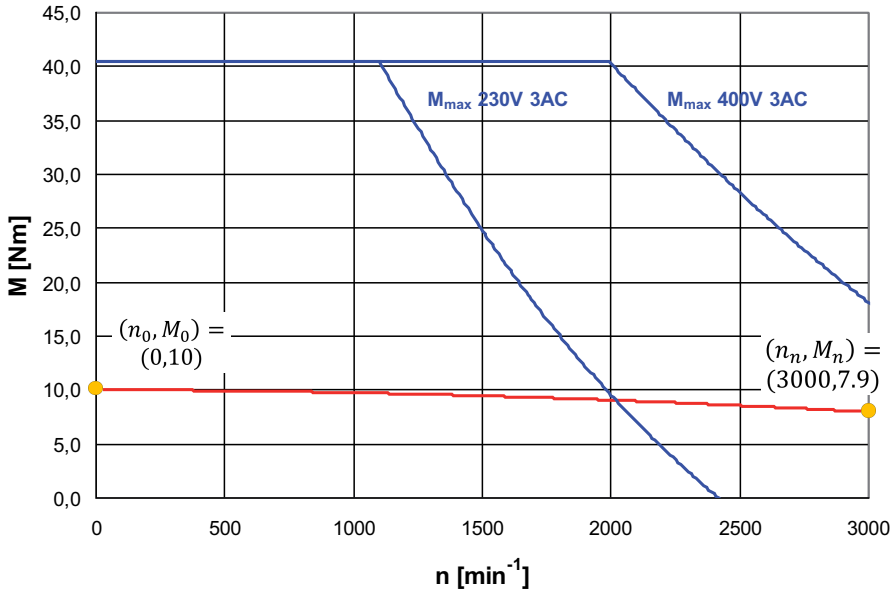

Figure 3.5: SH100 motor characteristic [51]. The rated values are $(n_n, M_n) = (3000, 7.9)$; the maximum speed is $n_{max} = 6000$ rpm; the stall values are $(n_0, M_0) = (0, 10)$

Available Data

In manufacfurers' catalogs, data at specific operating points can be found. In particular, rotational speed n [rev/min], torque M [Nm] and root-mean-square (RMS) (effective) phase current I are relevant to our study.

Mass moment of inertia is denoted by J_m and maximum rotating speed by n_{max} (or $\omega_{m,max}$). The per-phase resistance R is measured at 20°. Torque constant k_t is expressed in [Nm/A].

In Fig. 3.5, a motor speed-torque characteristic is reported for a ELAU motor [51]. The red line highlights the continuous service. If the RMS value of load torque is smaller than the continuous service admissible torque, the motor can achieve the task. This line is close to being horizontal, but decreases slightly from stall torque M_0 (torque provided at zero speed) to nominal torque M_n.

Nominal service is indefinitely possible if environmental conditions are met. Nominal (or rated) data are the most representative values for a motor. At rated speed n_n, the motor can provide rated torque M_n while drawing the rated current I_n.

Maximum torque or peak torque M_{max} can be briefly provided by the motor while absorbing the peak current I_{max}. At any instant, these values cannot be overcome by the motor. Peak torque value is constant and starts to decrease when n reaches a threshold depending on supply voltage (blue line in Fig. 3.5).

The stall torque the output torque of the motor while rotating at speed n_0 and drawing the stall current I_0. The speed n_0 is usually small, but it must be high enough so that the winding temperature is uniform and steady. For example, for ELAU motors, n_0 is usually set at 5 rpm.

Operative Model

The proposed model is defined in a domain the domain $[0, I_{\max}]$. It assumes a quadratic torque current dependence:

$$M(I) = k_{t0} + k_{t1} I + k_{t2} I^2 \tag{3.16}$$

To determine the unknown coefficients, first note that no torque is produced with a zero current or $M(0) = 0$, which leads to $k_{t0} = 0$. Besides, the working points relative to stall, rated and max operations lie on the torque-current function curve, and leads to the following sets of equations:

$$\begin{cases} M(I_0) = k_{t1} I_0 + k_{t2} I_0^2 = M_0 \\ M(I_n) = k_{t1} I_n + k_{t2} I_n^2 = M_n \\ M(I_{max}) = k_{t1} I_{max} + k_{t2} I_{max}^2 = M_{max} \end{cases} \tag{3.17}$$

Eq. (3.17) has two unknown quantities, k_{t1} and k_{t2}, and three equations. The least squares curve fitting method is used to find a pair of values k_{t1}, k_{t2} that minimize the sum of the squares of the residuals. The torque-current dependency is then given by:

$$M(I) = g_q(I) = k_{t1} I + k_{t2} I^2 \tag{3.18}$$

where the subscript q emphasizes teh quadratic relation between M and I. Let $M_i = g_q(I_i)$ be the i-th known value of g_q at I_i and let γ be a column vector with parameters k_{t1}, k_{t2}. The value of vector γ that minimizes the square sum S of residuals $r_i = M_i - g_q(I, \gamma)$, i.e.,

$$S = \sum_{i=1}^{3} r_i^2 = \sum_{i=1}^{3} \left(M_i - g_q(I, \gamma)\right)^2 \tag{3.19}$$

is the desired solution. As long as the direction flow of the current is irrelevant (such as when evaluating windings losses that depend on square current), the current can be evaluated by its magnitude alone. That being said, the resulting torque of Eq. (3.18) is the magnitude of the actual torque, which can be positive or negative, but does not influence the magnitude of the current. This helps to evaluate the inverse function for the torque-current conversion.

$$I = g_q^{-1}(|M|) = -\frac{k_{t1}}{2k_{t2}} + \frac{\sqrt{k_{t1}^2 - 4k_{t2}\,|M|}}{2k_{t2}} \tag{3.20}$$

Notice that the solution corresponding to $-\sqrt{k_{t1}^2 - 4k_{t2}\,|M|}$ is ruled out by the fact that $I \in [0, I_{\max}]$ is non-negative. The plus sign must be chosen since the curve in Eq. (3.18) is generally concave and, thus, k_{t2} is negative.

Application: ELAU SH100

The quadratic torque-current model is obtained for motor *PacDrive SH100/30*, a self-cooled servo motor with no brake by ELAU[51]. The motor has four poles ($p = 4$) and is supplied by a $400V$ main voltage. The catalog data for this motor are reported in Tab. 3.1. In the $I - M$ graph, function g is determined in order to minimize the residual distance from reference points: stall, rated and max values(see Eq. (3.17)). The resulting value of vector γ leads to $k_{t1} = 1.6275$ and $k_{t2} = -0.0116$. The function is visualized in Fig. 3.6 under the

Table 3.1: SH100 motor rated data, obtained from catalog [51]

Name	Symbol	Value
Rated speed	n_n [rpm]	3000
Standstill torque	M_0 [Nm]	10.0
Peak torque	$M_{\max}$ [Nm]	40.5
Rated torque	M_n [Nm]	7.9
Standstill current	I_0 [A]	6.2
Peak current	$I_{\max}$ [A]	32.3
Rated current	I_n [A]	5.3
Linear Torque Constant	k_t [Nm/A]	1.62
Ohmic resistance	R [Ohm]	1.81
Moment of Inertia	J_m $[kgcm^2]$	4.22
Maximum speed	n_max [rpm]	6000

quadratic label. Note that it does not strictly pass through the reference points (M_n, n_n), $(M_0, 0)$ and (M_{max}, I_{max}). Actual currents in reference points are defined as:

$$I'_0 = g^{-1}(M_0) \tag{3.21}$$
$$I'_n = g^{-1}(M_n) \tag{3.22}$$
$$I'_{max} = g^{-1}(M_{max}) \tag{3.23}$$

For the case study of SH100, $I'_0 = 6.43\,A$, $I'_0 = 5.03\,A$ and $I'_{max} = 32.3\,A$.

3.3.3 Experimental ELAU Torque-Current Model

We present here an experimental model obtained by manufacturer ELAU [52]. A new parameter is now introduced: the temperature difference ΔT between motor windings and environment. This parameter influences electrical quantities that depends on temperature (i.e. Ohmic resistance). In order to take temperature variation into account temperature variation, a thermal model must be made to consider the heat dissipation system. The thermal model depends on motor mounting (wall, surface plate, etc), materials (aluminum structure, steel, etc.) and also the eventual insulation required for the application (protected atmosphere application, under-water application). The creation of a thermal model is not trivial, and goes beyond the scope of this work. From now on, the motor is assumed to work at reference condition (i.e. winding temperature of 120°). This assumption is reasonable when the motor is properly selected. In fact, a motor working under near nominal conditions is designed to exploit its potential to reach its maximum allowed temperature, determined by isolation material and conductors capacity. Over-sized motors may reach a lower temperature with respect to reference ones. Nevertheless, such case is automatically excluded from our optimal selection process. An under-sized-motor situation should not be taken into consideration for its increased risk of failure.

The ELAU ambient reference temperature is set to $T = 40°$ and catalog quantities (as those reported in Tab. 3.1) are measured at winding motor temperature $T = 120°$. Thus, the parameter ΔT can be set to $\Delta T = 80°$ from now on. First, the parameter y is defined,

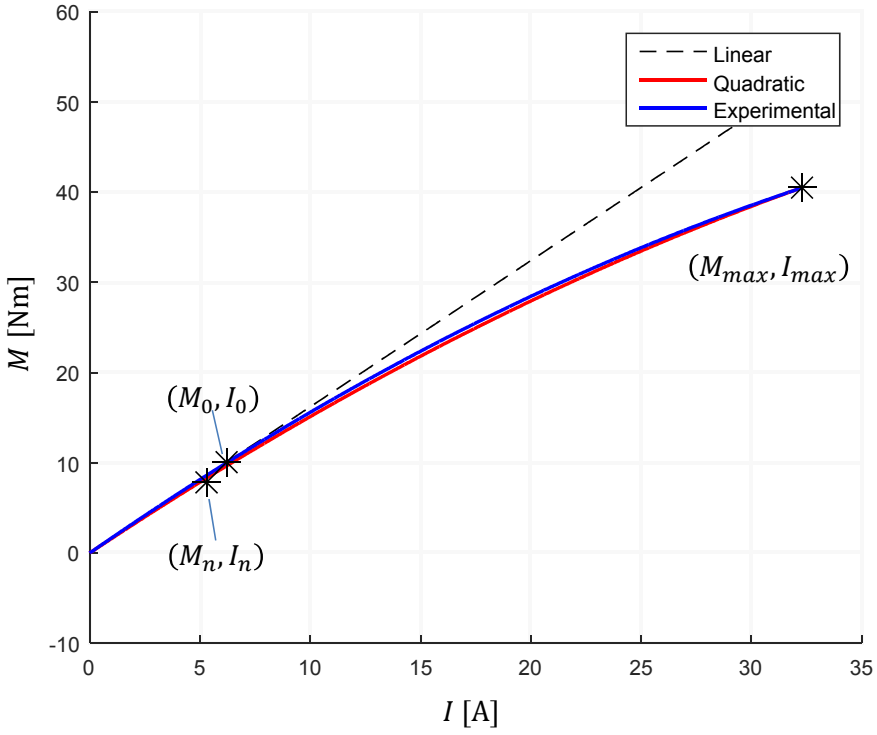

Figure 3.6: Confrontation of linear model, quadratic model and experimental model

which depends on torque and temperature:

$$y(M,T) = \frac{M}{\frac{\sqrt{3}}{2\pi}\Phi_{20}(1+\alpha\Delta T)I_0} \tag{3.24}$$

For the motor SH-100/30 whose data are reported in Tab. 3.1, the temperature coefficient is $\alpha_T = -9 \cdot 10^{-4}$ and the magnetic flux is $\Phi_{20} = 6.18$ Wb at 20°. the inverse torque-current relation can be written as:

$$I = g^{-1}(M) = 11,82 \cdot 10^4 I_0 \left(8423 - \sqrt{7.0947 \cdot 10^7 - 1.3536 \cdot 10^7 y}\right) \tag{3.25}$$

3.3.4 Comparison: Linear versus Custom

In Fig. 3.6, a comparison between the three models defined in Sec. 3.3, namely *linear, quadratic, experimental*, is presented for ELA motor SH100/30. It is clear that in the first part of the graph, the linear model can be used to approximate the relation between torque and current until I reaches a value approximately equal to $2I_n$, beyond which the saturation phenomena and iron losses cause a decrease in the ratio of torque versus current. At a given torque value, the linear model underestimates the current and hence also losses. Besides, for the motor in consideration, quadratic and experimental model have no substantial differences.

Table 3.2: SH100 motor rated data, obtained from catalog [52]

Module type	**5 kHz**			**10 kHz**			**20 kHz**		
	k_{i0}	k_{i1}	k_{i2}	k_{i0}	k_{i1}	k_{i2}	k_{i0}	k_{i1}	k_{i2}
8BVI0014HxS	0.60	1.30	60	0.97	0.50	110	1.70	-0.70	225
8BVI0028HxS	0.60	1.30	60	0.97	0.50	110	1.70	-0.70	225
8BVI0055HxS	0.60	1.30	60	0.97	0.50	110	1.70	-0.70	225
8BVI0110HxS	0.15	5.60	55	0.49	4.70	95	0.87	-10.00	200
8BVI0220HxS	0.13	5.50	40	0.43	3.70	110	1.40	1.97	230
8BVI0330HxS	0.07	7.30	40	0.20	11.10	130	1.85	3.80	300
8BVI0440HxS	0.07	7.30	40	0.20	11.10	130	1.85	3.80	300
8BVI0660HxS	0.03	7.90	90	0.11	11.00	185	0.1	27.00	310
8BVI0880HxS	0.03	7.90	90	0.11	11.00	185	0.1	27.00	310

3.4 Losses Model

The purpose of this section is to relate electric losses to motor mechanical operating conditions: given axis architecture and load (torque-speed characteristic), the motor model defined in Sec. 3.3 can achieve the task by transforming (M, ω_m) quantities in (I, ω) space. In particular, Eq. (3.14) and Eq. (3.7) allows for going from mechanical quantities to electrical ones, and vice versa (the functions are defined to be invertible inside their domain). In Sec. 3.4.1, every source of losses is analyzed and a mathematical model is defined.

3.4.1 Mathematical model

Inverter Losses

For a IGBT-based VSI the losses are expresses as [53][54]

$$P_{inv} = \frac{6}{\pi} \cdot f_s \cdot (E_{ON.I} + E_{OFF.I} + E_{OFF.D}) \cdot \frac{V_{dc}}{V_{ref}} \frac{i_L}{i_{ref}} \tag{3.26}$$

where f_s is the VSI switching frequency; V_{dc} is the DC bus voltage; I_L is the peak value of the line current, assumable to be in a sinusoidal form. $E_{ON.I}, E_{OFF.I}, E_{OFF.D}$, are the turn-on and turn-off energy of the IGBT and turn-off energy of the diode, respectively. Including factors depending on devices and load, the power loss can be modeled by an experimental curve depending on current, according to [55]:

$$P_{inv} = k_{i0} + k_{i1} |I| + k_{i2} I^2 \tag{3.27}$$

Switching losses are mainly responsible for P_{inv}, but conduction losses and load-independent losses are not negligible. The coefficients k_i's depend on the switching frequency and have to be experimentally determined for several frequency values. Unfortunately this approach is limited by the scarce availability of inverter experimental data. An interpolation of available manufacturer data can be done to associate the parameters of modules having similar size but produced by different manufacturers, as long as the main characteristics remain the same. In Tab. 3.2, B&R inverter data are reported for $f_s = 5, 10, 20$ kHz [52].

Iron losses and Copper losses

The per-phase resistance R is available form manufacturer data, while the current can be determined from the torque using Eq. (3.14). Windings losses are easily evaluated by:

$$P_{Cu} = \frac{3}{2} R I^2 \tag{3.28}$$

Both eddy currents and hysteresis losses are proportional to peak flux density (see Eq. (3.3) and Eq. (3.4)) and excitation frequency ω. The assumption of fundamental frequency (no superior harmonics are considered) allows the equivalent resistance to be used as discussed in Sec. 3.3.2. A further simplification is presented in [38], where a model with core losses proportional to the square of the rate of change of flux density is shown and an average measured value is used for flux density. The result shows that the main influence of core losses is excitation frequency. In [55] a similar model is proposed. Hysteresis magnetizing losses are proportional to the fundamental frequency:

$$P_{Hy} = \widetilde{k}_{f1} \mid \omega_m| \tag{3.29}$$

The frequency ω is replaced with rotational speed given in Eq. (3.7) (different values of p corresponds to different coefficient values). Eddy current losses are assumed to increase quadratically with the fundamental frequency:

$$P_{Ed} = \widetilde{k}_{f2}\, \omega_m^2 \tag{3.30}$$

Accordingly, the motor electric losses P_{loss} are:

$$P_{loss} = \frac{3}{2} R I^2 + \widetilde{k}_{f1}\ |\omega_m| + \widetilde{k}_{f2}\, \omega_m^2 \tag{3.31}$$

Thus, the total electric power drawn by the servo-axis can be calculated by adding mechanical power $P_m = M\, \omega_m$:

$$P_{el,tot} = M\, \omega_m + \frac{3}{2} R I^2 + \widetilde{k}_{f1}\ |\omega_m| + \widetilde{k}_{f2}\, \omega_m^2 + k_{i0} + k_{i1}\, |I| + k_{i2} I^2 \tag{3.32}$$

By introducing the torque-current model, the electric power function of M and ω_m can be expressed as:

$$\begin{aligned} P_{el,tot}(M, \omega_m) =& M\, \omega_m + \frac{3}{2}\,(R + k_{i2})\, \left(g^{-1}(M)\right)^2 + \widetilde{k}_{f1}\ |\omega_m| + \\ &+ \widetilde{k}_{f2}\, \omega_m^2 + k_{i0} + k_{i1} \left| g^{-1}(M) \right| \end{aligned} \tag{3.33}$$

3.4.2 Speed-Torque characteristic

In order to infer the coefficients of Eq. (3.29) and Eq. (3.30) from rated data, several assumptions must be made. In Section 3.3.3 the thermal behavior of the motor was introduced. Let R_{th} be the thermal resistance measured in K/W; R_{th} can be assumed to be constant that mainly depends mainly on the type of installation. For thermal equilibrium, the temperature increase ΔT is proportional to heat dissipation due to motor electric losses:

$$P_{loss} = \frac{\Delta T}{R_{th}} \tag{3.34}$$

In fact, without dissipation, windings would be at ambient temperature. Assuming ΔT as constant implies that stationary working points are considered. The maximum value of P_{loss} that the conductors can bear without overheating is determined by the allowed temperature increase ΔT with respect to ambient conditions. When the stationary operating points are considered, in order to map the maximum continuous service that the motor can achieve, this maximum value can be assumed to be a constant, denoted P^*_{loss}.

It is useful to introduce power losses depending on rotational speed n expressed in [rev/min] (or rpm), with $n = \omega_m \cdot 60/2\pi$. By introducing coefficients k_{f1} and k_{f2} instead of $\widetilde{k}_{f1}$ and $\widetilde{k}_{f2}$ to take into account such a difference, the motor electric losses P_{loss} becomes:

$$P_{loss} = \frac{3}{2} R I^2 + k_{f1} \left| n \right| + k_{f2}\, n^2 \tag{3.35}$$

Equating losses and dissipation yields:

$$P^*_{loss} = \frac{3}{2} R I^2 + k_{f1} \left| n \right| + k_{f2}\, n^2 = \frac{\Delta T}{R_{th}} \tag{3.36}$$

Isolating current I in Eq. (3.36) gives the analytical expression of motor torque-speed characteristic, depending on which function g is implemented:

$$M(n) = g\left(\sqrt{\frac{2}{3} \frac{P^*_{loss} - k_{f1} \left| n \right| - k_{f2}\, n^2}{R}} \right) \tag{3.37}$$

3.4.3 Coefficient determination

In order to completely define the torque-speed characteristic, a total of three points on the continuous torque characteristic curve must be given to fully determine the three unknown quantities in Eq. (3.37), namely P^*_{loss}, k_{f1} and k_{f2}. Typically, two of them are listed in catalogs: nominal operation point (M_n, n_n) and stall point $(M_0, 0)$, and a third point (M_2, n_2) must be computed. This can be achieved by solving Eq. (3.36) after transforming the problem from the torque space to the current space.

Imposing Eq. (3.36) for the stationary operating point provides the constant quantity P^*_{loss}:

$$P^*_{loss} = \frac{\Delta T}{R_{th}} = P_{loss}\Big|_{n=0} = \frac{3}{2} R I_0'^{\,2} \tag{3.38}$$

Then, expressing losses in given points generates the following system of equations:

$$\begin{cases} P^*_{loss} = \dfrac{3}{2} R I_0'^{\,2} = \dfrac{3}{2} R I_n'^{\,2} + k_{f1} \left| n_n \right| + k_{f2}\, n_n^2 \\ P^*_{loss} = \dfrac{3}{2} R I_0'^{\,2} = \dfrac{3}{2} R I_2'^{\,2} + k_{f1} \left| n_2 \right| + k_{f2}\, n_2^2 \end{cases} \tag{3.39}$$

Equation (3.39) can be solved by taking the difference of the two equations and rearranging, leading to the following expression for k_{f1} and k_{f2}:

$$\begin{cases} k_{f1} = \dfrac{3}{2} R \left(I_0'^{\,2} \dfrac{n_n + n_2}{n_n\, n_2} + I_n'^{\,2} \dfrac{n_2}{n_n(n_n - n_2)} - I_2'^{\,2} \dfrac{n_n}{n_2(n_n - n_2)} \right) \\ k_{f2} = \dfrac{3}{2} R \left(-\dfrac{I_0'^{\,2}}{n_n\, n_2} - \dfrac{I_n'^{\,2}}{n_n(n_n - n_2)} + \dfrac{I_2'^{\,2}}{n_n(n_n - n_2)} \right) \end{cases} \tag{3.40}$$

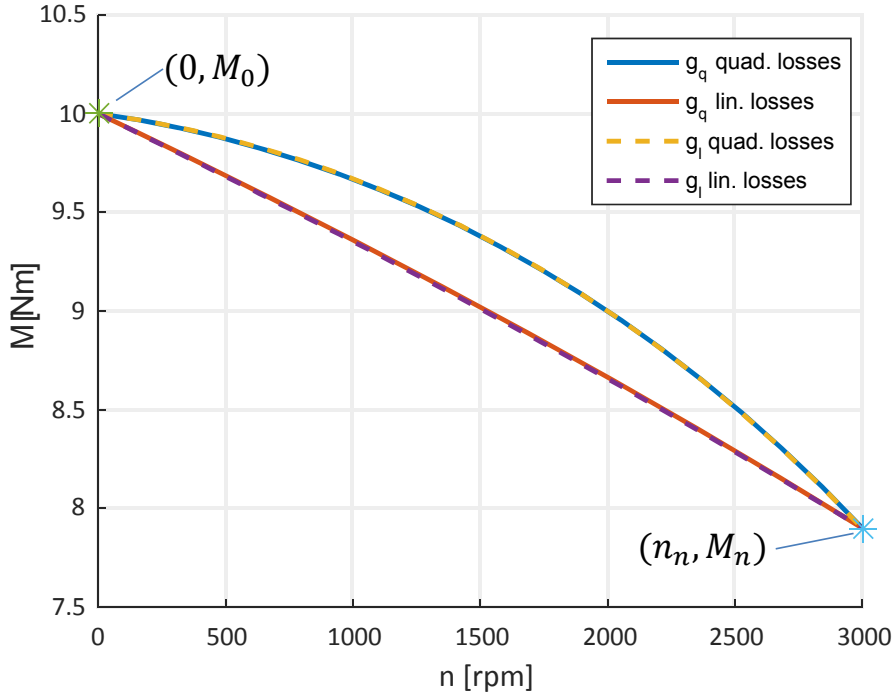

Figure 3.7: Comparison of linear, quadratic model and experimental models

If (M_2, n_2) is unknown or cannot be determined with sufficient precision (graphical determination from torque speed curve), the term proportional to k_{f2} can be disregarded and the system reduces to:

$$\frac{3}{2}RI_0^2 = \frac{3}{2}RI_n'^2 + k_{f1}\left|n_n\right| \longrightarrow k_{f1} = \frac{3}{2}\frac{R}{n_n}\left(I_0'^2 - I_n'^2\right) \tag{3.41}$$

Our loss model was applied to ELAU motor SH100, whose data reported in Tab. 3.1. An additional speed-torque point $(M_2, n_2) = (9, 2000)$ was determined from the graphical representation in Fig. 3.5. Coefficients k_{f1}, k_{f2} Were determined from Eq. (3.40) for both the linear-current model g_l and the quadratic torque-current model g_q. In Fig. 3.7, the torque-speed characteristic defined by Eq. (3.37) is presented for both quadratic (solid blue line) and linear loss model (solid red line). Linear-current models are represented as well with dotted lines (quadratic losses in yellow and linear losses in violet). As it can be seen, the torque-current model does not affect the speed torque characteristic in a considerable way, as the curves are almost overlapping. The quadratic loss model represents in a very satisfying way the manufacturer speed-torque characteristic given in Fig. 3.5.

On the other hand, the calculation of k_{f1}, k_{f2} and P_{loss} is indeed affected by the choice of torque current model. In Tab. 3.3 the mentioned coefficients for a quadratic loss model are reported, while in Tab. 3.4 coefficients for a linear loss model are reported. As can be seen, linear torque-current model underestimate losses.

3.4.4 Experimental ELAU loss model and validation

As for torque-current model in Sec. 3.3.3, an experimental loss model is available from ELAU for motor SH [52]. The model is based on internal measurement. The model is presented

Table 3.3: Quadratic Losses coefficients

	Quadratic current g_q	Linear Current g_l
k_{f1}	$4.268 \cdot 10^{-3}$	$3.558 \cdot 10^{-3}$
k_{f2}	$3.439 \cdot 10^{-6}$	$3.134 \cdot 10^{-6}$

Table 3.4: Linear Losses coefficients

	Quadratic current g_q	Linear Current g_l
k_{f1}	$14.5877 \cdot 10^{-3}$	$12.962 \cdot 10^{-3}$
k_{f2}	0	0

here and coefficients are reported, and used for comparison with our model.

Regarding iron losses, both linear and quadratic dependency on the fundamental frequency are present, along with temperature and square current term:

$$P_{Fe,xp} = \left(c_{f,1}\,|n| + c_{f,2}\,n^2\right)\left(1 + c_{f,3}\,I^2 - c_{f,4}\Delta T\right) \tag{3.42}$$

For windings losses, the dependence of resistance on temperature is emphasized. As previously stated, ΔT is kept constant at 80°.

$$P_{Cu,xp} = c_{c,1} I^2 + c_{c,2}\Delta T\, I^2 \tag{3.43}$$

Inverter losses are dependent on switching frequency, and are approximated by a 4-th degree polynomial function of the rotational speed. In Tab. 3.5, coefficients c_i's are given for two values of the switching frequency f_s: 4 kHz and 8kHz.

$$P_{inv,xp} = c_{inv,0} + c_{inv,1}\,|n| + c_{inv,2} n^2 + c_{inv,3}\,|n|^3 + c_{inv,4} n^4 \tag{3.44}$$

A simple dynamic task is now analyzed in order to compare mode presented in Sec. 3.4l with the experimental model. The system consists of a PMSM motor driving a four-bar mechanism, with a constant resistant force acting on the rocker. An harmonic trajectory is considered. The acceleration motor profile is $\ddot{\theta}_m = A_p \sin(\omega_0\, t)$, $t \in [0, t_c]$, where $\omega_0 = 2\pi/t_c$. Initial position and velocity are set to zero ($\theta_m(0) = \dot{\theta}_m(0) = 0$); since the acceleration has an average mean value of zero, after a period t_c the velocity returns to zero ($\dot{\theta}_m(t_c) = 0$). Coefficient A_p is set to achieve the condition $\theta_m(t_c) = 2\pi$, i.e. to make a full motorshaft revolution, so $A_p = 2\,\pi\omega_0/t_c$. The system is at full stop at $t = 0$, it accelerates and it decelerates to achieve a full motor revolution, and then returns to a full stop. The load profile $M(t)$ is given in Fig. 3.8 and the time cycle is set to $t_c = 0.1$. Under these conditions, the maximum motor speed is $n = 1200$ rpm and the maximum acceleration is $\ddot{\theta}_m = 3947$ rad/s^2. The mechanical power for achieving the task and the corresponding electric power drawn by the motor is shown in Fig. 3.9. The dotted red line represents the electric power computed by means of the experimental model of motor SH100, i.e. the sum of mechanical power P_m and $P_{Fe,xp}$, $P_{Cu,xp}$. The solid yellow line represents the same quantity computed with the custom electric motor model. In this particular case, the custom model slightly underestimates electric losses, but nevertheless is satisfyingly consistent with the experimental model.

Table 3.5: Experimental ELAU SH100 coefficients

	$i=0$	$i=1$	$i=2$	$i=3$	$i=4$
$c_{f,i}$		$8.77 \cdot 10^{-3}$	$7.99 \cdot 10^{-3}$	$1.12 \cdot 10^{-2}$	$7.9 \cdot 10^{-3}$
$c_{c,i}$		2.517	$1.0718 \cdot 10^{-2}$		
$c_{inv,i}$ (4kHz)	4.859	$5.725 \cdot 10^{-3}$	$4.791 \cdot 10^{-6}$	$-1.925 \cdot 10^{-9}$	$1.621 \cdot 10^{-13}$
$c_{inv,i}$ (8kHz)	3.661	$8.263 \cdot 10^{-3}$	$9.069 \cdot 10^{-6}$	$-4.167 \cdot 10^{-9}$	$4.387 \cdot 10^{-13}$

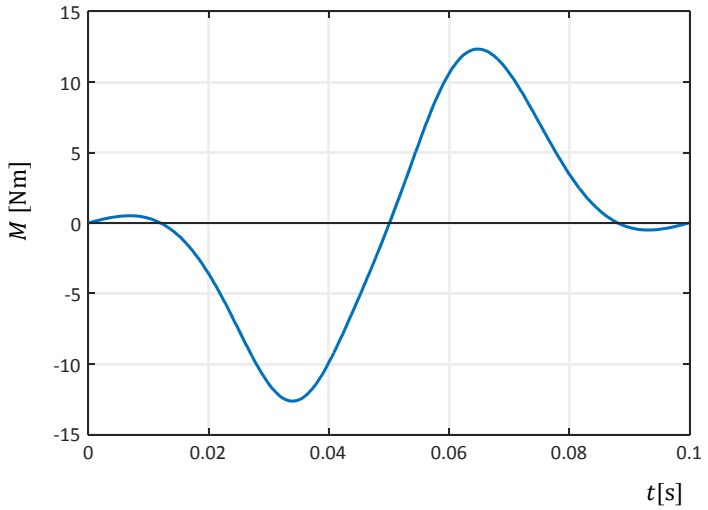

Figure 3.8: Motor torque for a harmonic law of motion and constant resistive torque on a 4-bar linkage

3.5 Motor Efficiency

Generally speaking, efficiency can be evaluated as the ratio of the energy required to achieve the task versus the actual energy used to achieve the task. The efficiency of an electric motor can be defined as:

$$\eta = \frac{P_m}{P_{el}} = \frac{P_m}{P_m + P_{loss}} \tag{3.45}$$

Electric motor efficiency is often disregarded during the drive selection process. In other words, if the motor can provide the mechanical power P_m, the absorbed power P_{el} is often not taken into account.

Mechanical power is the product of torque M and rotational speed ω_m. Electric motor loss P_{loss} was defined in Sec. 3.4.1 as a function of excitation frequency and stator current. The introduction of the torque-current model in Eq. (3.14) and rotational speed relation in Eq. (3.7), makes η a function of (M, ω_m) as well. The motor efficiency is thus evaluated as:

$$\eta(M, \omega_m) = \frac{M\,\omega_m}{M\,\omega_m + \frac{3}{2}R\,[g^{-1}(M)]^2 + \widetilde{k}_{f1}\,|\omega_m| + \widetilde{k}_{f2}\,\omega_m^2} \tag{3.46}$$

It is useful to combine motor efficiency with the speed-torque characteristic: the full expres-

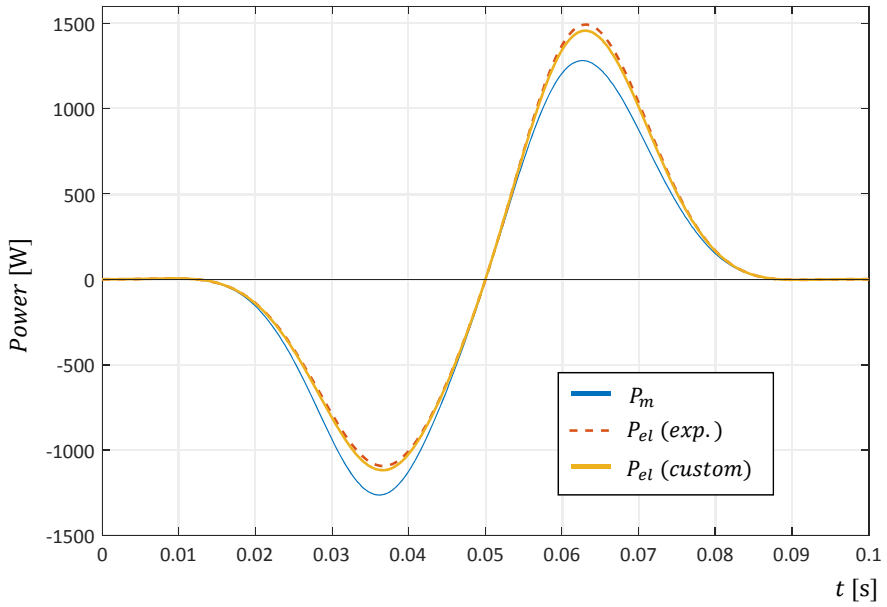

Figure 3.9: In blue: mechanical power to be provided to the shaft. Dotted red: electric power drawn by the motor, computed by the experimental model. In yellow: electric power drawn by the motor, compute with custom model.

sion can be obtained from Eqs. (3.14), (3.35) and (3.45). The contour map for ELAU motor SH100 is presented in Fig. 3.11, where iso-efficiency curves are drawn. The best efficiency zone is around and above the nominal conditions.

It is obvious that the efficiency drops at low speed or low torque. The reason for this phenomenon is that the amount of losses remains more or less unchanged while the mechanical power is at its minimum, and therefore the former has a bigger impact. The figure reported represents the custom loss model proposed in this chapter, with quadratic current-torque relation and iron losses being proportional to both linear and square rotational speed terms.

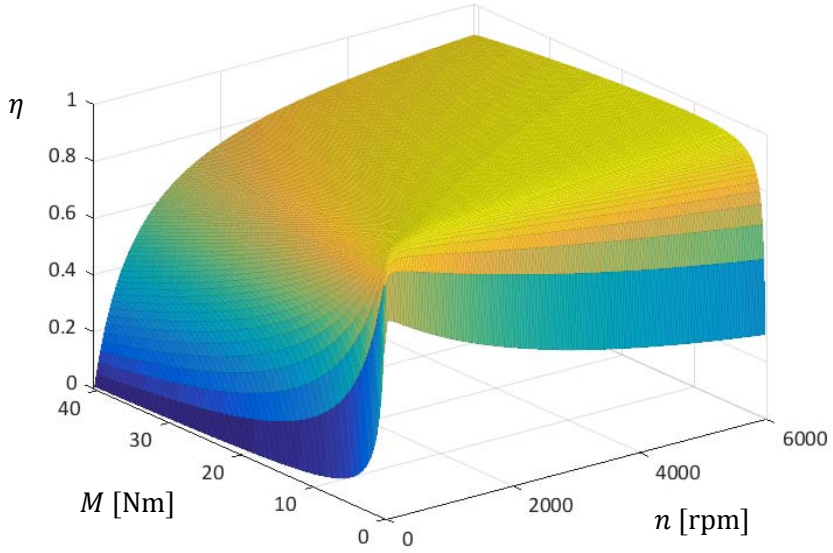

Figure 3.10: Efficiency for ELAU SH100 motor, represented as a function of torque M, rotational speed n

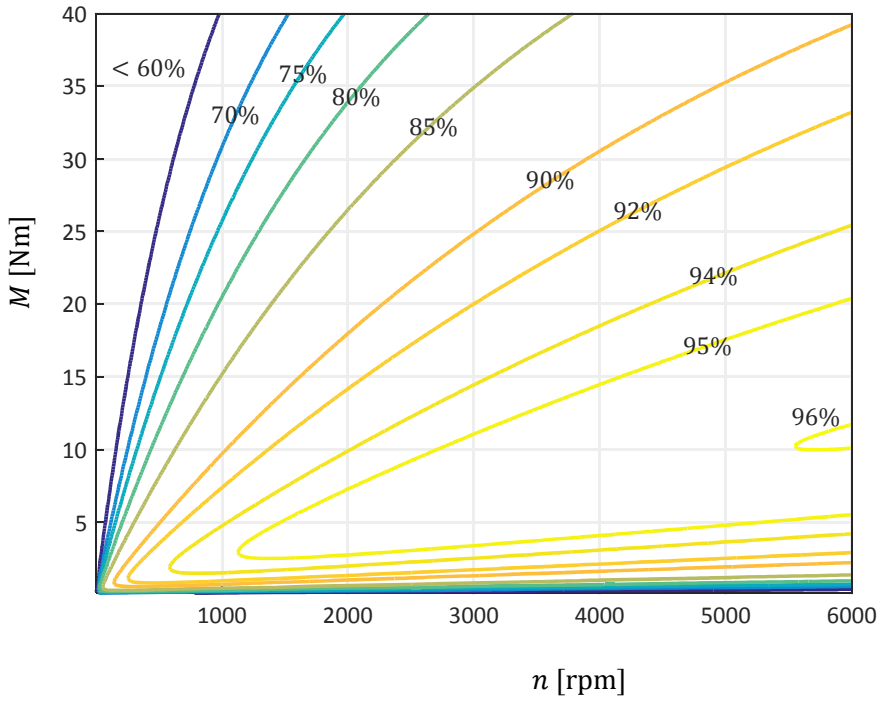

Figure 3.11: Efficiency of motor ELAU SH100, represented as a contour map over motor operating range. The iso-efficiency lines are highlighted.

Chapter 4

Optimal selection of the motor-reducer unit: discrete approach

In this chapter the optimal selection of the motor-reducer unit for a servo-axis is analyzed. The motor and the reducer are selected from a list of manufacturers' catalog. The optimal choice minimizes a user-defined objective function. Section 4.1 and Section 4.2 present the problem formulation and the most common objective functions used for the optimization. Section 4.3 deals with the selection procedure for different objective functions.

4.1 Introduction

4.1.1 Description of the problem

The selection of components is a ubiquitous and critical process in the design phase of an automatic machine. The definition of a generic optimal selection procedure is the key to efficient design of automatic machines.

Several issues may arise during component selection. First, the information available for selection may be inadequate to accurately account for the actual impact of the components that are chosen, since the model may still be incomplete: the introduction of unmodeled inertias, energy loss and elasticity may drastically modify the dynamic behavior of the system. In other words, the exact dynamic analysis cannot be performed before all components are chosen, and yet components cannot be properly chosen before the dynamic analysis is performed. For instance, the selection of the motor-reducer unit is bounded by several constraints that depend both on the motor and the gearbox reducer, which are not known before the selection is completed.

The sizing of the motor-reducer unit has a great impact on the dynamic performance of the system, and the goal of this chapter is to define a method that allows the selection of the best motor-reducer pair that minimizes a user-defined objective function.

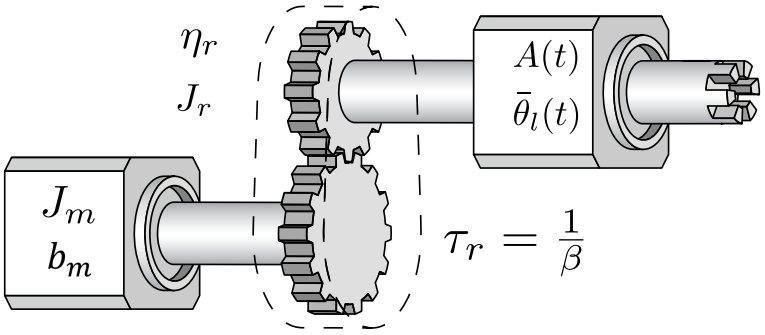

Figure 4.1: Notation for a Gearbox reducer.

4.1.2 Introduction of ideal gearbox reducer

As shown in Fig. 4.1, a gearbox reducer is introduced after the motor, at the beginning of the transmission chain. The reducer is assumed to have a constant transmission ratio τ_r, an inertia J_r reduced to the shaft connected to the motor, and a global reducer efficiency η_r.

A generic load linked to the output shaft of the reducer exerts a torque $A(t)$ at rotational speed ω_l. Since in most cases the load rotational speed is lower than the motor high-efficiency speed range, τ_r is often lower than 1. The reciprocal of transmission ratio $\beta = 1/\tau_r$ is referred to as the *gear ratio*.

The torque M that the electric motor can provide was introduced in Chapter 3 as a function of the drawn current; once the motor is attached to the transmission chain, it is always equal to the torque C_m provided at the motor shaft. Introducing the viscous damping effect on the motor as a resistive torque (Sec. 2.4.4), the total torque M is:

$$\begin{aligned} M(t) &= (J_m + J_r)\,\dot{\omega}_m(t) + \frac{A(t)}{\beta\,\hat{\eta}_r} + b_m\omega_m(t) \\ &= \beta\,[(J_m + J_r)\,\dot{\omega}_l + b_m\omega_l] + \frac{A}{\beta\,\hat{\eta}_r} \end{aligned} \tag{4.1}$$

where $\omega_m = \beta\,\omega_l$, J_r is the gearbox inertia reflected at the motor shaft. The efficiency function $\hat{\eta}_r$ is the defined as (see Eq. (2.23)):

$$\hat{\eta} = \begin{cases} \eta_{r,dir} & A\omega_l > 0 \\ \dfrac{1}{\eta_{r,inv}} & A\omega_l < 0 \end{cases} \tag{4.2}$$

where it is assumed $\eta_{r,dir} = \eta_{r,inv} = \eta_r$, and $A\omega_l$ is the power that the load is exchanging with the reducer. Sometimes, the reducer is assumed to be ideal: in this case, it is responsible of speed variation, but it does not introduce further inertia or losses (i.e. $J_r = 0$ and $\hat{\eta}_r = 1$). The zero reducer inertia assumption is often reasonable because of the dominating motor inertia. The coefficient b_m is the damping coefficient as defined in Eq. (2.39). In most of the optimization studies about the selection of moto-reducer unit, this term is disregarded [10], [16].

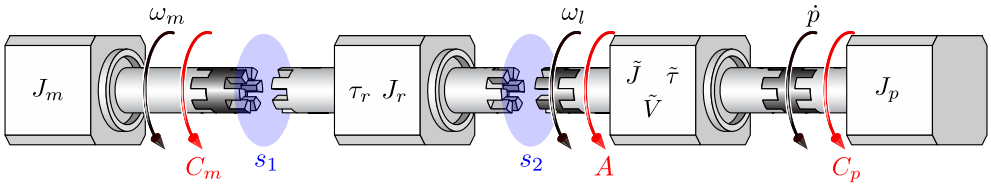

Figure 4.2: Model diagram of a servo-axis, with the introduction of a gearbox reducer between the motor and the rest of the transmission

Evaluation of load torque $A(t)$

The torque $A(t)$ depends on end-effector motion, load profile and the transmission architecture. In automatic machinery applications, the load can often be assumed to be purely inertial, since usually no external forces are applied to the end-effector (e.g., in a motion task). In [3, 56, 6] A is analytically determined only in the case of a purely inertial load with a constant inertia rotating at velocity ω_l,. When a generic load is considered [6], $A(t)$ is obtained from a multi-body simulation. In this section, the generic analytical expression of A is given for a 1-DoF serial system with variable inertia and external load.

In order to do that, we use the lumped-parameter model defined in Sec. 2.4. Consider the model including the gearbox reducer, as shown in Fig. 4.2. In the absence of the gearbox, section s_1 coincides with section s_2; the torque A applied at the first node of the transmission chain coincides with C_m, and the equation of motion is given by Eq. (2.40). When the gearbox is present, the torque A at s_2 is found by subtracting from Eq. (2.40) the motor inertia contribution and the motor damping torque (Eq. (2.39)). Alternatively, Eq. (2.29) can be applied sequentially to infer A. In both cases, the expression of A is:

$$A = \tilde{J}\dot{\omega}_m + \frac{1}{2}\tilde{J}'\omega_m^2 + \tilde{V}' - \tilde{C}_p \tag{4.3}$$

In the above equation, $\tilde{J}, \tilde{J}', \tilde{V}'$ are known functions since the transmission architecture is assumed to be known at this design stage. Moreover, once the target task is assigned to the servo-axis, both end-effector motion $\overline{p}(t)$ and force profiles $C_p(t)$ are known. Then, the motion profile $\overline{\theta}_l(t)$ is a known quantity[1], since it can be determined by means of inverse kinematic analysis from $\overline{p}(t)$. In particular, if we denote the transmission ratio of the equivalent block by $\tilde{\tau}$, $\omega_l = \dot{p}/\tilde{\tau}$ (see Eq. (2.30)). Since $\tilde{J}, \tilde{J}'$, $\tilde{V}'$ and $\tilde{C}_p$ are dependent on position θ_l, A is a function of the motion law $\overline{\theta}_l(t)$ and it ca be present and explicit dependence on time.

4.2 Objective functions

Before addressing the optimization phase, optimal selection criteria must be defined. First, the motor-gearbox pair must be able to achieve the target task. As seen in Sec. 3.3.2, PMSM have limitations on operating range, due to thermal and mechanical reasons. Consequently, there are also limitations on maximum motor torque and speed. The gearbox is responsible for torque and speed limitations as well (e.g. the maximum torque that the slow shaft can bear and the maximum speed of roller bearings), but is dominated by the PMSM limitations.

[1]For consistency, the vector containing displacement, velocity and acceleration at s_2 is defined as $\overline{\theta}_l = (\theta_l, \dot{\theta}_l, \ddot{\theta}_l) = (\theta_l, \omega_l, \dot{\omega}_l)$.

On the other hand, there is a big impact of gearbox reducer on the operating range of the motor (and consequently of the system), because the transmission ratio significantly influences the dynamic performances, such as required torques and speeds.

The optimization problem consists in the minimization of a user-defined objective function f_o, where f_o depends on system parameters and operating conditions. The constraints on motor and gearbox are expressed as inequalities, where a given parameter f_b computed for the system (e.g., maximum load speed) must be smaller than a given bound f_{limit}. One can naturally define f_b as an objective function. In facts, since $f_b \leq f_{limit}$, the minimization of f_b leads to two results: first, the feasibility analysis of the inequality constraints is included in the optimization; second, it allows for the selection of the most suitable component.

The choice of f_o depends on the application: even quantities which do not set constraints on the system can be chosen. For instance, we may want to minimize the system energy consumption from the electric grid: the upper bound for such functions are undefined.

4.2.1 The constraints on motor selection

First, the motor selection conditions are presented. As previously mentioned, the motor usually presents the strictest limitations on both torque and velocity.

Root-Mean-Square Torque

The root-mean-square value of the required motor torque M over a period t_c is:

$$M_{RMS} = \sqrt{\frac{1}{t_c}\int_0^{t_c} M^2(t)\,dt} \tag{4.4}$$

As discussed in Sec. 3.4, the current circulating in a conductor causes heat to be dissipated into the environment, thereby causing an increase of winding temperature. Since the motor torque is proportional to the current, and the Joule effect is proportional to square current, the RMS value takes into account of the heating of conductors. The RMS torque must be smaller than the nominal torque M_n given by the motor manufacturer, in order to prevent the winding insulation from reaching unsafe overheating temperature. Therefore, the thermal behavior of PMSM in a cycle is represented by the scalar quantity M_{RMS}, which is time independent. The torque $M(t)$ can instantaneously assume values bigger than M_n, only if the $M_{RMS} \leq M_n$ condition still holds over a cycle.

It is easily noticed that M_{RMS} is equal to the L_2-norm [2] of M, so $M_{RMS} = \|M\|_2$. Thus, the thermal limit for continuous operation is $\|M\|_2 \leq M_n$.

[2] The L_p-norm of a quantity f is defined as:

$$\|f\|_p = \left(\frac{1}{t_c}\int_0^{t_c} |f(t)|^p dt\right)^{\frac{1}{p}}$$

Table 4.1: PMSM limits: continuous torque, peak torque and maximum speed.

Continuous torque limit	$\|M\|_2 \leq M_n$
Peak torque limit	$\|M\|_\infty = \max(M) \leq M_{\max}$
Maximum speed limit	$\|\omega_m\|_\infty = \max(\omega_m) \leq \omega_{m,\max}$

Maximum torque

If the current value in stator windings becomes too large, it will cause the permanent magnets to demagnetize [44], even irreversibly. Since the torque is proportional to the stator current, the motor must never exceed the maximum torque value $M_{\max}$. The value of $M_{\max}$ is not constant and depends on motor speed ω_m; in fact, over a certain speed range, the demagnetization current curve is cut by the voltage drop curve, generating the characteristic curve pictured in Fig. 3.5.

Following the L_p-norm convention, the L_∞-norm is the maximum value of L. Accordingly, the maximum-torque condition may be expressed as:

$$\|M\|_\infty = \max_{t\in[0,t_c]} \{|M(t,\omega_m)|\} \leq M_{\max}(\omega_m(t)),\ \forall \omega_m \geq 0 \tag{4.5}$$

Maximum speed

There are both mechanical and electric limitations on maximum motor speed. In the former case, the centrifugal forces generated by the rotation of masses affects bearings' life. In the latter case, if the rotor speed is too high, the magnetic field generated by permanent magnets unlocks from the magnetic filed generated by motor windings and loses synchronicity. The intersection of the two constraints defines the maximum rotor speed, which we denote by $\omega_{m,\max}$ or $n_{\max}$. Usually the mechanical limit is dominating [46]. The mathematical expression is given in Tab. 4.1, where all types of motor limits are summarized.

4.2.2 Unbounded objective functions

While the motor limits must be respected in every application, the definition of objective functions depends on specific needs and is therefore strongly task-oriented. For example, if fixed costs are taken into account, the minimization of the RMS torque may be sufficient, since the size, and thus the cost, of a PMSM is proportional to the rated torque M_n. In a new generation automatic machine, electric energy is exchanged between the DC bus and the single servo-axes; several energy fluxes are present, and electric losses have an appreciable impact on the global efficiency.

In Chapter 3 the expression of instantaneous electric power $P_{el,tot}$ drawn by the drive was presented (see Eq. (3.1)). The energy drawn by the servo-axis over a period t_c is:

$$E_{total} = \int_0^{t_c} P_{el,tot}\, dt = \int_0^{t_c} P_m\, dt + \int_0^{t_c} P_{Cu}\, dt + \int_0^{t_c} P_{Fe}\, dt + \int_0^{t_c} P_{Inv}\, dt \tag{4.6}$$

which is a sum of four contributions: mechanical power P_m, windings losses P_{Cu}, iron losses P_{Fe} and inverter losses P_{inv}, integrated over a cycle. Minimizing the energy E_{total} is the same as minimizing the average electric power $(P_{el,tot})_{mean}$, since they differ only by a constant $1/t_c$.

Considering only the motor and recalling that P_{el} is defined as the power provided by the inverter to the motor (see Eq. (3.45)), , the energy absorbed by the motor over a cycle is:

$$E_{mot} = \int_0^{t_c} P_m\, dt + \int_0^{t_c} P_{Cu}\, dt + \int_0^{t_c} P_{Fe}\, dt \tag{4.7}$$

which differs from E_{mot} since the inverter contribution is not considered. The RMS value of the power exchange is not as indicative as the RMS torque, since there is no relation to physical quantities. The L_∞-norm of P_{el} or $P_{el,tot}$ is occasionally relevant, since some electrical components, such as capacitors, are sized according to the maximum power transfer value.

4.3 Discrete approach

As we have briefly introduced at the beginning of this chapter, a main issue arises during the selection of moto-reducer unit: the motor and gearbox characteristics, which are unknown at the moment of the selection, influence the dynamic behavior of the system. Consequently, the constraints that the components impose on the system cannot be verified until a choice is taken. For instance, the torque required from the motor to achieve the task is influenced by the motor inertia J_m, the reducer inertia J_r and the efficiency $\hat{\eta}_r$, which are unknown, as it is the motor rated torque M_n. Usually several assumptionsare made to simplify the problem, e.g., considering an ideal reducer (with zero inertia and unitary efficiency). Moreover, the selection procedure must be tailored for the information available from catalogs of motors and gearboxes. It is important to find a good balance between the theoretical rigor of the procedure and the practicality of its implementation. Various researchers addressed the problem (see, among others, the series of works by Cusimano [6], Van de Straete [3], and Giberti [12]) and proposed procedures where, under specific assumptions, an ideal selection is first made; then, the accuracy of the solution is verified under real-case conditions. If the solution is not correct, a new selection is made. The process is thus iterative, and each step consists of two phases:

- *Feasibility analysis phase*, where a population of motors is evaluated, and for each motor a range of admissible transmission ratios is found. The motors that cannot drive the load are excluded, regardless of transmission ratio.
- *Optimization phase*, where additional criteria are introduced in order to select the best motor-reducer pair. Comparisons are made between admissible motors paired with different transmission ratios, and the best choice is found.

Since the motor collection is a discrete list, on the basis of their commercial availability, we refer to this try-and-verify approach as a *discrete approach*.

4.3.1 Optimization for the root-mean-square torque value

For the feasibility analysis, aimed at establishing whether the motor can drive the load or not regardless the value of β, an ideal transmission is considered. At this stage, the motor moment of inertia is supposed to be known, since the procedure is repeated for every motor available in the catalog. By implementing the selection criterion used in [12], the value for an optimal gear ratio that minimizes the RMS torque of the motor is found for an ideal transmission without motor damping. Thus, assuming $J_r = 0$, $\hat{\eta}_r = 1$ and $b_m = 0 : \; b_m = 0$, the torque Eq. (4.1) becomes:

$$M(t, \beta) = J_m \beta \dot{\omega}_l(t) + \frac{A(t)}{\beta} \tag{4.8}$$

Computing the RMS value of Eq. (4.8) gives:

$$\begin{aligned} M_{RMS}^2 =& \int_0^{t_c} \frac{1}{t_c} \left(J_m \beta \dot{\omega}_l + \frac{A}{\beta} \right)^2 dt \\ =& J_m^2 \beta^2 \int_0^{t_c} \frac{1}{t_c} \dot{\omega}_l^2 dt + \frac{1}{\beta^2} \int_0^{t_c} \frac{1}{t_c} A^2 dt + 2 J_m \int_0^{t_c} \frac{1}{t_c} \left(A \dot{\omega}_l \right) dt \\ =& J_m^2 \beta^2 \dot{\omega}_{l,RMS}^2 + \frac{A_{RMS}^2}{\beta^2} + 2 J_m \left(A \, \dot{\omega}_l \right)_{mean} \end{aligned} \tag{4.9}$$

where $A_{RMS} = \|A\|_2$ and $\dot{\omega}_{l,RMS} = \|\dot{\omega}_l\|_2$ are the L_2-norm of load quantities and $\left(A \, \dot{\omega}_l \right)_{mean}$ is the average value of the mutual product. The inequality representing the thermal problem is $M_{RMS}^2 \leq M_n^2$(see the first of Tab. 4.1). Dividing both sides by the motor moment of inertia J_m gives:

$$J_m \beta^2 \dot{\omega}_{l,RMS}^2 + \frac{A_{RMS}^2}{J_m \beta^2} + 2 \left(A \, \dot{\omega}_l \right)_{mean} \leq \frac{M_n^2}{J_m} \tag{4.10}$$

Equation (4.10) is solved for a given motor to find the range of transmission ratios under which the motor can drive the load. It is a second order inequality where β is the unknown. We also introduce the *accelerating factor* ε and the *load factor* ν:

$$\begin{aligned} \varepsilon =& \frac{M_n^2}{J_m} \\ \nu =& 2 \left[\dot{\omega}_{l,RMS} A_{RMS} + \left(A \, \dot{\omega}_l \right)_{mean} \right] \end{aligned} \tag{4.11}$$

where the accelerating factor ε is also referred to as *power factor*. The coefficient ε does not depend on the task and it is defined exclusively by the motor parameters. Both ε and ν are measured in $[W/s]$. Substituting Eq. (4.11) in Eq. (4.10) leads to:

$$\nu + \left[\frac{A_{RMS}}{\beta \sqrt{J_m}} - \dot{\omega}_{l,RMS} \, \beta \sqrt{J_m} \right]^2 \leq \varepsilon \tag{4.12}$$

Since the second term at the RHS is always nonnegative, ν is the minimum value that the RHS can assume. The ideal transmission gear ratio that minimizes the RMS value of the torque may be obtained by equaling to zero the term inside the bracket in Eq. (4.12):

$$\beta_{M_{RMS}}^* = \sqrt{\frac{A_{RMS}}{J_m \, \dot{\omega}_{l,RMS}}} \tag{4.13}$$

Equation (4.12) also gives the range of admissible gear ratios. Solving the inequality, the boundary values for the admissible gear ratios are:

$$\begin{cases} \beta_{\max} = \dfrac{\sqrt{A_{RMS}}}{J_m} \dfrac{1}{\sqrt{\varepsilon - \nu + 4\ \dot{\omega}_{l,RMS}\ A_{RMS}} - \sqrt{\varepsilon - \nu}} \\ \beta_{\min} = \dfrac{\sqrt{A_{RMS}}}{J_m} \dfrac{1}{\sqrt{\varepsilon - \nu + 4\ \dot{\omega}_{l,RMS}\ A_{RMS}} + \sqrt{\varepsilon - \nu}} \end{cases} \tag{4.14}$$

The motor is able to drive the load if the range defined by boundaries $[\beta_{\min}, \beta_{\max}]$ is not empty, i.e. if, $\beta_{\min}$ and $\beta_{\max}$ exist and are real numbers. Every $\beta \in [\beta_{\min}, \beta_{\max}]$ is suitable for achieving the task.

4.3.2 Optimization for the energy drawn by the motor

The results obtained in Sec. 4.3.1 only refer to minimization of RMS torque. If the energy drawn by the servo mechanism is considered as an objective function instead, the optimization seeks an optimal gear ratio that is generally different from the one provided by Eq. (4.13). Nevertheless, since Eq. (4.10) still holds, suitable gear ratios must still be inside the range defined in Eq. (4.14).

Rezazadeh *et al.* [17] derived the optimal gear ratio that minimizes the total energy drawn by the motor from the electric source. The analysis is performed for DC motors, but it may be extended to PMSM as well. While the gearbox is considered to be ideal, the electric windings losses and the losses generated by the resistive viscous damping torque are taken into account: the former are proportional to square current, the latter are obtained by multiplying the damping torque in Eq. (2.39) by the motor speed . No iron losses are considered, and the current-torque relation is modeled as purely linear. This is the most general case found in literature.

Here, a complete electric motor model is considered and we derive the most general expression of the gear ratio minimizing the absorbed energy, which we denote by $\beta^*_{E_{mot}}$. The gearbox reducer is ideal, but along the windings losses and damping losses, the motor iron losses are taken into account. In Chapter 3, the losses coefficients of the model were defined for a generic motor and extracted from rated data; the drawn energy is evaluated by Eq. (4.7).

The total power drawn by the motor is the sum of mechanical power P_m and electrical losses P_{loss}. The motor torque is given by Eq. (4.1). Since an ideal transmission is studied, introducing $\hat{\eta} = 1$ and $J_r = 0$ leads to:

$$M = \beta \left(J_m \dot{\omega}_l + b_m \omega_l \right) + \frac{A}{\beta} \tag{4.15}$$

We compute P_m as the product between the motor speed ω_m and the torque in Eq. (4.15). We also introduce $\omega_m = \beta \omega_l$, obtaining:

$$\begin{aligned} P_m = M\, \omega_m &= \left[\beta \left(J_m \dot{\omega}_l + b_m \omega_l \right) + \frac{A}{\beta} \right] \beta \omega_l \\ &= \beta^2 \left(J_m \dot{\omega}_l \omega_l + b_m \omega_l^2 \right) + A \omega_l \end{aligned} \tag{4.16}$$

For the sake of convenience, we recall here Eq. (3.14) for torque-current relation and Eq. (3.31) for modeling P_{loss}. Accordingly, the two components of P_{loss} are the windings losses (see Eq. (3.28)) and the iron losses (see Eqs. (3.29), (3.30)):

$$\begin{aligned} P_{Cu} &= \frac{3}{2} R I^2 = \frac{3}{2} R \left[g(M)^{-1} \right]^2 \\ P_{Fe} &= \widetilde{k}_{f1}\, \omega_l\, \beta + \widetilde{k}_{f2}\, \omega_l^2\, \beta^2 \end{aligned} \tag{4.17}$$

The minimum value of $E_{mot}(\beta)$ may be found by setting $dE_{mot}/d\beta = 0$, namely:

$$\begin{aligned} \frac{dE_{mot}}{d\beta} =& \frac{dE_m}{d\beta} + \frac{dE_{Cu}}{d\beta} + \frac{dE_{Fe}}{d\beta} \\ =& \frac{d}{d\beta}\left(\int_0^{t_c} P_m\, dt \right) + \frac{d}{d\beta}\left(\int_0^{t_c} P_{Cu}\, dt \right) + \frac{d}{d\beta}\left(\int_0^{t_c} P_{Fe}\, dt \right) \\ =& \int_0^{t_c} \frac{\partial P_m}{\partial \beta} + \int_0^{t_c} \frac{\partial P_{Cu}}{\partial \beta} + \int_0^{t_c} \frac{\partial P_{Fe}}{\partial \beta} = 0 \end{aligned} \tag{4.18}$$

where Leibniz integral rule is used [57] to switch integral and differential operators as long as the integral function P_m and its derivative with respect to β are both continuous in $t \in [0, t_c]$. For the sake of clarity clarity, each term in Eq. (4.18) is evaluated separately. First,

$$\begin{aligned} \frac{dE_m}{d\beta} =& \int_0^{t_c} \frac{\partial P_m}{\partial \beta}\, dt = \int_0^{t_c} \left[2\beta \left(J_m \dot{\omega}_l \omega_l + b_m \omega_l^2 \right) \right] dt = \\ =& 2\beta \left(J_m \int_0^{t_c} \dot{\omega}_l \omega_l\, dt + b_m \int_0^{t_c} \omega_l^2\, dt \right) \end{aligned} \tag{4.19}$$

where the gear ratio β and J_m are not function of time and can be moved outside the integral operator. On the other hand, the terms $\dot{\omega}_l \omega_l$ and ω_l^2 are a function of time. As far as iron losses are concerned:

$$\begin{aligned} \frac{dE_{Fe}}{d\beta} =& \int_0^{t_c} \frac{\partial\, P_{Fe}}{\partial \beta}\, dt = \int_0^{t_c} \left(\widetilde{k}_{f1}\, |\omega_l| + 2\beta\, \widetilde{k}_{f2}\, \omega_l^2 \right) dt \\ =& \widetilde{k}_{f1} \int_0^{t_c} |\omega_l|\, dt + 2\beta\, \widetilde{k}_{f2} \int_0^{t_c} \omega_l^2\, dt \end{aligned} \tag{4.20}$$

In order to formulate $dE_{Cu}/d\beta = 0$, several considerations must be made about $g(I)$ and its inverse $g^{-1}(M)$. It is assumed that the function g has class C^1 and is invertible in the domain $[-I_{\max}, I_{\max}]$, with co-domain $[-M_{\max}, M_{\max}]$. Although this condition is sufficient for our computation, further considerations can be made on g. It is assumed that the torque-current characteristic of PMSM is the same regardless of the electric machine working as a motor or as a generator. This means that the characteristic curve of the motor is symmetric, i.e., the bijective function g can be defined in the first quadrant of reference system (I, M) and then be mirrored onto all other quadrants. For every point (I, M) inside the box $I \times M = [-I_{\max}, I_{\max}] \times [-M_{\max}, M_{\max}]$, the relation $|M| = g(|I|)$ is true. Conversely, the relation $|I| = g^{-1}(|M|)$ completely defines the inverse function. This assumption simplifies the analytical definition of function g, without loss of any generality.

That being said, the derivative dg/dI is well defined and continue in its domain. The differentiation of energy due to copper losses is thus:

$$\frac{dE_{Cu}}{d\beta} = \int_0^{t_c} \frac{\partial P_{Cu}}{\partial \beta}\, dt = \frac{3}{2} R \int_0^T \frac{\partial}{\partial \beta} \left[g^{-1}(M(\beta, t)) \right]^2 dt = \\ = \frac{3}{2} R \int_0^T 2\, g^{-1}(M)\, \frac{\partial g^{-1}(M)}{\partial M} \frac{\partial M}{\partial \beta} dt$$

where the partial derivative of M with respect to β is computed from Eq. (4.15) as:

$$\frac{\partial M}{\partial \beta} = J_m \dot{\omega}_l + b_m \omega_l - \frac{A}{\beta^2} \tag{4.21}$$

By using the differentiation rule for inverse function [58], we obtain:

$$\frac{dE_{Cu}}{d\beta} = \frac{3}{2} R \int_0^T 2\, g^{-1}(M) \frac{1}{\dfrac{dg}{dI}\left(g^{-1}(M)\right)} \frac{\partial M}{\partial \beta}\, dt \tag{4.22}$$

Hence, the gear ratio $\beta^*_{E_{mot}} \in \mathbb{R}^+$ that minimizes the energy drawn by the motor is the solution of equation:

$$2\beta \left[J_m \int_0^{t_c} \dot{\omega}_l \omega_l\, dt + b_m \int_0^{t_c} \omega_l^2\, dt + \widetilde{k}_{f2} \int_0^{t_c} \omega_l^2\, dt \right] + \widetilde{k}_{f1} \int_0^{t_c} |\omega_l|\, dt + \\ + \frac{3}{2} R \left[\int_0^{t_c} \frac{2\, g^{-1}(M)}{\dfrac{dg}{dI}\left(g^{-1}(M)\right)} \left(J_m \dot{\omega}_l + b_m \omega_l - \frac{A}{\beta^2} \right) dt \right] = 0 \tag{4.23}$$

The solution $\beta^*_{E_{mot}}$ covers the most general case presented in the literature, and it depends on the torque-current model implemented. Here two cases are presented, on the basis of the two models defined in Chapter 3.

Linear torque-current model

The linear torque current model is characterized by the function g_l defined in Eq. (3.15):

$$\begin{cases} M = g_l(I) = k_t\, I \\ I = g_l^{-1}(M) = \dfrac{M}{k_t} \\ \dfrac{dg_l}{dI}(I) = k_t \end{cases} \tag{4.24}$$

Hence, the contribute to differential energy of windings losses defined in Eq. (4.22) can be rearranged as:

$$\begin{aligned} \frac{dE_{Cu}}{d\beta} &= \frac{3}{2} R \int_0^{t_c} 2 \frac{M}{k_t^2} \left(\frac{\partial M}{\partial \beta} \right) dt \\ &= \frac{3R}{2\, k_t^2} \int_0^{t_c} \left(\beta \left(J_m \dot{\omega}_l + b_m \omega_l \right) + \frac{A}{\beta} \right) \left(J_m \dot{\omega}_l + b_m \omega_l - \frac{A}{\beta^2} \right) dt \\ &= \frac{3R}{2\, k_t^2} \int_0^{t_c} \left(\beta \left(J_m \dot{\omega}_l + b_m \omega_l \right)^2 - \frac{A^2}{\beta^3} \right) dt \\ &= \beta \frac{3R}{2\, k_t^2} \left(J_m^2 \int_0^{t_c} \dot{\omega}_l^2\, dt + b_m^2 \int_0^{t_c} \omega_l^2\, dt + 2 J_m b_m \int_0^{t_c} \dot{\omega}_l \omega_l \right) - \frac{1}{\beta^3} \frac{3R}{2\, k_t^2} \int_0^{t_c} A^2\, dt \end{aligned} \tag{4.25}$$

where Eqs. (4.21), (4.15) were introduced. Since the function g_l is particularly simple, it is possible to derive an analytical expression for $\beta^*_{E_{mot}}$. Summing the components defined in Eqs. (4.16), (4.17), and substituting $I^2 = M^2/k_t^2$, the electric motor power P_{el} is expressed as:

$$P_{el} = \beta^2 w + \beta q + s + \frac{u}{\beta^2} \tag{4.26}$$

where w, q, s, u are time-dependent coefficients hence defined by:

$$\begin{cases} w(t) = \dfrac{3\,R}{2\,k_t^2}\left(J_m\dot{\omega}_l + b_m\omega_l\right)^2 + \omega_l^2\widetilde{k}_{f2} + J_m\dot{\omega}_l\omega_l \\ q(t) = |\omega_l|\widetilde{k}_{f1} \\ s(t) = A\,\omega_l + \dfrac{3\,R}{k_t^2}\,J_m\dot{\omega}_l\,A \\ u(t) = \dfrac{3\,A^2\,R}{2\,k_t^2} \end{cases} \tag{4.27}$$

The energy drawn by the motor is given by:

$$E_{mot} = \beta^2 W + \beta Q + S + \frac{U}{\beta^2} \tag{4.28}$$

where capital letters indicate the integral of the aforementioned coefficients for $t \in [0, t_c]$,

By deriving and multiplying every term by β^3, and excluding the trivial solution $\beta = 0$, the optimum condition emerges from the following quartic equation:

$$\frac{dE_{mot}}{d\beta} = 2\,\beta^4 W + Q\,\beta^3 - 2\,U = 0 \tag{4.29}$$

which can be solved analytically [59] or numerically. Disregarding iron losses, Eq. (4.29) becomes a bi-quadratic equation ($q = 0$) and $\beta^*_{E_{mot}}$ coincides with the one found in [17]. It may be interesting noticing that for a cyclic load the integral of the terms $\dot{\omega}_l\omega_l$ and $\dot{\omega}_l^2$ over a cycle are zero. If b_m is set to zero, $\beta^*_{E_{mot}}$, coincides with $\beta^*_{M_{RMS}}$ of Eq. (4.13).

Quadratic torque-current model

The quadraatic torque-current model is characterized by the function g_q defined by Eq. (3.18) and Eq. (3.20).

$$\begin{cases} g_q(I) = k_{t1}|I| + k_{t2}I^2 \\ g_q^{-1}(|M|) = -\dfrac{k_{t1}}{2k_{t2}} + \dfrac{\sqrt{k_{t1}^2 - 4k_{t2}\,|M|}}{2k_{t2}} \\ \dfrac{dg_q}{dI}(I) = k_{t1} + 2\,k_{t2}I \end{cases} \tag{4.30}$$

Since the domain of g_q is defined as $[0, I_{\max}]$, g_q is always positive. In order to guarantee that the co-domain of g_q coincides with the domain of g_q^{-1}, M is replaced by its the absolute value in the equation. This does not affect the motor behavior, under the assumption that a PMSM has a symmetric operating range. The derivative of E_{Cu} with respect to β is the only term that is affected by the change of the torque-current model, and is given by:

$$\frac{dE_{Cu}}{d\beta} = \frac{3}{2}R\int_0^T \left(\frac{1}{k_{t2}} - \frac{\operatorname{sgn}(M)\,k_{t1}}{k_{t2}\sqrt{k_{t1}^2 - 4k_{t2}\,|M|}}\right)\frac{\partial M}{\partial\beta}dt$$

which is obtained from Eq. (4.22) and with further simplification. For the quadratic torque-current model, no analytic expression is available for $\beta^*_{E_{mot}}$ and the Eq. (4.18) is solved numerically. The function *sign* takes into account in the derivative of the absolute value introduced on M.

4.3.3 Optimization for Energy drawn by the electric grid

If the power loss during switching P_{inv} is taken into account, the corresponding energy loss must be introduced and denoted by E_{inv}. The total energy E_{total} is evaluated by summing E_{mot} and E_{inv}. Since E_{mot} is already known from Sec. 4.3.2, we shall only consider E_{inv} here. By recalling Eq. (3.27):

$$\begin{aligned}\frac{dE_{inv}}{d\beta} &= \int_0^{t_c} \frac{\partial P_{inv}}{\partial \beta}\, dt = \int_0^{t_c} \frac{\partial}{\partial \beta}\Big(k_{i0} + k_{i1}\,|I| + k_{i2} I^2\Big) dt = \\ &= k_{i1} \int_0^T \frac{\operatorname{sgn}(I)}{\dfrac{dg}{dI}\Big(g^{-1}(M)\Big)} \frac{\partial M}{\partial \beta}\, dt + k_{i2} \int_0^T \frac{2\, g^{-1}(M)}{\dfrac{dg}{dI}\Big(g^{-1}(M)\Big)} \frac{\partial M}{\partial \beta}\, dt\end{aligned} \tag{4.31}$$

where the square current term inside the integral is the same as that in Eq. (4.22). If g^{-1} is defined for the first torque-current quadrant, I is always positive and the signature function $\operatorname{sgn}(I)$ is equal to $+1$ (see considerations in Sec. 4.3.2).

The optimal gear ratio that minimizes total energy $\beta^*_{E_{total}}$ is the solution of the following equation:

$$\frac{dE_{total}}{d\beta} = \frac{dE_{mot}}{d\beta} + \frac{dE_{inv}}{d\beta} = 0 \tag{4.32}$$

where the switching loss contribution in Eq. (4.31) is introduced along the differential motor energy (see Eq. (4.29)).

4.3.4 Discrete selection criterion: a case study

In this section, a case study is presented related to motor database composed of SH motors, by manufacturer ELAU [51]. Motor data are obtained from the standard catalog: motors from small ($M_n \leq 1$ Nm) to medium-large size (M_n up to 45 Nm) are taken into account. The database is reported in Tab. 4.2.

The motion law $\omega_l, \dot{\omega}_l$ and the load torque A are presented in Fig. 4.3, and are obtained from a real case scenario, concerning an end-effector used for positioning the product inside an automatic machine. The load is cyclic with period $t_c = 0.12$.

The feasibility analysis begins by evaluating, for each motor, the accelerating factor ε and comparing it to load factor ν (see Eq. (4.11)). If $\varepsilon \leq \nu$, the motor cannot drive the load regardless of the transmission ratio. Since $\nu = 8.2 \cdot 10^4$ [W/s], motors $\mathcal{M}1$, $\mathcal{M}2$, $\mathcal{M}4$, $\mathcal{M}7$ and $\mathcal{M}15$ are discarded, as it is shown in Fig. 4.4. For each of the remaining motors, the available gear ratio range is calculated using Eq. (4.14). Please notice that, for motor $\mathcal{M}3$, that the accelerating factor is barely larger than the load factor; with $\varepsilon \simeq \nu$, the available gear ratio range approaches zero. Hence, $\mathcal{M}3$ is not a stable selection, since the minimum difference with the ideal case would lead to a non-feasible region.

Then, the optimal gear ratio that minimizes the energy drawn by the motor is found, without damping torque included in the analysis ($b_m = 0$). The procedures presented in

Table 4.2: Motor database: ELAU SH series [51]

Index	Name	M_n [Nm]	n_n [rpm]	J_m [kg cm^2]
$\mathcal{M}1$	SH-05580005	0.48	8000	0.059
$\mathcal{M}2$	SH-05580009	0.72	8000	0.096
$\mathcal{M}3$	SH-05580013	1.05	8000	0.134
$\mathcal{M}4$	SH-07060010	1.3	6000	0.25
$\mathcal{M}5$	SH-07060020	1.9	6000	0.41
$\mathcal{M}6$	SH-07060030	2.3	6000	0.58
$\mathcal{M}7$	SH-10050030	2.7	5000	1.4
$\mathcal{M}8$	SH-10040060	4.6	4000	2.31
$\mathcal{M}9$	SH-10040080	5.7	4000	3.22
$\mathcal{M}10$	SH-10030100	7.9	3000	4.22
$\mathcal{M}11$	SH-14030120	9.2	3000	7.41
$\mathcal{M}12$	SH-14030200	12.3	3000	12.68
$\mathcal{M}13$	SH-14030270	12.9	3000	17.94
$\mathcal{M}14$	SH-14030330	16.1	3000	23.7
$\mathcal{M}15$	SH-20530360	21	3000	71.4
$\mathcal{M}16$	SH-20520650	34	2000	129
$\mathcal{M}17$	SH-20520900	45	2000	190

Sec. 4.3.2 are compared, with results shown in Fig. 4.5. For the sake of clarity, only the results for motors from $\mathcal{M}8$ to $\mathcal{M}14$ are represented in the figure (the complete results are given in Tab. 4.3). Moreover, the reciprocal of the gear ratio β, i.e., the transmission ratio $\tau_r = 1/\beta$, is presented with a logarithmic scale. The range of available transmission ratio is bounded by a minimum value (blue triangle) and a maximum value (red triangle) (see Eq. (4.14)). The value of $\beta^*_{M_{RMS}}$ that minimizes M_{RMS} is denoted by a blue dot; notice that $\beta^*_{M_{RMS}}$ is centered inside the range, if a logarithmic scale is used [12]. A yellow circle represents the optimal value $\beta^*_{E_{mot}}$ considering only windings losses and no iron losses, as in [17]. However, for a cyclic load without motor damping ($b_m = 0$), this value coincides with $\beta^*_{M_{RMS}}$. Since in automatic machines this scenario is common, it does not provide extra information for optimal selection. The green cross and the black asterisk represent values of $\beta^*_{E_{mot}}$ obtained with different torque-current models: the former is obtained if the liner torque-current model is used (i.e. the solution of Eq. (4.29)), whereas the latter is obtained if the quadratic torque current-model is used. The linear model provides a quadratic equation to be analytically solved. On the other hand, the quadratic model guarantee a higher accuracy, and the method is still relatively simple to implement and Eq. (4.18) can be solved numerically. The results for motor $\mathcal{M}9$ are shown on the right side of Fig. 4.5, in order to highlight the differences between methods. In this case, $\beta^*_{M_{RMS}} = 1.968$. The linear torque-current model leads to $\beta^*_{E_{mot}} = 1.772$ ($\tau_r = 0.566$), whereas the quadratic torque-current model leads to $\beta^*_{E_{mot}} = 1.801$ ($\tau_r = 0.555$).

Once the above analysis is performed, the actual energy absorbed by every available motor is evaluated. The optimal motor choice features the lowest energy consumption per cycle. In Fig. 4.6, the motor energy consumption as a function of the transmission ratio $\tau_r = 1/\beta$ is shown for motors $\mathcal{M}8$ through $\mathcal{M}14$. Every curve represents a different motor, with the minimum of each curve highlighted; $\mathcal{M}10$ is the best motor within the subset, with $\beta^* = 1.5623$ and corresponding value $E_{mot} = 7.59$ J.

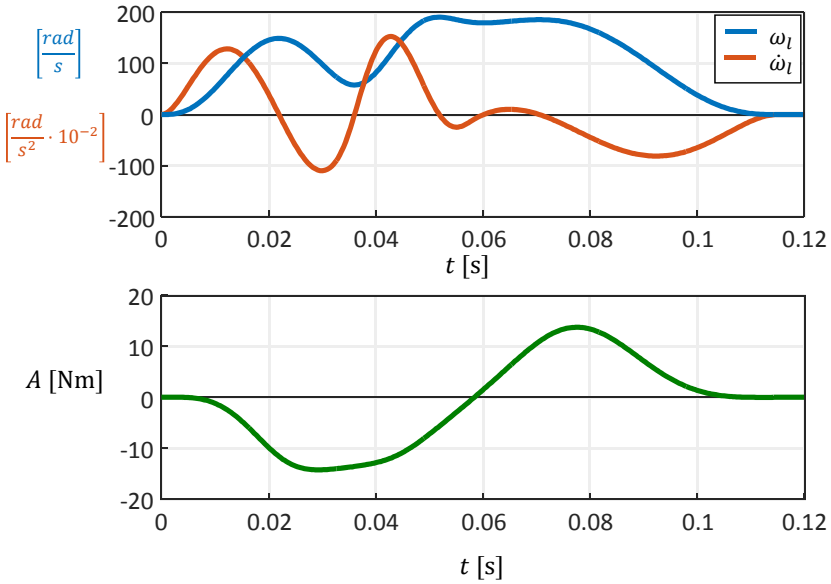

Figure 4.3: Load profile of motion and load torque A for an end-effector utilized in a packaging automatic machine

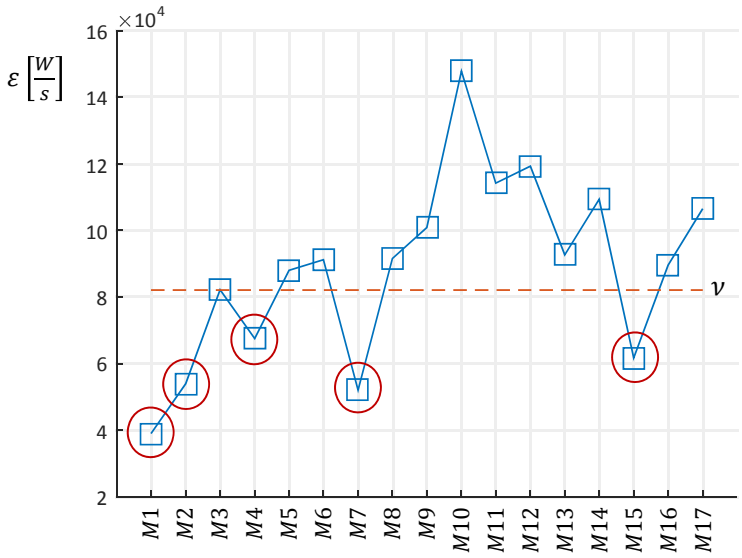

Figure 4.4: Feasibility analysis: motors $\mathcal{M}1$, $\mathcal{M}2$, $\mathcal{M}4$, $\mathcal{M}7$ and $\mathcal{M}15$ cannot drive the load regardless of transmission ratio

Overall results

In Tab. 4.3, the results of the analysis for all motors are given. First, the value $\beta^*_{M_{RMS}}$ is shown for each available motor, along with the corresponding value $M_{RMS}(\beta^*_{M_{RMS}})$. The value $\beta^*_{E_{mot}}$ is found by implementing the quadratic torque-current model, and the correspondent value of E_{mot} is shown, computed in $\beta^*_{E_{mot}}$. Then, $\beta^*_{E_{tot}}$ and the correspondent value of objective function $E_{tot}(\beta^*_{E_{tot}})$ are given.

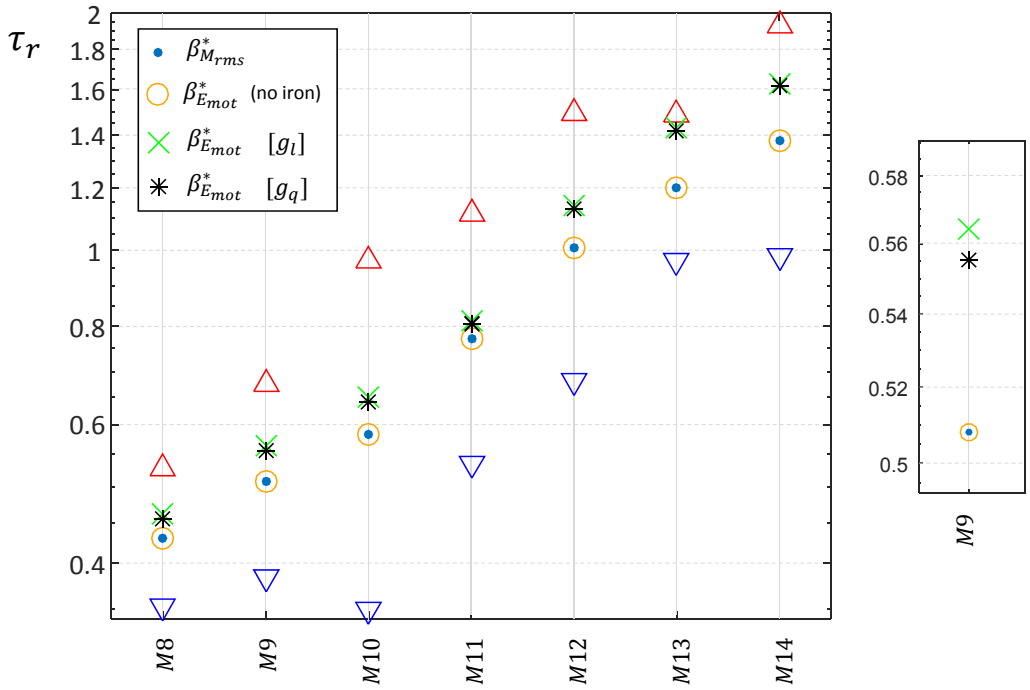

Figure 4.5: Optimal values of τ_r for motors from $\mathcal{M}8$ through $\mathcal{M}14$, with a focus on motor $\mathcal{M}9$.

Motor $\mathcal{M}3$ is the best overall choice for all the considered objective functions M_{RMS}, E_{mot} and E_{tot}. It should be noticed, however, that $\mathcal{M}3$ has an accelerating factor ε barely larger than the load factor ν (see Fig. 4.4). Hence, the range of values β that satisfy Eq. (4.12) is small, since, from Eq. (4.14), it must be $9.41 < \beta < 9.89$. This situation is not suitable for a practical selection, since the real-case scenario uncertainties may lead to a not feasible choice. Therefore,s the selection of motor $\mathcal{M}5$ is more consistent. The choice of motor $\mathcal{M}10$ minimizes both E_{mot} and E_{tot} in the subset $\mathcal{M}8$ through $\mathcal{M}14$.

Once the optimal motor has been determined, several checks must be performed in order to ensure that the selected combination can achieve the task. The gearbox reducer was represented as an ideal transmission ratio, so far. The first issue to be addressed is the discretization of the transmission ratios available on the catalog: since β^* is determined analytically, it is unlikely that this exact value is commercially available. If we rule out custom made reducers, a first gap between real and ideal conditions is introduced. Furthermore, once the reducer is selected, the transmission inertia and the real operation efficiency must be introduced, which cause a further discrepancy. Eventually, the inequalities in Tab. 4.1 must be checked after a choice is made, and if the requirements are not fulfilled, the process must be repeated. Although we will not consider this phase detail, several authors have addressed this problem and defined corresponding guidelines for automatized procedures. For instance, in [10], a comprehensive approach is presented for the motor thermal problem. It features the alternation of direct and inverse power flow and the introduction of transmission inertia. The problem is solved by means of graphical diagrams.

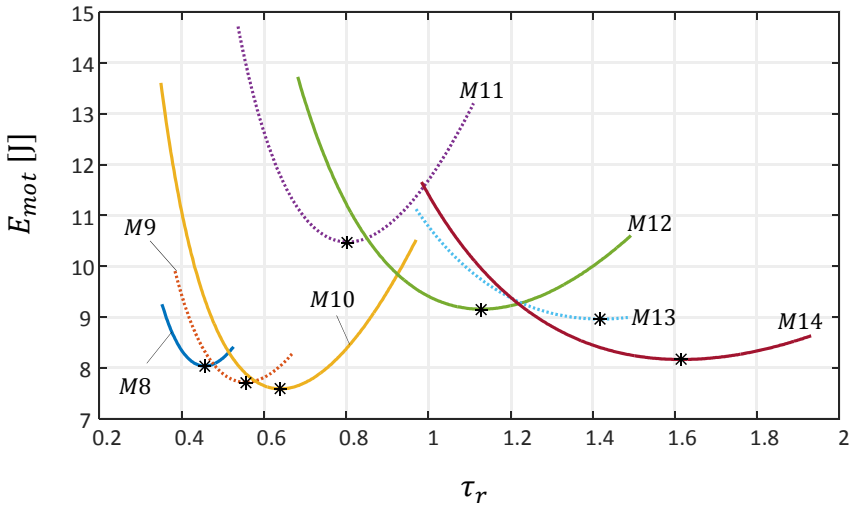

Figure 4.6: Motor energy E_{mot}, computed for every motor from $\mathcal{M}9$ through $\mathcal{M}14$, with the minimum being highlighted.

4.3.5 Optimization for motor torque peak value

The motor torque peak value $\|M\|_\infty$ is given in Eq. (4.5). The problem of minimizing the peak value of function $M(\beta, t)$ is not trivial even for the ideal case (see Eq. (4.8)). The shape of the function $M(\beta, t)$ highly depends on functions $\dot{\omega}(t)$ and $A(t)$, which depend on the specific application. [14, 15] addressed the problem by presenting an analytical procedure for selecting the optimal transmission ratio and motor minimizing $\|M\|_\infty$. The procedure is comprehensive, but rather complex. In this work, the same problem is addressed from a different viewpoint: we aim at giving an interpretation of the mathematical problem more than defining an alternative optimization procedure.

The first step is to isolate the local stationary points of function $M(\beta, t)$. Fixing β, differentiating M with respect to time and imposing the first-order optimality condition give the time instants at which $M(\beta, t)$ reaches a stationary point. For each value of β, these time instants assume different values. Considering the ideal case with no damping ($\hat{\eta} = 1$, $J_r = 0$ and $b_m = 0$), the motor torque is given by Eq. (4.8). Differentiating with respect to time yields:

$$\frac{\partial M(\beta, t)}{\partial t} = J_m \beta \ddot{\omega}_l + \frac{\dot{A}}{\beta} = 0 \qquad \Longrightarrow \qquad t_i(\beta) \quad (i = 1, \ldots, n) \tag{4.33}$$

Eq. (4.33) may be solved numerically, and it generally admits several solutions, say n, i.e., the curve $M(\beta, t)$ has n stationary points. Among these points, the one with the largest absolute value is the one we wish to minimize. The number of stationary points and the times t_i depend on the gear ratio β. From a geometrical point of view, the curves $t_i(\beta)$ $(i = 1, \ldots, n)$, represent what we call *time patterns* of stationary points with respect to β. We indicate by $M_{st,i}$ the value of the torque along the i-th pattern, i.e. $M_{st,i}(\beta) = M(\beta, t_i(\beta))$. The objective function that must be minimized is the maximum value of the absolute values of $M_{st,i}$ $(i = 1, \ldots, n)$ for each β:

$$\|M\|_\infty = \max\left(|M_{st,i}(\beta)|\right) \quad \forall \beta \tag{4.34}$$

Table 4.3: Results of discrete optimization, for all motors. The values presented in the table include $\beta^*_{M_{rms}}$, $\beta^*_{E_{mot}}$ (computed with quadratic torque-current model) and $\beta^*_{E_{tot}}$. The value of M_{RMS}, E_{mot} and E_{tot} are given for the corresponding optimal gear ratio.

Index	$\beta^*_{M_{RMS}}$	$M_{RMS}(\beta^*_{M_{RMS}})$	$\beta^*_{E_{mot}}$	$E_{mot}(\beta^*_{E_{mot}})$	$\beta^*_{E_{tot}}$	$E_{tot}(\beta^*_{E_{tot}})$
$\mathcal{M}1$	-	-	-	-	-	-
$\mathcal{M}2$	-	-	-	-	-	-
$\mathcal{M}3$	9.6467	1.05 Nm	9.2704	6.025 J	9.2858	13.614 J
$\mathcal{M}4$	-	-	-	-	-	-
$\mathcal{M}5$	5.5149	1.83 Nm	5.2545	6.437 J	5.2760	14.395 J
$\mathcal{M}6$	4.6368	2.18 Nm	4.1765	6.884 J	4.2347	15.056 J
$\mathcal{M}7$	-	-	-	-	-	-
$\mathcal{M}8$	2.3234	4.36 Nm	2.1947	8.036 J	2.1986	16.698 J
$\mathcal{M}9$	1.9679	5.14 Nm	1.8014	7.715 J	1.8177	16.830 J
$\mathcal{M}10$	1.7190	5.89 Nm	1.5623	7.587 J	1.5755	14.471 J
$\mathcal{M}11$	1.2972	7.80 Nm	1.2442	10.475 J	1.2434	18.550 J
$\mathcal{M}12$	0.9917	10.02 Nm	0.8860	9.156 J	0.9057	18.242 J
$\mathcal{M}13$	0.8337	12.14 Nm	0.7049	8.960 J	0.7385	18.661 J
$\mathcal{M}14$	0.7254	13.95 Nm	0.6191	8.165 J	0.6490	19.627 J
$\mathcal{M}15$	-	-	-	-	-	-
$\mathcal{M}16$	0.3109	32.54 Nm	0.2908	15.666 J	0.2932	31.689 J
$\mathcal{M}17$	0.2562	39.50 Nm	0.2374	12.874 J	0.2409	29.992 J

Here, a graphical representation of the mathematical problem is provided, taking into consideration the case study presented in Sec. 4.3.4. For the sake of clarity, the problem is studied in the domain $\beta \in [2, 100]$, which corresponds to $\tau_r = \in [0.01, 0.5]$, with $J_m = 0.06 \cdot 10^{-4}$ kgm^2. Such choices may not be appropriate for a practical selection, but nevertheless they lead to a satisfactory representation, which is the goal of this section. By numerically solving Eq. (4.33), we can find the time patterns $t_i(\beta)\,(i = 1, \ldots, 6)$, at which M has a stationary point. In Fig. 4.7, patterns t_i's are shown as functions of $\tau_r = 1/\beta$, which is presented with a base-10 logarithmic scale. A total of $n = 6$ solutions are found, where the solution t_3 presents a bifurcation (black line) into two branches t_{3a} and t_{3b}. Besides, the pattern t_3 does not assume real values in every point of the considered domain.

In order to investigate the nature of these stationary points, M is represented by a surface dependent on time and transmission ratio τ_r (linear scale). In Fig. 4.8, the curves representing $M_{st,i}\,(i = 1, \ldots, n)$ are shown with colors consistent with those of the patterns t_i's in Fig. 4.7. As β approaches infinity (τ_r approaches zero), the torque presents the same trend as $\dot{\omega}_l$, since the term $J_m\dot{\omega}_l\beta$ approaches infinity and the term A/β approaches zero. When β approaches zero (τ_r approaches infinity), the inertial term approaches zero whereas the term A/β becomes dominant. The trend of function M is influenced by this behavior, and so is the distribution of stationary points. The stationary points denoted by $M_{st,3}$ (black line) vanish when the contribution of A/β becomes dominant; this happens for low values of β (high values of τ_r).

Finally, we evaluate the objective function $\|M\|_\infty$ defined in Eq. (4.34). In Fig. 4.9, the absolute values of $M_{st,i}(\beta)\,(i = 1, \ldots, n)$ are shown. For each β, $\|M\|_\infty$ is given by the largest of $|M_{st,i}|\,(i = 1, \ldots, n)$. In this case, the objective function to minimize is:

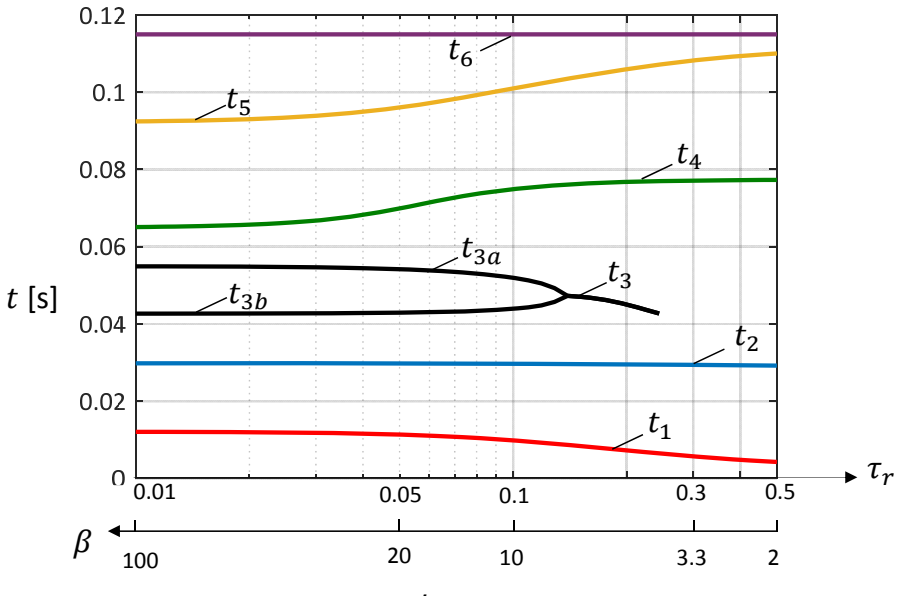

Figure 4.7: Time patterns $t_i\,(i = 1, \ldots, n)$ of Eq. (4.33) in a domain $\beta \in [2, 100]$.

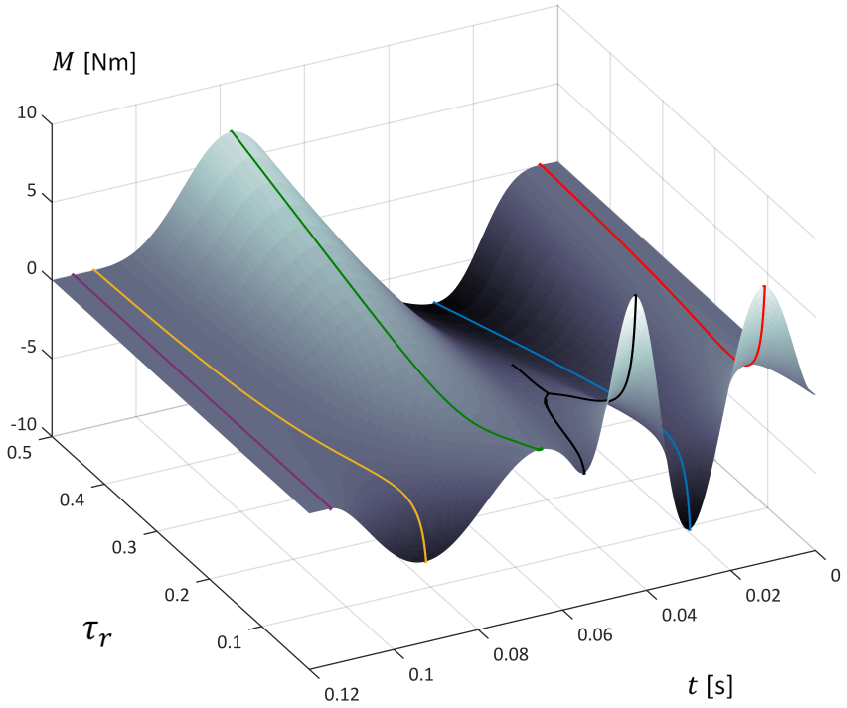

Figure 4.8: Values of the torque $M_{st,i}\,(i = 1, \ldots, n)$, computed along $t_i(\beta)$

$$\|M\|_\infty = \begin{cases} |M_{st,3b}| & \beta < 32.26 \\ |M_{st,2}| & \beta > 32.26 \end{cases} \tag{4.35}$$

We can see that the optimal transmission ratio, that minimizes the peak value of the motor torque, is $\beta^*_{M_{peak}} = 14.71$.

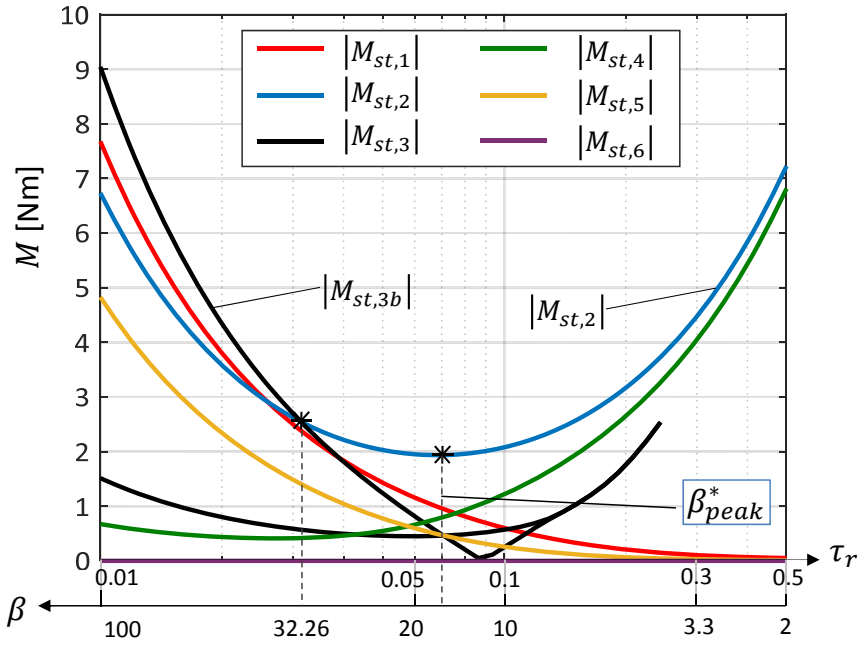

Figure 4.9: Values of $|M_{st,i}|\,(i = 1, \ldots, n)$. $\|M\|_\infty$ is given, for each β, by the largest value of $|M_{st,i}|\,(i = 1, \ldots, n)$.

Chapter 5

Optimal selection for the motor-reducer unit: continuous approach

In Chapter 4 the optimal selection of the motor-reducer unit was carried out by a discrete approach, namely the motor catalog was scanned in order to find the optimal operating conditions of each motor. The motor-reducer unit selection process is iterative in nature, since every motor has its own characteristics that influence the dynamic behavior of the system, which in turn influences the selection. The procedure is applied under specific assumptions; after a first choice is made, the solution is verified in a real case scenario; if verification fails, the process is repeated. In this chapter, in order to overcome these limitations, a new mathematical procedure is developed. Section 5.1 introduces a continuous version of the discrete approach, while Sec. 5.2 presents a method to extend the available motor list to a continuous virtual catalog. Section 5.3 casts the selection process into a constrained nonlinear optimization problem. Sections 5.4, 5.5 and 5.6 present an application of the optimization procedure to several objective functions including RMS motor torque, energy absorbed by the motor and energy absorbed by the servo-axis.

5.1 Introduction

Given a list of commercially available components, a *size index* is defined to identify the size of a single component with respect to the size of the total population. Consider the motors listed in Tab. 4.2 for example. The list is ordered by nominal torque. The size index α maps the list, such that each value of the index represent a different motor. Since the range of α is arbitrary, the simplest choice is to assign $\alpha = 0$ to represent the smallest motor and $\alpha = 1$ for the largest. In a commercially available catalog, α can assume only a discrete sequence of values $\alpha_j \, (j = 1, \dots, N_{mot})$, where N_{mot} is the number of motors considered. Each α_j is associated to a set of parameters $\xi_i \, (i = 1, \dots, N_{par})$ characterizing the $j-$th motor, such as the mass moment of inertia J_m or the statoric resistance R. N_{par} is the number of parameters taken into consideration. We denote the set of parameters depending on α, i.e. on the motor size, as $\overline{\xi}_\alpha$. The values $\overline{\xi}_\alpha(\alpha_j) \, (j = 1, \dots, N_{mot})$, can be found in manufacturers' catalogs.

In this chapter, the discrete population of available components is extended to a con-

tinuous catalog, such that each value of $\alpha \in [0,1]$ represents an available choice, thereby establishing a one-to-one correspondence. The selection problem is reduced to the determination of a suitable value of α. Consequently, the i-th parameter, denoted ξ_i, is a continuous function of α defined over the interval $[0,1]$. Once the continuous set $\overline{\xi}_\alpha(\alpha)$ is defined, the continuous component catalog is fully characterized.

Analogously, the size index β maps the reducer catalog. The set of continuous functions $\overline{\xi}_\beta(\beta)$ is determined, comprising the characteristic parameters of the reducer. The union of the two continuous sets forms the set $\overline{\xi}(\alpha,\beta)$, where $\overline{\xi} = (\overline{\xi}_\beta, \overline{\xi}_\beta)$. This set of continuous functions allows us to solve the optimal selection problem without iterations, since all inertia and efficiency parameters may be introduced at the beginning of the optimization. After the determination of the optimal values α^* and β^*, the nearest components available in the commercial catalog may be chosen and then verified; alternatively, custom components can also be built.

5.2 Definition of a continuous catalog

5.2.1 Discrete values of set $\overline{\xi}$

Consider the motor population defined in Table 4.2, where $N_{mot} = 17$. The value α_j corresponds to motor $\mathcal{M}_j$. By definition, $\alpha_1 = 0$ and $\alpha_{N_{mot}} = 1$. Using a linear interpolation, we can assign to each motor a unique value α_j according to the following uniformly spaced sequence:

$$\alpha_j = \frac{j-1}{N_{mot}-1} \qquad j = 1, \ldots, N_{mot} \tag{5.1}$$

As for the gearbox reducer, the gear ratio β may serve as a size index: in fact, during the discrete optimization approach, it was already used as a continuous variable. The commercial catalog gives us a list of discrete values $\beta_k\,(k = 1, \ldots, N_{red})$ and parameters $\xi_i(\beta_j)$ (e.g., reducer inertia, efficiency), where N_{red} is the number of available reducers. If β is smaller than one, the reducer performs as a velocity multiplier, i.e., the velocity of the motor is smaller than $\dot{\omega}_l$. Accordingly, we consider the possibility of mounting a reducer with flipped sides, turning it into a multiplier. The actual reducer list is thus mirrored in order to cover the case $\beta < 1$, by using the reciprocal values of $\beta_k\,(k = 1, \ldots, N_{red})$, thereby effectively providing a total of $2\,N_{red}$ gearboxes. In Table 5.2, an example list is given, by manufacturer B&R (series 8GA [60]).

The complete set of parameters $\overline{\xi}$ comprises both motor-related and reducer-related quantities. As far as the motor is concerned, the main parameters are those presented in Tab. 3.1. [1]. Moreover, by applying the electric motor model defined in Chapter 3, additional parameters can be appended to $\overline{\xi}_\alpha$, such as the loss coefficients of each motor, as reported in Tab. 5.1.

As far as the reducer is considered, the subset $\overline{\xi}_\beta$ has fewer components, since the only parameters worth considering are the inertia J_r, the efficiency η_r and the transmission ratio τ_r (see Tab. 5.2) [2]

[1] Only the main parameters are reported in Table 4.2. Further data can be found in [51]

[2] Reducer catalogs provide the inertia reflected to the input shaft. Since there is no way to figure out how the inertia is actually distributed between the two shaft, it is assumed that all the inertia is concentrated on the input. Thus, disregarding efficiency, the inertia reflected at the output shaft is given by $J_{out} \simeq J_{in}\,\beta^2$.

Table 5.1: Size index α, winding and iron losses coefficients k_{t1}, k_{t2}, k_{f1} for every motor in the catalog. The coefficient k_{f2} is equal to zero because the two-points characteristic-curve model is used (see Section 3.4.3)

.

Motor	α_j	k_{t1} [Nm/A]	k_{t2} [Nm/A^2]	k_{f1} [J/rpm]
$\mathcal{M}1$	0	0.787	$-93.0 \cdot 10^{-3}$	$0.3 \cdot 10^{-3}$
$\mathcal{M}2$	0.0625	0.705	$-38.5 \cdot 10^{-3}$	$0.3 \cdot 10^{-3}$
$\mathcal{M}3$	0.1250	0.797	$-39.8 \cdot 10^{-3}$	$0.8 \cdot 10^{-3}$
$\mathcal{M}4$	0.1875	0.870	$-45.0 \cdot 10^{-3}$	$1.3 \cdot 10^{-3}$
$\mathcal{M}5$	0.2500	0.777	$-11.3 \cdot 10^{-3}$	$1.2 \cdot 10^{-3}$
$\mathcal{M}6$	0.3125	0.786	$-7.2 \cdot 10^{-3}$	$2.4 \cdot 10^{-3}$
$\mathcal{M}7$	0.3750	1.007	$-17.3 \cdot 10^{-3}$	$5.2 \cdot 10^{-3}$
$\mathcal{M}8$	0.4375	1.257	$-10.9 \cdot 10^{-3}$	$4.8 \cdot 10^{-3}$
$\mathcal{M}9$	0.5000	1.245	$-8.7 \cdot 10^{-3}$	$8.0 \cdot 10^{-3}$
$\mathcal{M}10$	0.5625	1.627	$-1.1 \cdot 10^{-3}$	$12.3 \cdot 10^{-3}$
$\mathcal{M}11$	0.6250	1.442	$-6.9 \cdot 10^{-3}$	$14.6 \cdot 10^{-3}$
$\mathcal{M}12$	0.6875	1.474	$-2.5 \cdot 10^{-3}$	$33.5 \cdot 10^{-3}$
$\mathcal{M}13$	0.7500	1.584	$-1.7 \cdot 10^{-3}$	$50.5 \cdot 10^{-3}$
$\mathcal{M}14$	0.8125	1.584	$-2.1 \cdot 10^{-3}$	$51.2 \cdot 10^{-3}$
$\mathcal{M}15$	0.8750	1.801	$-6.2 \cdot 10^{-3}$	$41.1 \cdot 10^{-3}$
$\mathcal{M}16$	0.9375	2.243	$0.3 \cdot 10^{-3}$	$121.8 \cdot 10^{-3}$
$\mathcal{M}17$	1	2.543	$-0.9 \cdot 10^{-3}$	$136.4 \cdot 10^{-3}$

5.2.2 Extension to a continuous domain

In this section, a method to extend the definition of the set $\overline{\xi}$ over a continuous domain is presented. First, $\overline{\xi}_\alpha$ is defined for $\alpha \in [0,1]$ by fitting the data of the discrete subset $\overline{\xi}_\alpha(\alpha_j)$, for $j = 1, \dots, N_{mot}$. Then, the same extension is applied to the discrete subset $\overline{\xi}(\beta_k)$, for $k = 1, \dots, N_{red}$. The continuous domain of β is bounded between the maximum value β_{max} and its reciprocal, i.e., the domain for β is given by $[1/\beta_{max}, \beta_{max}]$. In any case, $\beta \in (0, +\infty)$.

Consider for instance the i-th parameter function ξ_i, which belongs to the subset $\overline{\xi}_\alpha$. The problem is to find a curve that best fits the data $\xi_i(\alpha_j)$ $(j = 1, \dots, N_{mot})$. The concept of *best* fit is rather general, since it must be specified whether the fitting curve must include the data points (i.e a strict interpolation is needed) or a certain degree of approximation can be tolerated. Here these two different methods are considered and then compared.

The first method features a cubic-spline piece-wise interpolation. Each segment between two points is interpolated by a cubic curve (a third order polynomial): under the constraint that the interpolant passes through a specified sequence ofpoints, the spline minimizes bending while guaranteeing the continuity of first and second derivatives of the function [61]. The second method introduces a single n-th order polynomial $p_n(\alpha)$ to best fit all points. The polynomial coefficients are determined by minimizing the sum of squares of the errors computed at points $\xi_i(\alpha_j)$ [62]. In reference to Eq. (3.19), the vector γ containing the $n+1$

Table 5.2: Reducer database: 1-stage planetary gearboxes by B&R [60]. The entries with $\beta < 1$ are obtained by mirroring the data corresponding to entries with $\beta > 1$.

Index	Name	β_k	Inertia J_r [kgm^2]	Efficiency η_r
$\mathcal{R}_1$	8GA50-070hh010 (flip)	1/10	$2.000 \cdot 10^{-4}$	0.96
$\mathcal{R}_2$	8GA50-070hh008 (flip)	1/8	$1.6000 \cdot 10^{-4}$	0.96
$\mathcal{R}_3$	8GA50-070hh005 (flip)	1/5	$0.900 \cdot 10^{-4}$	0.96
$\mathcal{R}_4$	8GA50-070hh004 (flip)	1/4	$0.752 \cdot 10^{-4}$	0.96
$\mathcal{R}_5$	8GA50-070hh003 (flip)	1/3	$0.107 \cdot 10^{-4}$	0.96
$\mathcal{R}_6$	8GA50-070hh003	3	$0.119 \cdot 10^{-4}$	0.96
$\mathcal{R}_7$	8GA50-070hh004	4	$0.047 \cdot 10^{-4}$	0.96
$\mathcal{R}_8$	8GP45-070hh005	5	$0.036 \cdot 10^{-4}$	0.96
$\mathcal{R}_9$	8GA50-070hh008	8	$0.025 \cdot 10^{-4}$	0.96
$\mathcal{R}_{10}$	8GP45-070hh010	10	$0.020 \cdot 10^{-4}$	0.96

unknown coefficients is found by minimizing the sum:

$$S = \sum_{j=1}^{N_{mot}} [\xi_i(\alpha_j) - p_n(\alpha_j, \gamma)]^2 \tag{5.2}$$

where p_n denotes a n-th order polynomial with coefficients γ.

As shown in Fig. 5.1 the two methods are applied to torque-current coefficients k_{t1} and k_{t2}, as an example. The green line represents a 4-th order polynomial fitting the given data with the least square method. The blue line is a cubic spline interpolation, while the orange markers denote the data points. As can be seen, the fitting polynomial represents the data in a satisfying way, because the pattern of the coefficients is well represented as a function of independent variable α. The spline is indeed a more accurate representation, but the fitting polynomial offers two dominating advantages: first, the analytic expression is simpler, and it can be easily derived or rearranged. Second, the fitting curve is smoother than the spline, and thus so is the behavior of the generic motor. In order to clarify this concept, consider the continuous extension of the torque-current relation $g_q(I)$ defined in Sec. 3.3.2. Since the torque coefficients k_{t1} and k_{t2} depend on size index α, the generic torque expression becomes a function of two variables, thereby defining a surface indicated by g_s:

$$M(I, \alpha) = g_s(I, \alpha) = k_{t1}(\alpha)|I| + k_{t2}(\alpha)I^2 \tag{5.3}$$

By assigning a value the index α, the quadratic torque-current relation $g_{q,\alpha}$ for the α-sized motor is obtained. As mentioned in Sec. 3.3.2, $g_{q,\alpha}$ is invertible in the domain $[0, I_{max}]$, where here I_{max} is a function of α , since it is a parameter $\xi_i \in \overline{\xi}_\alpha$. If the values (M, α) are given and the current must be found, the relation $I(M, \alpha) = g^{-1}_{q,\alpha}(M)$ is used (see Eq. (3.20)). In Fig. 5.2, the torque-current-size surface g_s is shown. The blue lines represent the quadratic torque-current model for each motor $\mathcal{M}_j$ (see Eq. (3.18)). The surface does not necessarily contain these curves, since a polynomial fitting curve has been used to define coefficients. However, the approximation is satisfying, since the surface does not appear to have any discontinuity point.

The rated torque M_n and the stator resistance fitting curves are shown in Fig. 5.3. In the top part the rated torque is fitted by means of a second order polynomial. In this case, a

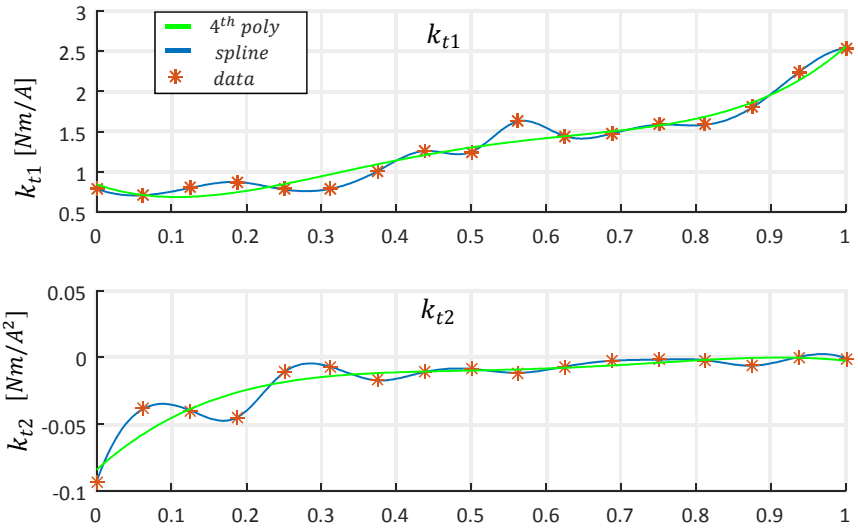

Figure 5.1: Curve fitting (green line) and spline interpolation (blue line) for torque coefficients k_{t1} and k_{t2}

Table 5.3: Fitting methods for functions ξ_i, interpolated on set of data α_j $(j = 1, \ldots, N_{mot})$ and β_k $(k = 1, \ldots, 2N_{red})$

ξ_i	*Fitting*	*data*	ξ_i	*Fitting*	*data*
M_n	spline	α_j	R	spline	α_j
J_m	spline	α_j	M_{max}	spline	α_j
k_{t1}	poly 4	α_j	k_{t2}	poly 4	α_j
k_{f1}	poly 2	α_j	k_{f2}	poly 2	α_j
I_{max}	spline	α_j	n_{max}	poly 2	α_j
J_r	spline	β_k	η_r	linear	β_k

polynomial function is not suitable to fit the data, because M_n may assume negative values which are not physically feasible. Raising the order of the fitting polynomial often introduces additional inflation points that will corrupt the fitting results. In the bottom part, the fitting curves of stator resistance R is shown. A fourth order polynomial is used to fit the data, which also introduces negative values for the rated torque R. As it can be seen, increasing the order of the polynomial doesn't fix the problem, since the asymptotes are not correctly fitted by a polynomial curve. In these cases the cubic spline is a better representation for its higher accuracy. On the other hand, the analytic expression of parameter function can not be easily determined. The fitting methods for each parameter function of the motor and the reducer are listed in Tab. 5.3.

5.3 The optimization problem subject to constraints

The optimization of a nonlinear objective function of a set of unknown variables subject to a set of equality and inequality constraints is referred to as *nonlinear programming*. In our

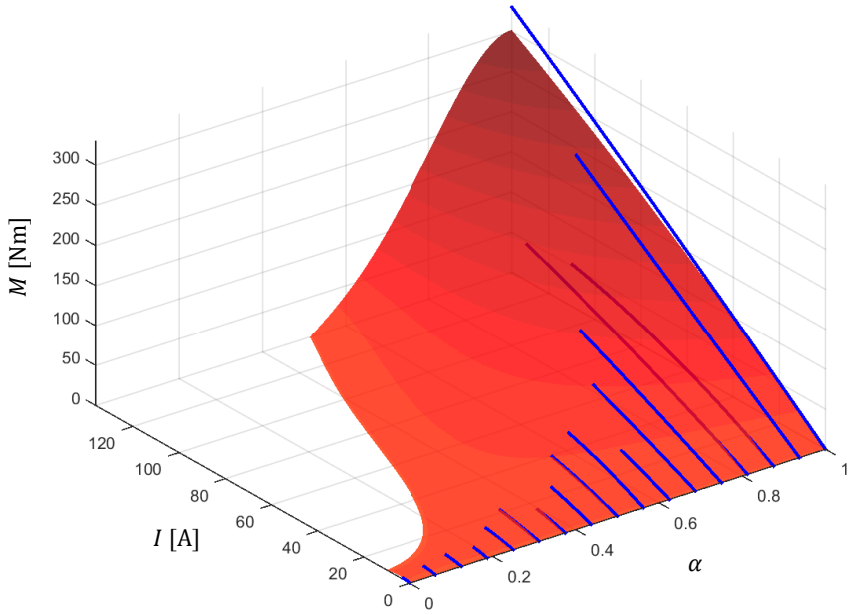

Figure 5.2: Torque-current-size relation $M(I, \alpha)$ represented by the surface g_s. The blue lines represent the quadratic torque-current models for each motor $\mathcal{M}_j$ $j = (1, \ldots, N_{mot})$

case, the motor-reducer selection process may be considered as a nonlinear programming problem of a generic objective function $f(\alpha, \beta)$ of two unknown variables α and β, which we simply refer to as a two-dimensional problem.

5.3.1 Objective Functions

The objective functions remain the same as those presented in Sec. 4.2. The motor torque is a function of time and size indexes α and β. Recalling Eq. (4.1), the general expression for motor torque is:

$$M(\alpha, \beta, t) = \beta \left[(J_m(\alpha) + J_r(\beta))\, \dot{\omega}_l(t) + b_m(\alpha)\omega_l(t) \right] + \frac{A(t)}{\beta\, \hat{\eta}_r(\beta)} \tag{5.4}$$

The damping coefficient b_m is a parameter that may be included in the set $\overline{\xi_\alpha}$. However, it is not available on the motor catalog ; moreover, it depends on several factor (mounting, environment, etc.) and not only on the motor. In this analysis, the motor damping effect is disregarded and the expression of the torque becomes [5]:

$$M(\alpha, \beta, t) = \beta \left[J_m(\alpha) + J_r(\beta) \right] \dot{\omega}_l(t) + \frac{A(t)}{\beta\, \hat{\eta}_r(\beta)} \tag{5.5}$$

The square value of the RMS motor torque is thus (see Eq. (4.9)):

$$M^2_{RMS}(\alpha, \beta) = (J_m + J_r)^2\, \beta^2 \dot{\omega}^2_{l,RMS} + \frac{A^2_{RMS}}{\beta^2\, \hat{\eta}^2_r} + 2\,(J_m + J_r)\, \frac{(A\, \dot{\omega}_l)_{mean}}{\hat{\eta}_r} \tag{5.6}$$

The energy absorbed by the motor is evaluated by integrating over a cycle the electric

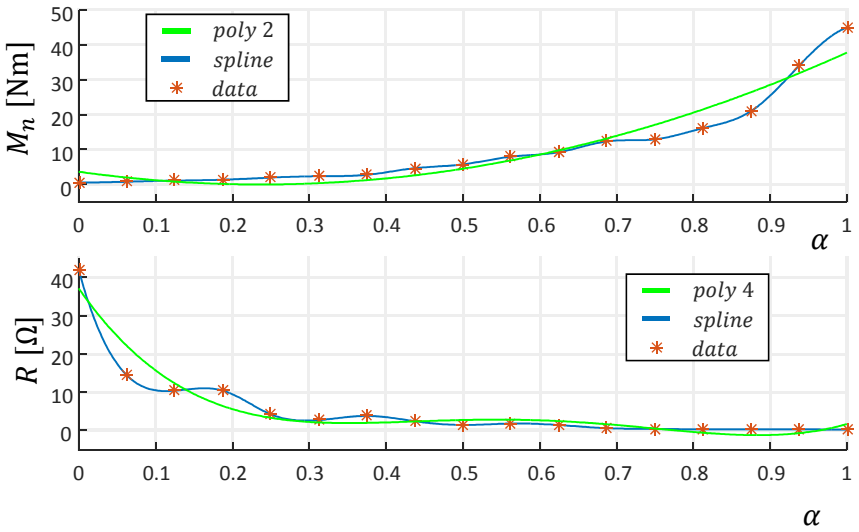

Figure 5.3: Curve fitting and interpolation for rated torque M_n (top) and stator resistance R (bottom)

power P_{el}, which accounts for the mechanical power and the motor losses (see Eq. (4.17)):

$$\begin{aligned} P_{el}(\alpha,\beta,t) =& \beta^2(J_m + J_r)\dot{\omega}_l\omega_l + \frac{A\omega_l}{\hat{\eta}_r} + \\ &+ \frac{3}{2}R\left(g_{q,\alpha}^{-1}(M)\right)^2 + \widetilde{k}_{f1}\,\omega_l\,\beta + \widetilde{k}_{f2}\,\omega_l^2\,\beta^2 \end{aligned} \tag{5.7}$$

where the instantaneous current $I = g_{q,\alpha}^{-1}(M)$ is evaluated at a point (M,α). Here, note that M is already a function of (α,β,t), as defined in Eq. (5.5). Integrating Eq. (5.7) over a cycle t_c, the energy E_{mot} drawn by the motor in a cycle is:

$$E_{mot}(\alpha,\beta) = \int_0^{t_c} P_{el}(\alpha,\beta,t)\,dt \tag{5.8}$$

In order to find the total energy E_{tot} absorbed by the motor, the total power must be integrated, including the inverter losses (see Eq. (3.27)).

$$P_{el,tot} = P_{el}(\alpha,\beta,t) + k_{i0} + k_{i1}\,|I| + k_{i2}I^2 \tag{5.9}$$

The evaluation of $P_{el,tot}$ is not straightforward since the inverter coefficients do not admit a direct dependence on α or β. This issue is addressed in Sec. 5.6. The total energy is then given by:

$$E_{tot}(\alpha,\beta) = \int_0^{t_c} P_{el,tot}(\alpha,\beta,t)\,dt \tag{5.10}$$

5.3.2 The Karush-Kuhn-Tucker conditions

Let x be a subset of $\mathbb{R}^n$, and let f_o, u_i be real-valued functions of x $\forall i \in \{1,\dots,m\}$. Function f_o is the objective function while function u_i is a constraint function. The optimization

problem is expressed in the form:

$$\begin{aligned} &\min f_o(x) \\ &\text{subject to } u_i(x) \leq 0 \ \ \forall i \in \{1, \ldots, m\} \end{aligned} \tag{5.11}$$

If the *qualification conditions* of the constraints are fulfilled [63], the *Karush-Kuhn-Tucker* (or KKT) theorem can be applied to find the *local optimum* x^* for the problem 5.11. The *Lagrangian* $\mathcal{L}$ is defined as:

$$\mathcal{L}(x, \lambda) = f_o(x) - \sum_{i=1}^{m} \lambda_i u_i(x) \tag{5.12}$$

where the λ_i $(i = 1, \ldots, m)$ are called KKT multipliers. The KKT theorem states that a vector λ_i^* $(i = 1, \ldots, m)$ exists such that x^*, λ^* are solution of the system:

$$\begin{cases} \dfrac{\partial \mathcal{L}}{\partial x_k} = \dfrac{\partial f_o}{\partial x_k} - \displaystyle\sum_{i=1}^{m} \lambda_i \frac{\partial u_i}{\partial x_k} = 0 & k = 1, \ldots, n & \text{(5.13a)} \\ \dfrac{\partial \mathcal{L}}{\partial \lambda_i} = -u_i \geq 0 & i = 1, \ldots, m & \text{(5.13b)} \\ \lambda_i \geq 0 & i = 1, \ldots, m & \text{(5.13c)} \\ \lambda_i \, u_i(x^*) = 0 & i = 1, \ldots, m & \text{(5.13d)} \end{cases}$$

The conditions (5.13) are called *KKT conditions*. Equation (5.13a) is called the stationarity condition, Eq. (5.13b) and (5.13c) the primal and dual feasibility respectively, and Eq. (5.13d) the complementary slackness condition. The KKT conditions are the generalization of the method of *Lagrange multiplier*, for an optimization problem with inequality constraints.

5.3.3 System resolution

The non-linear system in Eq. (5.13) is seldom solvable in closed form, and therefore several algorithms have been developed to solve it numerically. In this work, the *interior-point* algorithm is used [64, 65, 66]. It consists in solving a sequence of approximate minimization sub-problems: a logarithmic term called *barrier function* is added to the original function f, and a sequence of equality constrained problems are solved, which are easier to solve with respect to the original inequality-constrained problem. As the barrier function term is brought to zero, the approximate minimum tends to the real one. The KKT conditions hold for every local minimum, and the interior-point algorithm output depends on the initial guess. In case of multiple local minimums inside the function domain, the solution is not guaranteed to be global. A possible remedy is a "smart" choice of the initial guess. In any case, in order to ensure a global minimum, an iterative process must be carried on. Alternatively, the minimization problem can be solved by a *genetic algorithm* [67] in order to find a global minimum. In the next section, the nonlinear programming problem is applied to the task defined in Sec. 4.3.4.

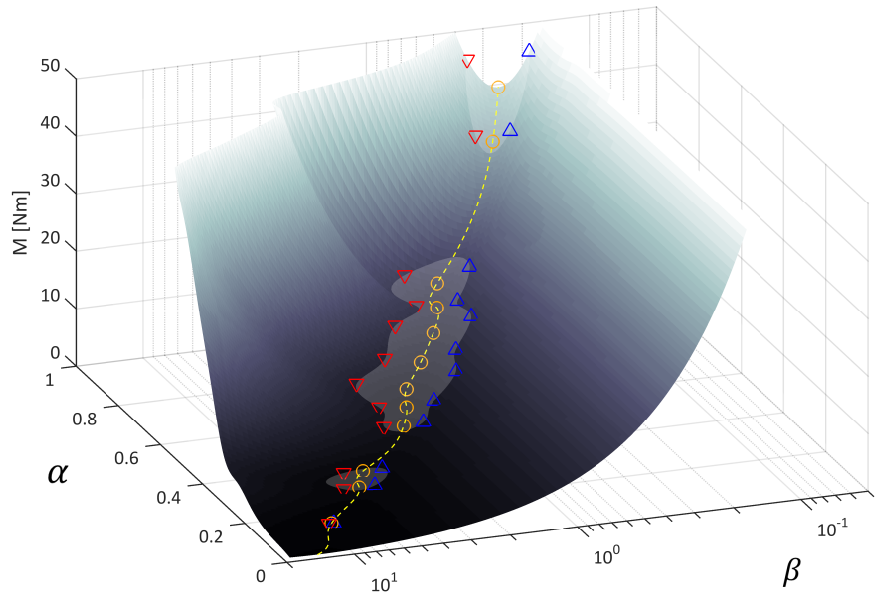

Figure 5.4: RMS torque surface in α, β for the ideal transmission case. The shaded gray surface represents M_n in the regions where it is $M_{RMS} < M_n$. The markers indicate the value obtained by the discrete optimization algorithm

5.4 Optimization for root-mean-square torque

The first objective function analysed is the root-mean-square value for motor torque.

5.4.1 Feasibility

A comparison with the discrete approach

Before solving the nonlinear programming problem, in this section we make several considerations on the feasibility conditions for a parameter pair (α, β) to be a solution. First, the function M_{RMS} is evaluated for the case with an ideal transmission (with unitary efficiency and zero reducer inertia, see Eq. (4.8)), as considered in Chapter 4. The function M_{RMS} over $(\alpha, \beta) \in [0, 1] \times [0.1, 10]$ under a logarithmic scale for axis β is shown in Fig. 5.4. Also shown in the same figure it is the surface representing $M_n(\alpha)$, when $M_n > M_{RMS}$ (shaded gray): if M_{RMS} is below $M_n(\alpha)$, the selection is feasible. The values obtained by the discrete optimization algorithm for α_j $(j = 1, \ldots, N_{mot})$, are reported: the orange circles represent the values of $\beta^*_{M_{RMS}}$ computed in Eq. (4.13), while the blue and red triangle delimits, for each motor, the range of admissible value for β (see Eq. (4.14)). It can be seen that the discrete range limits are, as expected, at the intersection between the continuous surfaces M_{RMS} and M_n. Since the same simplifications are considered, the solution of the discrete approach is a particular case of the one obtained with the continuous approach.

The dotted yellow line traces the pattern of the optimal value $\beta^*_{M_{RMS}}(\alpha)$ that is obtained by deriving $\partial M / \partial \beta$ and then evaluating it for each α. The following equation is the same

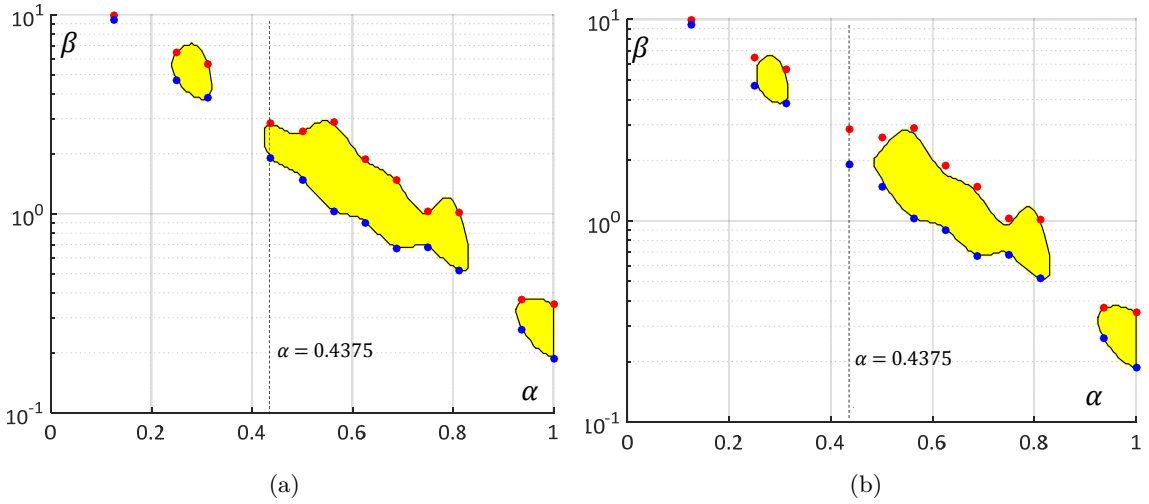

(a) (b)

Figure 5.5: Region of feasibility $\mathcal{A}(M_{RMS})$ with ideal reducer (a) and actual reducer (b). The range of admissible gear ratio, for each $\alpha_j\,(j = 1, \ldots, N_{mot})$, are shown, denoted by maximum (red) and minimum (blue) values. The value $\alpha_4 = 0.4375$ ($\mathcal{M}4$) leads to an admissible motor in the ideal case (a), while in the real case (b) the motor is not feasible regardless of transmission ratio.

as Eq. (4.13), where the dependence on α is introduced through $J_m(\alpha)$:

$$\beta^*_{M_{RMS}}(\alpha) = \sqrt{\frac{A_{RMS}}{\dot{\omega}_{l,RMS}\, J_m(\alpha)}} \tag{5.14}$$

It gives, for each α, the optimal value $\beta^*_{M_{RMS}}(\alpha)$ that minimizes the RMS torque.

Region of feasibility

We define a *region of feasibility* for a specific constraint as the subset $\mathcal{A}$ such that if $(\alpha, \beta) \in \mathcal{A}$, then the constraint is verified. As far as the motor thermal problem is concerned, the corresponding region of feasibility $\mathcal{A}(M_{RMS})$ is defined such that, for all $(\alpha, \beta) \in \mathcal{A}(M_{RMS})$, it is $M_{RMS}(\alpha, \beta) < M_n(\alpha)$.

In Fig. 5.5(a) the region of feasibility $\mathcal{A}(M_{RMS})$ is shown (in yellow) for the constraint $M_{RMS}(\alpha, \beta) < M_n(\alpha)$, computed for an ideal reducer (i.e. $\eta_r = 1$ and $J_r = 0$). In the same figure, the results of the discrete approach optimization are shown: for each $\alpha_j\,(j = 1, \ldots, N_{mot})$, Eq. (4.14) gives the range of admissible gear ratios, which are represented as red (maximum values of β) and blue dots (minimum values). It can be noticed that the discrete set of limit values belongs to the contour of $\mathcal{A}(M_{RMS})$. If Eq. (5.6) is used to compute M_{RMS}, i.e. a real reducer is considered, the region $\mathcal{A}(M_{RMS})$ changes accordingly. In Fig. 5.5(b), the region $\mathcal{A}(M_{RMS})$ is shown (yellow) for the real reducer case (i.e. $\eta_r < 1$ and $J_r \neq 0$). The limitation obtained by the ideal discrete optimization are also reported: as it can be seen, in this case the discrete limits obtained with the ideal reducer don't belong to the region contour. The region of feasibility is stricter, with respect to the case of Fig. 5.5(a). Considering the motor $\mathcal{M}8\,(\alpha_8 = 0.4375)$, we can see that for the ideal case there is a not-empty subset of feasible gear ratio ratios. In the real case, the motor is not admissible, regardless of the gear ratio.

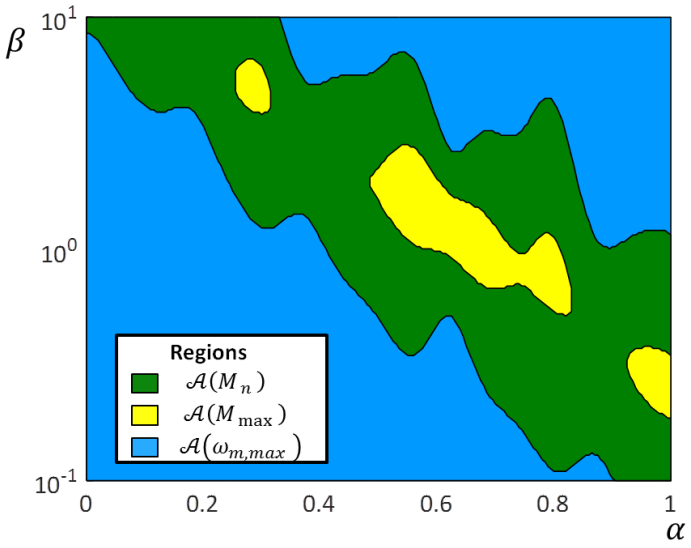

Figure 5.6: Region of feasibility: max speed limit (light blue), torque peak limit (green) and RMS torque limit (yellow)

In order to perform the feasibility analysis and the optimization simultaneously, the admissibility constraints must be implemented inside the nonlinear programming problem. Recall the other two limitations on the motor operating range besides the RMS torque (see Tab. 4.1): the maximum motor speed limit $\omega_{m,\max}$ and the maximum peak torque value $M_{\max}$. Both parameters are functions of the size index; as explained in Sec. 5.2.2, their dependency on α is obtained by fitting the discrete data available in commercial catalogs (see Table 5.3 for the fitting methods that are adopted). The condition on motor speed and maximum torque are expressed as:

$$\begin{cases} \max(\omega_m) = \beta \max(\omega_l) < \omega_{m,\max}(\alpha) & \text{(5.15a)} \\ \max(|M|) < M_{\max}(\alpha) & \text{(5.15b)} \end{cases}$$

where we have introduced the relation $\omega_m = \beta\omega_l$. The value $\max(\omega_l)$ is known once the cycle is defined, and Eq. (5.15a) can be easily implemented as an inequality constraint in the nonlinear programming problem. On the other hand, it is difficult to express Eq. (5.15b) in analytical form. In fact, the determination of the global maximum of the function $M(\alpha, \beta, t)$ is not straight-forward, since it requires traversing all stationary points. References [14, 15] present a graphic diagram-based method for minimizing the torque peak. In our case, the global maximum of M is determined numerically.

It is interesting to visualize the feasibility regions for our case study. In Fig. 5.6 the aforementioned regions are shown for maximum speed (light blue), peak torque (green) and RMS torque (yellow) limitations, denoted respectively as $\mathcal{A}(M_{max})$, $\mathcal{A}(\omega_{m,max})$, and $\mathcal{A}(M_{M_{RMS}})$. In particular, it can be noticed that $\mathcal{A}(\omega_{m,max})$ coincides with the entire domain $[0, 1] \times [10^{-1}, 10]$ for (α, β) whereas $\mathcal{A}(M_{M_{RMS}})$ is a proper subset of the other two regions. Then, imposing $M_{RMS} < M_n$ is a sufficient condition for the problem.

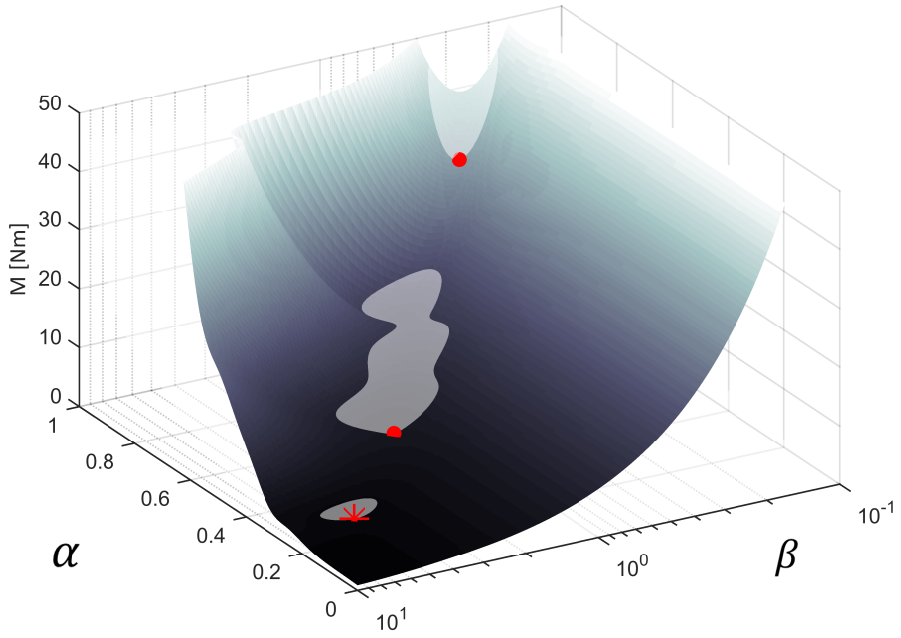

Figure 5.7: Surface representing the RMS motor torque for the real reducer case. The red dots represent the local minimums of the cosntrained surface and the asterisk represent the global minimum (see Tab. 5.4). The region of feasibility is represented in gray.

5.4.2 The nonlinear optimization equations

The objective function f_o of the problem 5.11 is the square value of $M_{RMS}(\alpha, \beta)$ as defined in Eq. (5.6), since the minimum of M_{RMS} coincides with the minimum of M^2_{RMS}. First, the inequality constraints regarding the domain limits for (α, β) are implemented. By definition, $0 \leq \alpha \leq 1$. The upper limit of β is given by the largest gear ratio $\beta_{\max}$ available in the reducer catalog. Conversely, the lower limit is given by the reciprocal of the same value, because it corresponds to the same reducer with switched sides. Therefore, the parameter functions $\overline{\xi}(\alpha, \beta)$ are defined for $1/\beta_{\max} \leq \beta \leq \beta_{\max}$ and $0 \leq \alpha \leq 1$. Then, motor operation range limits are implemented. The functions $u_i\,(i = 1, \ldots, 7)$ are given by:

$$\begin{cases} u_1 = \alpha - 1 & \leq 0 \\ u_2 = -\alpha & \leq 0 \\ u_3 = \beta - \beta_{\max} & \leq 0 \\ u_4 = -\beta + \dfrac{1}{\beta_{\max}} & \leq 0 \\ u_5 = M_{RMS} - M_n & \leq 0 \\ u_6 = \max(M) - M_{\max} & \leq 0 \\ u_7 = \beta \max(\omega_l) - \omega_{m,max} & \leq 0 \end{cases} \tag{5.16}$$

These, together with $f_o = M_{RMS}$, completely define the problem. In this particular case, u_5 contains u_6 and u_7, as shown in Fig. 5.6. By numerically solving the problem, we are able to find three solutions.

The surface of RMS torque for the real reducer case is shown in Fig. 5.7. The feasible

region $\mathcal{A}(M_{RMS})$ is shown in gray. Three stationary points are highlighted, with two local minimums indicated by a red dot and the global minimum indicated with an asterisk. The stationary points versus the value of f_o are reported in Tab. 5.4.

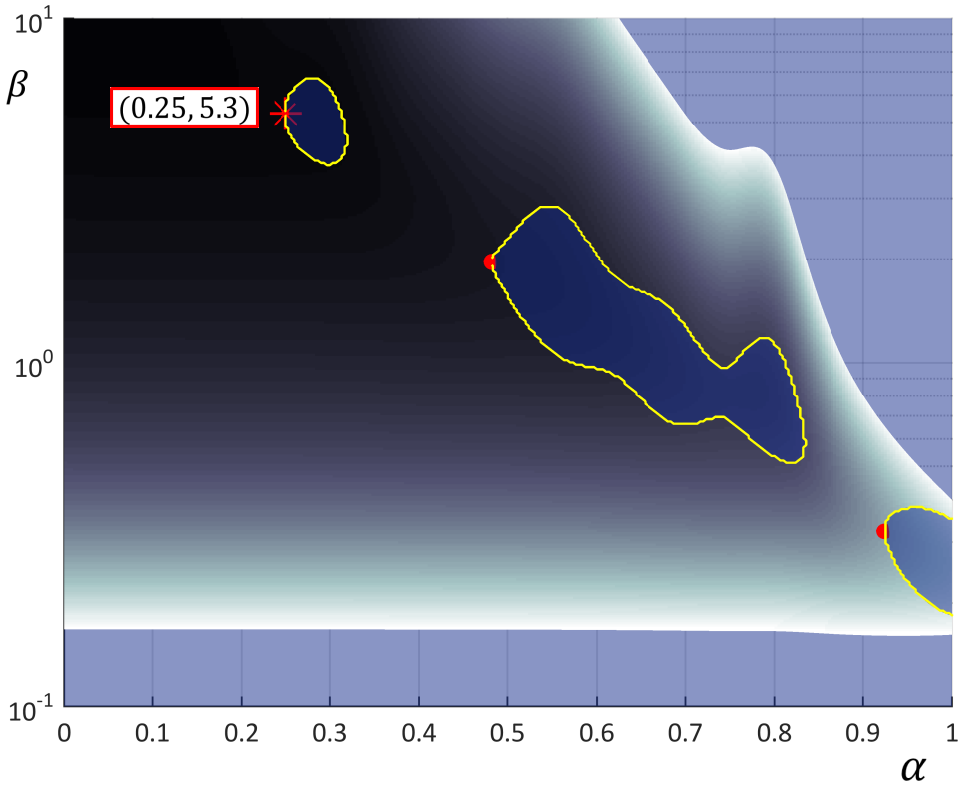

Figure 5.8: The position of the global optimum $(\alpha^*, \beta^*) = (0.25, 5.3)$ is denoted by a red asterisk, and $\mathcal{A}(M_{RMS})$ is denoted by a yellow line. The solution is on the boundary: while selecting the actual motor-reducer in the neighborhood of the optimum, the feasibility must be verified

In Fig. 5.8, the surface M_{RMS} is represented in the plane $\alpha - \beta$, and the region of feasibility is highlighted by a yellow contour. The position of the global optimum $(\alpha^*, \beta^*) = (0.25, 5.3)$ is denoted by a red asterisk, and it is on the boundary of $\mathcal{A}(M_{RMS})$. Notice that for $\alpha^* = 0.25$, the only feasible gear ratio is the optimum $\beta^* = 5.3$. When selecting the actual motor, the selection must be as close as possible to the optimum. However, it is unlikely to achieve precisely the value (α^*, β^*), but rather a point in the neighborhood; hence, it is possible that the feasibility is not achieved. Since the region of feasibility is convex, a solution to this issue may be considering, for the actual selection, the values $\alpha > 0.25$. For higher values of α, in fact, the range of available gear ratios widens; conversely, the selection is farther from the optimum. Therefore, a good balance between feasibility and optimization should be found.

Each solution is obtained starting from a different initial guess. Finding the global minimum may be achieved at the cost of an increasing number of initial guesses with an increasing computation time. Nevertheless, additional problem-specific knowledge may allow for fewer initial guesses to find the global solution.

Table 5.4: Global and local minimums of RMS torque value M_{rms}

.

α	β	M_{rms} [Nm]	*Type*
0.2500	5.301	1.900	global
0.4826	1.962	5.327	local
0.9241	0.323	30.873	local

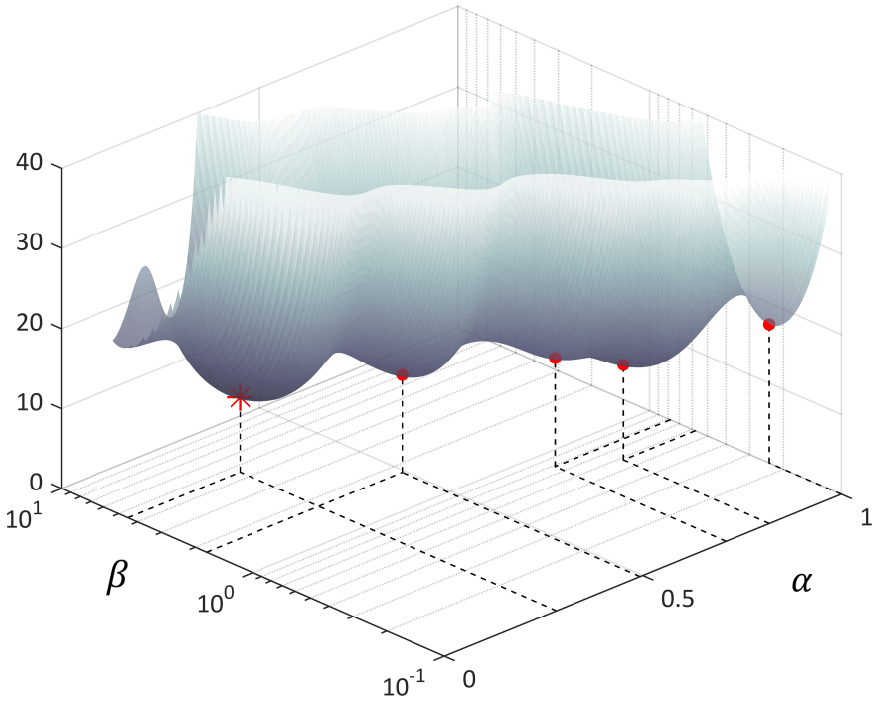

Figure 5.9: Surface representing the energy absorbed by the motor. Minima position are reported in Tab. 5.5: the red asterisk denotes the global minimum.

5.5 Optimization for the energy absorbed by the motor

In this section we define the objective function to be the energy absorbed by the motor, defined in Eqs. (5.7) and (5.8), namely $f_o = E_{mot}$. In particular, we consider the real reducer case. The constraints of the KKT systems are the same as the ones listed in Eq. (5.16). The list may be expanded by including the constraints on reducer (e.g., the peak torque on the reducer shaft, the maximum reducer rotational speed).

The surface representing E_{mot} for $(\alpha, \beta) \in [0, 1] \times [0.1, 10]$ is shown in Fig. 5.9. The global minimum is at $(\alpha, \beta) = (0.282, 4.48)$ which leads to an energy consumption equal to $E_{mot} = 9.34$ J per-cycle, represented by a red asterisk in the figure. Other local minima are represented by red dots, and the detailed values are reported in Tab. 5.5. The available region $\mathcal{A}(M_{RMS})$ in the plane $\alpha - \beta$ is shown in Fig. 5.10. The local minimum on the boundary $(\alpha, \beta) = (1, 0.237)$ is included in $\mathcal{A}(M_{RMS})$ and thus it must be considered as an admissible choice. However, the considerations on boundary solutions made in Sec. 5.4.2

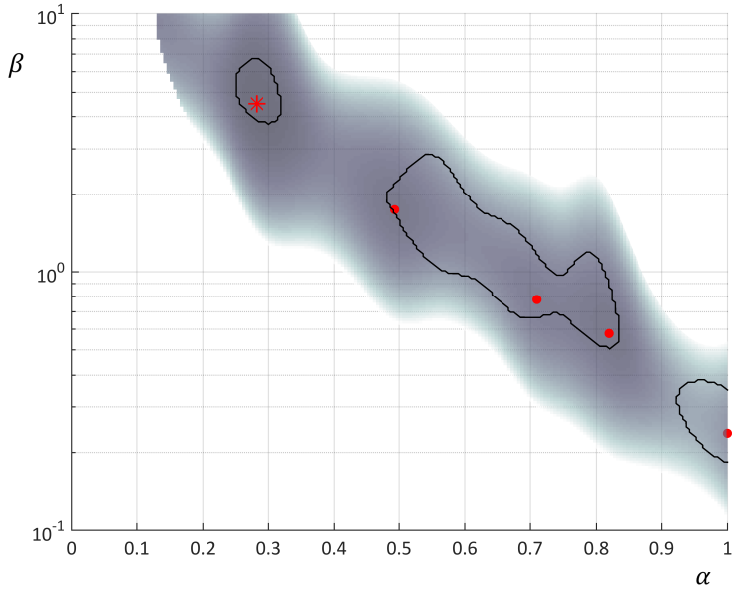

Figure 5.10: Region of feasibility $\mathcal{A}(M_{RMS})$. Minima position are reported in Tab. 5.5: the red asterisk denotes the global minimum.

still hold.

Table 5.5: Global and local minimums of energy absorbed by the motor E_{mot}
.

α	β	E_{mot} [J]	*Type*
0.282	4.4797	9.342	global
0.493	1.7439	12.206	local
0.701	0.7804	13.617	local
0.819	0.5779	11.914	local
1.00	0.2371	17.340	local

5.5.1 Comparison with the discrete approach

In the presented application, the motor and the reducer which are nearest to the global minimum are: a motor between $\mathcal{M}5$ and $\mathcal{M}6$ (see Tab. 5.1) and a reducer between $\mathcal{R}_7$ and $\mathcal{R}_8$ (see Tab. 5.2). However, the feasibility of these couplings must be verified. A feasible choice is, for example, motor $\mathcal{M}6$ ($\alpha_6 = 0.3125$) and reducer $\mathcal{R}_7$ ($\beta_7 = 4$); it leads to a value for energy absorbed by the motor of 9.96 J per cycle, which is close enough to the global optimum.

In Sec. 4.3.4, the discrete optimization approach for the same case study was carried out. The analysis featured an ideal reducer, and it led to the selection of motor $\mathcal{M}3$ ($\alpha_3 = 0.125$) with a gear ratio $\beta = 9.27$ (see Tab. 4.3). The computation of E_{mot} at $(\alpha, \beta) = (\alpha_3, 9.27)$ for the real case (see Eqs. (5.7), (5.8)) gives $E_{mot} = 15.35$ J. Comparing this results with the data in Tab. 5.5 , we can see that it is sub-optimal value. Moreover $(\alpha, (\alpha, \beta) = \beta) =$

(α_3, 9.27) is outside the feasible region $\mathcal{A}(M_{RMS})$. Thus, the discrete selection procedure leads to non-optimal (ot even not-feasible) choices, because the contribution of J_r and η_r is not disregardable.

Now consider the subset of $\mathcal{A}(M_{RMS})$ given by $\alpha_8 < \alpha \leq \alpha_{14}$. It corresponds to the subset of motor catalog comprising motors $\mathcal{M}8\,(\alpha_8 = 0.4375)$ through $\mathcal{M}14\,(\alpha_{14} = 0.8125)$, and it is represented in Fig. 5.10. The result of the discrete optimization for this subset is reported in Fig. 4.6. As reported in Fig. 5.10, the optimal choice was $\mathcal{M}10\,(\alpha_{10} = 0.5625)$ with $\beta = 1.5632$. The optimum for this subset computed by the continuous approach procedure is $(\alpha^*, \beta^*) = (0.82, 0.58)$ (see Fig. 5.10), which leads to the selection of motor $\mathcal{M}14$. Again, the two procedure lead to different results. In conclusion, it is confirmed that the contributions of J_r and η_r are not disregardable. Moreover, the continuous approach optimization allows to find the optimal choice without iterations.

5.6 Inverter Losses

5.6.1 Motor and inverter matching

Considering inverter losses for evaluating the total energy absorbed by the electric grid, the following issue arises: the inverter loss coefficients in Eq. (3.27) are not directly dependent on motor or reducer size indexes. A third size index can be defined to map a discrete inverters catalog. However, adding a third independent parameter and hence raising the dimension of the optimization problem makes the search for a solution more complicated, and it renders the extra effort questionable. Since the selection of motor and inverter are strictly related, a dependence of inverter losses coefficients on motor size index α is here inferred.

The criterion we use is the following: given the discrete catalog of motors $\mathcal{M}_j\,(j = 1, \ldots, N_{mot})$ represented by discrete values α_j, each motor is assigned a default inverter from a commercial catalog by manufacturer $B\&R$ [46]. A convenient inverters list is reported in Tab. 3.2. Inverters are identified by $\mathcal{I}_q\,(q = 1, \ldots, N_{inv})$, with N_{inv} being the number of available inverters. The motor-inverter assignment is based on the maximum current parameter. The j-th motor is characterized by the maximum current value $(I_{max})_{\mathcal{M}_j}$, such that it must be $I \leq (I_{max})_{\mathcal{M}_j}$. There is also a similar limitation for the inverter: the q-th inverter is characterized by the maximum current value $(I_{max})_{\mathcal{I}_q}$, such that it must be $I \leq (I_{max})_{\mathcal{I}_q}$. Then, the j-th motor is matched with the $q-$th inverter if and only if $(I_{max})_{\mathcal{M}_j} \leq (I_{max})_{\mathcal{I}_q}$, and $(I_{max})_{\mathcal{I}_q}$ is the smallest value available in the catalog that verifies this condition. In other words, this criterion assigns for each motor the smallest inverter available to achieve the task, and the choice is made on the basis of maximum current condition. In this way, both motor and inverter parameters are functions of α, and the inverter parameters are included in $\overline{\xi}$. For instance, for every $\alpha_j\,(j = 1, \ldots, N_{mot})$ the set of losses coefficients k_{i0}, k_{i1} and k_{i2}, as defined in Sec. 3.4.1, is known. Then, one of the method used in Sec. 5.2.2 may be used to define the inverter losses coefficients in a continuous domain $\alpha \in [0, 1]$, as it was done for any motor characteristic parameter belonging to the set $\overline{\xi}_\alpha$. Here, a second order polynomial fitting is used for inverter losses coefficients.

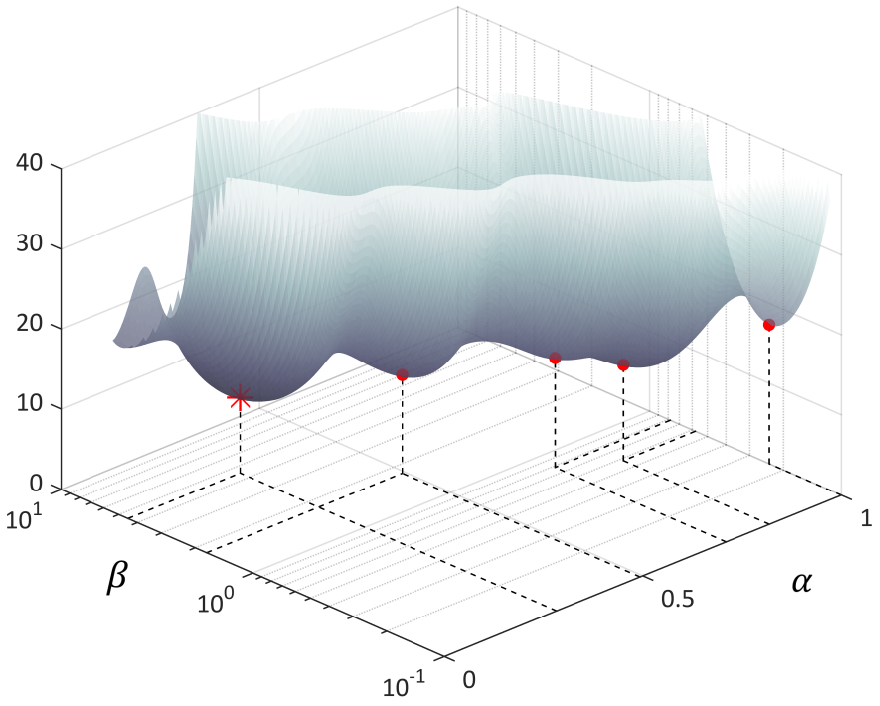

Figure 5.11: Surface representing the total electric energy absorbed by the servo-axis. Minima position are reported in Tab. 5.6: the red asterisk denotes the global minimum.

5.6.2 Optimization for the total absorbed energy

The total electric energy $P_{el,tot}$ absorbed by the servo-axis over a cycle, defined in Eqs. (5.9) and (5.10), is set as the objective function f_o, . In Tab. 5.6, the local and global minimums are reported. The function E_{tot} over the domain $[0, 1] \times [0.1, 10]$ is shown in Fig. 5.11. The red asterisk represents the global minimum. Comparing the surface E_{tot} with the one representing E_{mot} in Fig. 5.9, it can be seen that they are similar in terms of both shape and positions of the stationary points.

Table 5.6: Global and local minimums of total energy absorbed by servo-axis E_{tot}
.

α	β	E_{tot} [J]	*Type*
0.284	4.5283	16.9274	global
0.493	1.7629	20.6180	local
0.693	0.8629	23.9234	local
0.803	0.6653	22.6703	local
1.00	0.2395	34.0180	local

Table 5.7: Global minimums (α^*, β^*), computed for objective functions M_{RMS}, E_{mot} and E_{tot}. The values $f_o(\alpha^*, \beta^*)$ of the objective functions computed in its correspondent (α^*, β^*) are reported.

f_o	α^*	β^*	$f_o(\alpha^*, \beta^*)$	Suggested motor
M_{RMS}	0.2500	5.301	1.90 Nm	$\mathcal{M}5$
E_{mot}	0.282	4.4797	9.34 J	$\mathcal{M}5/\mathcal{M}6$
E_{tot}	0.284	4.5283	16.92 J	$\mathcal{M}5/\mathcal{M}6$

5.7 Discussion of the results

In Tab. 5.7 the results of optimization for the three objective functions, RMS motor torque M_{RMS}, energy absorbed by the motor E_{mot} and the energy absorbed by the servo axis E_{tot} are reported.

As far as the minimization of electric energy is concerned, we can see that considering E_{mot} or E_{tot} as objective function does not make a remarkable difference in determining the global optimum. The introduction of inverter losses causes the energy function to rise significantly, but it does not alter the position of the optimum. As for the selection of the motor, an optimization for energy leads to higher average values of α (i.e. bigger motors), with respect to the values obtained by optimizing M_{RMS}.

As for the comparison with discrete approach, the consideration made in Sec. 5.5.1 are valid for all the considered objective functions. The discrete optimization leads to a first-try optimal selection (motor $\mathcal{M}3$) , which is not feasible, since for $\alpha_3 = 0.125$, no values of β grants the inclusion in the feasibility region.

Different choices can be made by the designer once a generic optimal value (α^*, β^*) is known. First of all, the knowledge of the global minimum gives a strong and accurate indication for a first-try selection: the motor and the reducer which are nearest to the global minimum can be selected. This is not guaranteed to be the best choice, because the actual values of (α, β) are likely different from the theoretical ones (the same problem exists for the reducer in the discrete approach). However, since the objective functions are continuous function, the choice is close enough to the global optimum if the resolution of the catalog is good enough. It must be recalled that when evaluating a possible selection in the neighborhood of the optimum, if (α^*, β^*) belongs to the boundary, it is important to verify the feasibility (see Sec. 5.4.2).

Another alternative consists in designing a custom motor-reducer unit for the application, to approximate the solution with higher accuracy. The parameters that the motor-reducer unit must have are given by the evaluation of functions $\overline{\xi}(\alpha^*, \beta^*)$. However, given the size of the component (i.e. given the motor rated torque M_n), the other parameters (such as stator resistance R or nominal speed n_n), cannot be chosen in a completely arbitrary way, because several constructive relations exist. However, since the parameter functions are defined by means of fitting actual commercial data, the values $\overline{\xi}(\alpha^*, \beta^*)$ should be plausible.

Moreover, as it has already been noticed in in Sec. 5.5.1, the knowledge of other local minima provides a complete picture of the trend of the objective surface. If some limitations exist on motors availability, the local minima might give the best solution for a particular subset of the domain (α, β).

Chapter 6

Conclusions

A servo-controlled automatic machine comprises a significant number of 1-DoF electromechanical actuators, namely servo-axes. Each servo-axis is composed by a motor (a permanent magnet synchronous motor or PMSM), a mechanical transmission and an end-effector. The servo-axis provide the motion law and the required power to the end-effector, in order to achieve an desired task. The design of a such a machine must involve a detailed study from a mechatronic viewpoint, due to its electromechanical nature. The ultimate goal of our work was to develop a reliable tool which supports the optimal selection of a mechatronic actuator.

6.1 The electromechanical model

W first challenge addressed in Chapters 2 and 3 the development of a global model of the servo-axis, comprising both mechanical and electrical parts. The model provides a global view on the systems from the electric grid to the end effector. Such model allows the evaluation of the influence of all components, including the servo-motor, the mechanical transmission and the motion law of the system.

6.1.1 Mechanical Model

Chapter 2 presented the mechanical model. The mechanical transmission was modeled by means of lumped-parameters blocks. Each block is a single-input-single output element, characterized by a transfer function, which allows to infer relations between input and output quantities, such as torques and velocities. The transmission chain, going from the motor to the end-effector, was composed by adding subsequent blocks; this allowed the global equation of motion to be determined, thus leading to the solution of both forward and inverse dynamics. Each block may represent a single body in the transmission chain, or an entire mechanism. Eventually, each block is a transfer function between two nodes, thus making the approach intrinsically modular. Under this perspective, several standard 1-DoF mechanism were characterized, along with the possibility of implementing a generic mechanism outputted by a multi-body simulator. Sometimes a lumped-parameter block model may provide not sufficient details to represent the behavior of a complex mechanism. In particular, the implementation of efficiency may lead to different modeling choices, when the sources of mechanical losses are multiple. In this case, the resolution of the model

may be improved by increasing the number of blocks modeling the mechanism. In Sec. 2.5, several modeling techniques were given and discussed.

6.1.2 Electrical Model

Chapter 3 introduced the electric model of the servo-axis, from the permanent magnet synchronous motor (PMSM) to the electric grid, comprising the inverter. As for the PMSM, the motor equivalent electric circuit was determined by using the synchronous machines *dq* theory, thus finding the relation between mechanical quantities (motor torque, rotational speed) and electric quantities (stator current, excitation frequency). The torque-current relation was generalized. In particular, a procedure was presented to determine a quadratic torque-current relation, on the basis of rated data available on motor catalogs. Such model allows one to implicitly take into account electric phenomena such as saturation, which on the contrary would be hard to evaluate and would require experimental characterization. All the electric loss sources were considered, namely iron losses, windings losses and switching losses. Such losses were modeled as dependent on motor current and frequency (i.e. the rotational speed). Similarly to the case of the torque-current model, experimental characterization are not required to determine losses coefficients. The electric model was validated by mean of a comparison with experimental results obtained from manufacturer ELAU. Finally, the motor efficiency map was obtained over the motor operative range, and the total energy absorbed by the servo axis, was obtained. On the one hand, the model is simple and suitable to a practical use, since it only requires easily gatherable data. On the other hand, it is based on unavoidable simplifications, to limit the number of parameters to be determined. For instance, the temperature has a great influence on electrical parameters: in this work, the thermal model was assumed to be stationary, i.e. the system was assumed to be at thermal equilibrium in every operation instant. A further step may feature the introduction of a dynamic thermal model, taking into account the dependency of electric parameters on windings temperature. In this case, however, further information should be provided by the user/designer on motor mounting position (wall mounting, surface mounting, etc.), materials (alluminium, steel, etc.) and environment (temperature, aerodynamics), therefore introducing an additional degree of complexity.

6.2 The optimization procedures

Once the model was defined, the impact of several design choices, such as the selection of components and the motion profile, could be evaluated by simulation. In particular, Chapters 4 and 5, addressed the motor-reducer unit's selection. The following objective functions were considered: the RMS motor torque, the peak torque, the energy absorbed by the motor, and the energy absorbed by the servo-axis.

6.2.1 Discrete approach

Chapters 4 introduced a *discrete optimization approach*: a discrete set of candidate motors was analyzed, assuming the gearbox reducer to be ideal (i.e. with unitary efficiency and zero inertia). For each candidate, a feasibility optimization was carried out under several constraints (e.g. RMS motor torque must be smaller than motor rated torque), determining a feasible range of transmission ratios. We focused on the determination, for each

motor, of the optimal transmission ratio minimizing the assigned objective function, with ideal reducer conditions. The analytical expression of the optimal transmission ratio that minimizes energy consumption at the motor was derived. Iron and windings losses were considered, implementing the quadratic torque current relation. This value depends on motor characteristic data, other than application and transmission specifications. Adding the contribution of inverter losses, the transmission ratio that minimizes energy absorbed by the electric grid was found. In this case, some more specific coefficients are needed to evaluate the energy loss at the inverter. These data may be obtained by inverter manufacturers, or via experimentations. However, we saw that, for our case study, the transmission ratio that minimizes the energy absorbed by the motor is close to the one that minimizes the total energy.More precisely, the energy absorbed is significantly different, when inverter losses are introduced, but the optimal transmission ratio remains similar. In any case, the discrete optimization for the energy returned a optimum which is sensibly different from the one obtained considering only windings losses, as indicated by prior studies.

6.2.2 Continuous approach

The discrete approach is practical and automatable, but it is iterative and it must be repeated for each motor. In fact, the introduction of a non-ideal reducer impacts the dynamic behavior of the system and a feasibility verification must be made to take these changes into account. In order to overcome these drawbacks we presented a novel method, a so called *continuous approach*, where the discrete set of available motors was extended to a continuous domain by fitting manufacturer data. Under these circumstances, the optimization can be carried out without iterations, and it is applicable to the general case of a real reducer. The constraints on the system remains the same as the discrete one. The problem becomes a two-dimensional nonlinear optimization subject to nonlinear constraints, and the solution gives the optimal choice for the motor-reducer system. Similarly to what we did in the discrete approach, the evaluation of the objective functions is based on the presented electromechanical model, with the only difference being that every quantity is computed in its most general case (no inertia or efficiency is disregarded). Two continuous size indexes were defined, α and β, to map motor and reducer catalogs. All component characteristic parameters, and thus the objective functions, are dependent on those indexes. Since the component data were obtained by interpolating catalog data, the discrete optimization is a particular case of the continuous optimization. The nonlinear programming problem was solved by introducing the Karush-Khun-Tucker theorem, which gives the condition for a point (α, β) to be a local minimum. The subsequent system of equality and inequality was solved numerically via the interior-point algorithm, and all solutions were investigated in order to find the global optimum. Once the global minimum is known, it may be used as a first-try selection. Since the real catalog is not continuous, the actual values of (α, β) can likely be different from the theoretical ones. However, the choice of the nearest available components is close enough to the global optimum if the resolution of the catalog is good enough. Another alternative is designing a custom motor-reducer unit for the application. Comparing the continuous optimization results with the discrete ones, we notice that in the former case no unfeasible solutions are provided, whereas this may occur when using the discrete approach, the reason being that the selection is made in not ideal conditions. As far as the choice of objective function is concerned, it is confirmed that the addition of inverter losses does not significantly changes the optimal transmission ratio that minimizes the energy absorbed by the servo-axis.

As for the future perspectives, the implementation of a genetic algorithm (or the development of a custom hybrid algorithm) may directly lead to the global optimum. However, the information that the local optima provide are not disregardable, since the local trend that the objective function has may be important in the case that other constraints limit the problem, and only a subset of the domain is available. Moreover, the improvement of the optimization phase is heavily linked with the electromechanical model. In fact, the model is the basis for the optimization process: the introduction of further contributions on the model would lead to even more accurate indications on the optimal selection.

APPENDIX A: OptimusDrive - a simulation and optimization software

A simulation and optimization software, called *OptimusDrive* [26], is developed, that implements the electromechanical model and the optimization algorithms here presented. It is a powerful complete simulation tool for the study of servo-axis, which offers comprehensive guidance to machine designers when selecting component types and specifications. The versatility of OptimusDrive allows for the determination of a wide range of electric and mechanical parameters related to servo-axis operation, which the user can take advantage of to define an optimal machine set-up and the corresponding objective function. Moreover, the behavior of the system in different operating conditions can be simulated and evaluated. The program is coded using MATLAB graphic user interface (GUI).

Key features

- *Modeling of the mechanical transmission*: a library of pre-defined mechanisms is available; the user may compose the transmission by sequentially adding blocks in a graphic diagram: once the geometrical and inertial parameters are provided, the software will automatically compute the transmission transfer functions. If a generic mechanism is to be implemented, on the other hand, the transfer function must be manually provided. OptimusDrive also implemented a tool to characterize a generic mechanism block, with the aid of convenient simulations obtained from multi-body software. The pre-defined mechanism library includes:
  - gears drives,
  - pulley-belt drives,
  - 4-bar mechanism,
  - crank-lever mechanism,
  - crank and slotted lever mechanism,
  - Geneva wheel,
  - generic mechanism (transfer function provided by the user),
  - generic mechanism (transfer function obtained from multi-body simulations).
- *Dynamics solver*: in order to solve the inverse dynamics, either the motion law of the end-effector or the motion law of the motor must be provided. The kinematics and the

inverse dynamics are solved step-by-step for each node of the block diagram. In order to solve the forward dynamics, the motor torque and external load must be provided as a function of time. The subsequent differential equation is solved by numerical integration. The torques/forces and the velocities at each node of the block diagram are promptly evaluated.

- *Characterization of the motor (and inverter)*: using the motor coefficients obtained by the motor data available from catalogs, the software infers the torque-current relation, and it evaluates the windings and iron losses are evaluated. An efficiency map is defined over the motor operating range. If the inverter data are available, the switching losses are also modeled.
- *Optimization for candidate motor*: for each candidate motor, the introduction of a gearbox reducer is evaluated. The optimal transmission ratio that minimize a set of objective functions is given. The list of objective functions includes:
  - root-mean-square value of motor torque,
  - peak value of motor torque,
  - peak value of electric power absorbed by the motor,
  - root-mean-square value of electric power absorbed by the motor,
  - energy absorbed by the motor,
  - energy absorbed from the electric grid.
- *Complete optimization*: once a motor and a reducer catalog are provided by the user, the software generates a continuous catalog by interpolating available components data. An optimization algorithm then determines the best choice for the motor and reducer pair. The most general case is considered for the optimization, where both mechanical and electrical losses from the motors and also the reducers are taken into account.

Inputs and Outputs

The user is provided with a graphic interface for accessing the functionalities of the software. The user may introduce the input via data text file. The inputs the user must provide to the software are:

- Blocks sequence, composed using GUI.
- Geometrical and inertial block properties .
- External load and end-effector (or motor) motion law (inverse dynamics).
- Motor torque as a function of time (forward dynamics).
- Motor catalog data.
- Motor and reducer catalogs (for complete optimization only).

The output may be exported in several file format, such as *.xls* or *.mat*. Graphics contents are also exportable. The outputs the software provides are:

- Mechanical torque, power and rotational speed of the motor.
- Forces/torques and velocities, computed at each node of the block model.
- Electrical power/energy absorbed by the motor; motor efficiency.
- Total electrical power/energy absorbed from the grid; global efficiency.
- Optimal transmission ratio that minimizes a user-defined objective function, for the selected motor.
- Optimal selection for motor and reducer.

List of Figures

List of Tables

Acknowledgments

I would like to deeply thank Professor Marco Carricato, who guided my research by providing me with precious suggestions and ideas, and above all, supported me throughout these years.

I would also like to thank Professor Vincenzo Parenti Castelli as the coordinator of the PhD course, and all the GRAB (Group of Robotics, Automation and Articular Biomechanics) members.

Thanks to all my colleagues (and friends as well) for all the support. It has been a pleasure to work with them. A special thought goes to the guys in Aula Masi-Carducci, who supported me while I was writing this thesis.

I'm grateful to Dr. Troy Wu for his precious help in editing this work.

I would like to thank all the PhD students, researchers and professors from the University of Bologna that I met during my work: they kindly shared their experience and provided me different points of view.

Thank you to my girlfriend and to all my friends: they are always there and they know me more than I know myself.

Finally, my deepest gratitude goes to my family, for their guidance and for their unconditional support throughout my studies and my life. Nothing would have been possible without them.

Bibliography

[1] K. A. Pasch and W. P. Seering. On the drive system for high-performance machines. *Journal of Mechanisms, Transmissions, and Automation in Design*, 106(1):102–108, 1984.

[2] D. Z. Chen and L. W. Tsai. The generalized principle of inertia match for geared robotic mechanisms. In *Proceedings. 1991 IEEE International Conference on Robotics and Automation*, pages 1282–1287 vol.2, Apr 1991.

[3] H. Van de Straete, P. Degezelle, J. De Schutter, and R. J. M. Belmans. Servo motor selection criterion for mechatronic applications. *IEEE/ASME Transactions on Mechatronics*, 3(1):43–50, Mar 1998.

[4] H. Van de Straete, J. De Schutter, and K.U. Leuven. Optimal variable transmission ratio and trajectory for an inertial load with respect to servo motor size. *Journal of Mechanical Design*, 121(4):544–551, Dec 1999.

[5] F. Roos, H. Johansson, and J. Wikander. Optimal selection of motor and gearhead in mechatronic applications. *Mechatronics*, 16(1):63 – 72, 2006.

[6] Giancarlo Cusimano. A procedure for a suitable selection of laws of motion and electric drive systems under inertial loads. *Mechanism and Machine Theory*, 38(6):519 – 533, 2003.

[7] Giancarlo Cusimano. Generalization of a method for the selection of drive systems and transmissions under dynamic loads. *Mechanism and Machine Theory*, 40(5):530 – 558, 2005.

[8] Giancarlo Cusimano. Optimization of the choice of the system electric drive-device transmission for mechatronic applications. *Mechanism and Machine Theory*, 42(1):48 – 65, 2007.

[9] Giancarlo Cusimano. Choice of motor and transmission in mechatronic applications: Non-rectangular dynamic range of the drive system. *Mechanism and Machine Theory*, 85:35 – 52, 2015.

[10] Giancarlo Cusimano and Federico Casolo. An almost comprehensive approach for the choice of motor and transmission in mechatronics applications: Motor thermal problem. *Mechatronics*, 40:96–105, 2016.

[11] Adamini R. Legnani G, Tiboni M. *Meccanica degli Azionamenti*. Ed. Esculapio, 2nd edition, 2002.

[12] H. Giberti, S. Cinquemani, and G. Legnani. Effects of transmission mechanical characteristics on the choice of a motor-reducer. *Mechatronics*, 20(5):604 – 610, 2010.

[13] H. Giberti, S. Cinquemani, and G. Legnani. A practical approach to the selection of the motor-reducer unit in electric drive systems. *Mechanics Based Design of Structures and Machines*, 39(3):303–319, 2011.

[14] Giancarlo Cusimano. Choice of electrical motor and transmission in mechatronic applications: The torque peak. *Mechanism and Machine Theory*, 46(9):1207–1235, 2011.

[15] Giancarlo Cusimano. Influence of the reducer efficiencies on the choice of motor and transmission: Torque peak of the motor. *Mechanism and Machine Theory*, 67:122–151, 2013.

[16] H. Giberti, A. Clerici, and S. Cinquemani. Specific accelerating factor: One more tool in motor sizing projects. *Mechatronics*, 24(7):898–905, 2014. cited By 3.

[17] S. Rezazadeh and J. W. Hurst. On the optimal selection of motors and transmissions for electromechanical and robotic systems. In *2014 IEEE/RSJ International Conference on Intelligent Robots and Systems*, pages 4605–4611, Sept 2014.

[18] T. Verstraten, G. Mathijssen, R. Furnémont, B. Vanderborght, and D. Lefeber. Modeling and design of geared dc motors for energy efficiency: Comparison between theory and experiments. *Mechatronics*, 30:198–213, 2015. cited By 0.

[19] Tom Verstraten, Raphaël Furnémont, Glenn Mathijssen, Bram Vanderborght, and Dirk Lefeber. Energy consumption of geared dc motors in dynamic applications: Comparing modeling approaches. *IEEE Robotics and Automation Letters*, 1(1):524–530, 2016.

[20] R. H. Park. Two-reaction theory of synchronous machines generalized method of analysis-part i. *Transactions of the American Institute of Electrical Engineers*, 48(3):716–727, July 1929.

[21] M. A. Rahman and P. Zhou. Analysis of brushless permanent magnet synchronous motors. *IEEE Transactions on Industrial Electronics*, 43(2):256–267, Apr 1996.

[22] T. Herold, D. Franck, E. Lange, and K. Hameyer. Extension of a d-q model of a permanent magnet excited synchronous machine by including saturation, cross-coupling and slotting effects. In *2011 IEEE International Electric Machines Drives Conference (IEMDC)*, pages 1363–1367, May 2011.

[23] T. M. Jahns, G. B. Kliman, and T. W. Neumann. Interior permanent-magnet synchronous motors for adjustable-speed drives. *IEEE Transactions on Industry Applications*, IA-22(4):738–747, July 1986.

[24] R. Schifer and T. A. Lipo. Core loss in buried magnet permanent magnet synchronous motors. *IEEE Transactions on Energy Conversion*, 4(2):279–284, Jun 1989.

[25] L. Xu, X. Xu, T. A. Lipo, and D. W. Novotny. Vector control of a synchronous reluctance motor including saturation and iron loss. *IEEE Transactions on Industry Applications*, 27(5):977–985, Sep 1991.

[26] F. Meoni and M. Carricato. OptimusDrive - Simulation and Optimization software. http://grab.diem.unibo.it/OptimusDrive/, 2017. [Download link].

[27] J.E. Shigley and J.J. Uicker. *Theory of machines and mechanisms*. McGraw-Hill series in mechanical engineering. McGraw-Hill, 1995.

[28] Bruno Siciliano and Oussama Khatib. *Springer handbook of robotics*. Springer, 2016. 2nd ed.

[29] Robert Mahony, Vijay Kumar, and Peter Corke. Multirotor aerial vehicles. *IEEE Robotics and Automation magazine*, 20(32), 2012.

[30] Wei Wu. Dc motor parameter identification using speed step responses. *Modelling and Simulation in Engineering*, 2012:30, 2012.

[31] J.R. Dormand and P.J. Prince. A family of embedded runge-kutta formulae. *Journal of Computational and Applied Mathematics*, 6(1):19 – 26, 1980.

[32] P.L. Magnani and G. Ruggieri. *Meccanismi per macchine automatiche*. Collezione di ingegneria meccanica. UTET, 1986.

[33] A. Hughes and B. Drury. Chapter nine - synchronous and brushless permanent magnet machines and drives. In A. Hughes and B. Drury, editors, *Electric Motors and Drives (Fourth Edition)*, pages 281 – 313. Newnes, Boston, fourth edition edition, 2013.

[34] J. C. Gamazo-Real, E. Vazquez-Sanchez, and J. Gomez-Gil. Position and speed control of brushless dc motors using sensorless techniques and application trends. *Sensors*, 10(7):6901–6947, 2010.

[35] Ned Mohan, Tore M. Undeland, and William P. Robbins. *Power Electronics. Converters, Applications and Design*. John Wiley and Sons, Inc, third edition, 2003.

[36] A. E. Fitzgerald, J.R. Kingsley, and Umans D. *Electric Machinery. A.E. Fitzgerald, Charles Kingsley, JR., Stephen D. Umans*. McGraw-Hill, 6th edition, 2003.

[37] C. P. Steinmetz. On the law of hysteresis. *Proceedings of the IEEE*, 72(2):197–221, Feb 1984.

[38] G. R. Slemon and X. Liu. Core losses in permanent magnet motors. *IEEE Transactions on Magnetics*, 26(5):1653–1655, Sep 1990.

[39] W. Hassan and Bingsen Wang. Efficiency optimization of pmsm based drive system. In *Proceedings of The 7th International Power Electronics and Motion Control Conference*, volume 2, pages 1027–1033, June 2012.

[40] I. Boldea and S.A. Nasar. *Electric Drives, Second Edition*. Electric Power Engineering Series. Taylor & Francis, 2005.

[41] F. Meier and J. Soulard. dq theory applied to a permanent magnet synchronous machine with concentrated windings. In *2008 4th IET Conference on Power Electronics, Machines and Drives*, pages 194–198, April 2008.

[42] N. Urasaki, T. Senjyu, and K. Uezato. An accurate modeling for permanent magnet synchronous motor drives. In *APEC 2000. Fifteenth Annual IEEE Applied Power Electronics Conference and Exposition (Cat. No.00CH37058)*, volume 1, pages 387–392 vol.1, 2000.

[43] Z. Haigang, Q. Weiguo, W. Yanxiang, G. Shihong, and Y. Yuan. Modeling and simulation of the permanent-magnet synchronous motor drive. In *2011 International Conference on Uncertainty Reasoning and Knowledge Engineering*, volume 2, pages 256–260, Aug 2011.

[44] Juha Pyrhöonen, Valéria Hrabovcová, and Scott R Semken. *Permanent magnet synchronous machine drives*, pages 296–345. John Wiley & Sons Ltd, 2016.

[45] D. Y. Ohm. Dynamic model of pm synchronous motors. techreport, Drivetech Inc., Blacksburg, Virginia, 05 2000.

[46] B&R. *8LS three-phase synchronous motors*, 2.0 edition, 04 2016.

[47] J. E. Brown, K. P. Kovacs, and P. Vas. A method of including the effects of main flux path saturation in the generalized equations of a.c. machines. *IEEE Transactions on Power Apparatus and Systems*, PAS-102(1):96–103, Jan 1983.

[48] I. Boldea and S. A. Nasar. Unified treatment of core losses and saturation in the orthogonal-axis model of electric machines. *IEE Proceedings B - Electric Power Applications*, 134(6):355–363, November 1987.

[49] E. Levi and V. Vuckkovic. Field-oriented control of induction machines in the presence of magnetic saturation. *Electric Machines & Power Systems*, 16(2):133–147, 1989.

[50] R. S. Colby and D. W. Novotny. Efficient operation of surface-mounted pm synchronous motors. *IEEE Transactions on Industry Applications*, IA-23(6):1048–1054, Nov 1987.

[51] Schneider Electric. *PacDrive SH Servo Motor: Operating Manual*, 2009.

[52] K.D. Schmitt. Efficiency sh100 - formulas and coefficients. Schneider Electric, 01 2014.

[53] M. H. Bierhoff and F. W. Fuchs. Semiconductor losses in voltage source and current source igbt converters based on analytical derivation. In *2004 IEEE 35th Annual Power Electronics Specialists Conference (IEEE Cat. No.04CH37551)*, volume 4, pages 2836–2842 Vol.4, 2004.

[54] Q. K. Nguyen and J. Roth-Stielow. Analysis and modelling of the losses for the electrical drive system of an electric vehicle. In *2014 IEEE Vehicle Power and Propulsion Conference (VPPC)*, pages 1–6, Oct 2014.

[55] Forthuberf and A. Holzleitner. A guide to calculate power losses of a drive train. Tech report, B&R, 2013.

[56] H.J. Van de Straete, J. De Schutter, and R. Belmans. An efficient procedure for checking performance limits in servo drive selection and optimization. *Mechatronics, IEEE/ASME Transactions on*, 4(4):378–386, Dec 1999.

[57] David V. Widder. *Advanced Calculus: Second Edition*. DOVER PUBN INC, 1989.

[58] J.E. Marsden and A. Weinstein. *Calculus unlimited*. Benjamin/Cummings Publishing Company, 1981.

[59] Peter Borwein and Tamas Erdelyi. *Polynomials and Polynomial Inequalities*. Springer New York, 2012.

[60] B&R. Standard planetary gearboxes. online catalog :https://www.br-automation.com/en/products/motion-control/8g-standard-planetary-gearbox/, 2016.

[61] Carl De Boor. A practical guide to splines, 1978. Number 27 in Applied Mathematical Sciences.

[62] Ake Bjorck. *Numerical Methods for Least Squares Problems*. CAMBRIDGE UNIV PR, 1996.

[63] C.D. Pagani and Salsa S. *Analisi matematica*, volume 2. Zanichelli, first edition, 1991.

[64] Richard H Byrd, Mary E Hribar, and Jorge Nocedal. An interior point algorithm for large-scale nonlinear programming. *SIAM Journal on Optimization*, 9(4):877–900, 1999.

[65] Richard H Byrd, Jean Charles Gilbert, and Jorge Nocedal. A trust region method based on interior point techniques for nonlinear programming. *Mathematical Programming*, 89(1):149–185, 2000.

[66] Richard A Waltz, José Luis Morales, Jorge Nocedal, and Dominique Orban. An interior algorithm for nonlinear optimization that combines line search and trust region steps. *Mathematical programming*, 107(3):391–408, 2006.

[67] David E Goldberg. Genetic algorithms in search, optimization and machine learning. *Addison-Wesley*, 1989.